DISSERTATION

SPREAD OFDM VIA CARRIER INTERFEROMETRY SPREADING CODES: PERFORMANCE, THROUGHPUT, AND PAPR ENHANCEMENT

Submitted by

David A. Wiegandt

Department of Electrical and Computer Engineering

In partial fulfillment of the requirements

for the Degree of Doctor of Philosophy

Colorado State University

Fort Collins, Colorado

Summer 2003

COLORADO STATE UNIVERSITY

May 28, 2003

WE HEREBY RECOMMEND THAT THE DISSERTATION PREPARED UNDER OUR SUPERVISION BY DAVID A. WIEGANDT ENTITLED "SPREAD OFDM VIA CARRIER INTERFEROMETRY SPREADING CODES: PERFORMANCE, THROUGHPUT, AND PAPR ENHANCEMENT" BE ACCEPTED AS FULFILLING IN PART REQUIREMENTS FOR THE DEGREE OF DOCTOR OF PHILOSOPHY.

Committee on Graduate Work

Dr. V. Chandrasekar, Electrical & Computer Engineering

Dr. Derek Lile, Electrical & Computer Engineering

Dr. Fred Smith, Mechanical Engineering

Advisor: Dr. Carl R. Nassar, Electrical & Computer Engineering

Department Head: Dr. Derek Lile, Electrical & Computer Engineering

ABSTRACT OF DISSERTATION

SPREAD OFDM VIA CARRIER INTERFEROMETRY SPREADING CODES: PERFORMANCE, THROUGHPUT, AND PAPR ENHANCEMENT

Orthogonal Frequency Division Multiplexing (OFDM) has been an important technique in wireless communication architectures since the 1970's and 1980's. OFDM is now the protocol in the IEEE 802.11a and IEEE 802.11g Wireless Local Area Networks (WLANs) standards, as well as the IEEE 802.16 Fixed Broadband standard. It is also a front-runner for implementation in future cellular standards and satellite systems. However, OFDM is not without its limitations – both in terms of performance and Peak-to-Average Power Ratio (PAPR). In this dissertation, the author significantly enhances the performance of traditional OFDM systems via the introduction of novel Carrier Interferometry (CI) spreading codes. Specifically, this research demonstrates through computer emulation and RF testing, that the application of CI spreading codes to OFDM, leads to significant performance gains (relative to traditional OFDM), and an eliminated PAPR issue. The novel OFDM techniques introduced in this dissertation will significantly enhance the abilities of OFDM in the years to come.

David A. Wiegandt
Electrical and Computer Engineering Department
Colorado State University
Fort Collins, CO 80523
Summer 2003

ACKNOWLEDGEMENTS

The time spent in pursuit of this doctoral degree has been blessed with the love, friendship, and support of so many wonderful people. The road from undergraduate through Ph.D. is filled with many high points and a few bumps, and I could not have reached the end without my family and friends.

To begin, I would like to thank my advisor, Dr. Carl Nassar, for helping me discover so many opportunities along the way. Through the research and the travel, we had many good times, and I greatly appreciate all that you have helped me to accomplish. I would also like to thank my committee members for their guidance and friendship as well. To Dr. Lile, who is a major part of the reason I chose CSU, thank you for the opportunity to teach and for all of your continued assistance with my different pursuits. To Dr. Chandra, who always had an open door and a lesson to teach, I will always be grateful for your support both in and out of the classroom. And to Dr. Smith, who always showed an incredible interest in my research, thank you for helping to draw the passion out of this work and for the fun times we had with the Order of the Engineer and the Walking Machine competitions. While not technically on my doctoral committee, I would like to additionally thank those who have benefited my overall professional education, Dr. Kevin Lear, Dr. Carl Wilmsen, and Mike Murphy.

Aside from the academic side of things, my time here would not have been complete without the rest of the CSU family. I would like to thank Karen and Ray, Nancy, Laura, Beth, Tom, Cathy, and Mark for the friendship and the laughs we all have shared.

Finally, I would like to thank my parents, Karl and Elizabeth, for being the biggest fans and the best friends a person could ever hope to have. There was no greater feeling in the world then getting through a hurdle and knowing you were waiting on the other end of the phone to begin cheering. I would also like to thank my sister, Jennifer. While we did not talk everyday, seeing your screen name active brought me peace of mind, and it was like you were with me every step of the way. I am thankful that you, Ted, and Reese could be here to see the final leg of this degree. And last, but not least, I would like to thank Clint Lanier and Johanna Cox for providing the kind of support that only best friends can provide.

TABLE OF CONTENTS

LIST OF FIGURES

LIST OF TABLES

Part I:

Introduction

Chapter 1 Introduction

In the last decade, we have witnessed unprecedented growth in the areas of signal processing and wireless communications. Recent developments have led to, e.g., higher processing speeds, smaller processors, lower transmit powers, higher-bandwidth efficiencies, and lower costs. However, while these advances have led to impressive technological innovations, the spectrum is none-the-less becoming more and more cluttered. It is now, more than ever, important to continue reducing transmit powers and increasing bandwidth efficiencies (i.e., higher data rate/number of users within the same frequency band).

An important technological innovation, leading to the advancement of wireless systems, is Orthogonal Frequency Division Multiplexing, or OFDM. OFDM was first introduced in the late 1950's and first characterized in the mid 1960's (e.g. [1-5]). OFDM is able to divide the overall frequency-selective bandwidth into N smaller (narrower) bands that each experience flat fading, thereby overcoming the effect of ISI (Inter-Symbol Interference) due to the selectivity. While introduced many decades ago, it was not until more recent advances in signal processing (namely the advent of the FFT

and IFFT) (in the late 1980's [6-7]) that a true low-cost, easily implemented OFDM architecture became available. Today, OFDM's applications include variable rate modems [8], ADSL, VHDSL and HDSL subscriber line multichannel transceivers [9-13], digital terrestrial ATV broadcasting [14], fixed wireless [15], wireless ATM [16], and Wireless LANs such as the IEEE 802.11a standard [17] and the IEEE 802.11g standard [18].

In this chapter, the concept of OFDM is briefly reviewed, followed by the contribution of this dissertation to the arena of OFDM.

1.1 Orthogonal Frequency Division Multiplexing

OFDM's popularity stems, in part, from its ability to avoid frequency selectivity. Specifically, in OFDM, a high-rate symbol stream is fed into a serial-to-parallel converter, and N low-rate symbol streams are output. Each low-rate stream is then sent simultaneously over N orthogonal carriers, one symbol stream per unique carrier [19]. The data rate per carrier is a factor of N smaller then the original data rate (due to serial-to-parallel conversion), and hence, the bandwidth per carrier is only $(1/N)^{th}$ of the overall system bandwidth. As a result, each transmitted symbol (one per carrier) experiences a flat fade. This translates into simple receiver design and a system that avoids multipath.

However, OFDM is not without its disadvantages. Based upon this frequency division process, each carrier undergoes a flat fade and reaches the receiver with a different amplitude. As such, it is possible, even likely, that some of the N data symbols are completely lost due to deep fades. To account for this, Coded OFDM (COFDM) has been introduced (e.g., [20-25]).

In COFDM, incoming information symbols are channel coded prior to serial-to-parallel conversion by a rate m/n coder. The coded symbols are then interleaved and sent on one of the frequency carriers (where the interleaving ensures that adjacent coded symbols reside on non-adjacent frequency carriers). By inclusion of channel coding, a frequency diversity benefit is introduced, as are the usual channel coding gains. As a result, the resulting channel coded OFDM system, COFDM, represents a system with greatly improved performance. While enhancing performances, the COFDM systems have the drawback of reduced throughput.

An additional drawback in OFDM, and its method of orthogonal carrier transmission, is high (poor) PAPR (Peak-to-Average Power Ratio) [26]. Specifically, high peaks in power (up to N times the average) result from unstable envelopes, a consequence of using independently modulated carriers. Specifically, in-phase, coherent summations across the independently modulated data symbols can cause a peak in transmit power (within the transmit frame) that is dramatically higher than the average transmit power (within the transmit frame). These large spikes in transmit power drive the power amplifier into the

saturation region of operation, leading to spectral spreading. A number of solutions to OFDM's peak-to-average power ratio (PAPR) problem have been proposed in the literature (i.e., block coding [27], peak cancellation [28-29], partial transmit sequences [30], selective mapping [31], and clipping [32]), but, while reducing the PAPR, these methods typically increase system complexity, and may contribute to in-band distortions that lead to reduced bit-error-rate (BER) performances.

1.2 Statement of Work: The CI/OFDM System

In this dissertation, Carrier Interferometry (CI) spreading codes are introduced into OFDM systems, thereby improving OFDM's (1) performance, (2) throughput, and (3) peak-to-average power ratio (PAPR).

- *Performance*: By introducing novel Carrier Interferometry spreading codes into OFDM, we provide an innovative method for improved performance [33-38]. The resulting CI/OFDM system exploits the full frequency diversity benefit of the channel at the receiver, and as a result, significantly outperforms traditional OFDM systems in terms of bit error rate in multipath fading channels (i.e., channels exhibiting frequency selectivity over the entire bandwidth). These

results naturally extend to the wide range of modulation formats employed in OFDM, i.e., BPSK, QPSK, 16QAM and 64QAM.

- *Throughput*: By introducing pseudo-orthogonal Carrier Interferometry spreading codes into OFDM, we create PO-CI/OFDM systems which double throughput in OFDM systems with real-signaling (i.e., BPSK, ASK). The throughput gain is available without extra bandwidth requirements or performance degradations [39-41].

- *PAPR*: By introducing Carrier Interferometry and Pseudo-Orthogonal Carrier Interferometry spreading codes into OFDM, we create CI/OFDM and PO-CI/OFDM systems capable of eliminating the peak-to-average power ratio problems inherent in traditional OFDM systems [42-44].

- *WLANs*: By applying our CI/OFDM technology to enhance the IEEE 802.11a Wireless LAN standard, we show how the above benefits can be exploited in a modern-day indoor architecture [45-49]. Specifically, the resulting system achieves, e.g., a 5-7 dB performance gain at a probability of error of 10^{-3} in actual indoor environments.

- *Terrestrial Link Testing*: By applying our CI/OFDM technology to Fixed Broadband terrestrial systems, we show how the above benefits can be exploited in modern day outdoor architectures [50-52]. Specifically, the resulting CI/OFDM system significantly outperforms traditional architectures utilizing OFDM by (up to) an order of magnitude in actual outdoor terrestrial environments.

- *Satellite Testing*: By applying our CI/OFDM technology to satellite architectures, we show how the above benefits can be exploited in modern day satellite systems [53-54]. Specifically, CI/OFDM achieves small performance gains over actual satellite channels for BPSK, QPSK, and 16QAM. When CI/COFDM is applied, dramatic performance increases are observed for 64 QAM, leading to high-bandwidth efficiencies and a high-throughput system for use over satellites.

Orthogonal Frequency Division Muliplexing (OFDM) has become a key player for the future of the wireless communications industry. With this in mind, this dissertation introduces powerful and novel innovations to the OFDM architecture which improve performance, throughput, and peak-to-average power ratio.

Part II:

OFDM

Chapter 2 Introduction to Orthogonal Frequency Division Multiplexing

Orthogonal Frequency Division Multiplexing (OFDM) was first introduced in the late 1950's and first characterized in the mid 1960's (e.g. [1-5]). Since its introduction over four decades ago, advances in digital signal processing have led to OFDM's growing popularity. Applications include variable rate modems [8], ADSL, VHDSL and HDSL subscriber line multichannel transceivers [9-13], digital terrestrial ATV broadcasting [14], fixed wireless [15], wireless ATM [16], and Wireless LANs such as the IEEE 802.11a [17] and the IEEE 802.11g standards [18].

OFDM's popularity stems, in part, from its ability to avoid frequency selectivity. Specifically, in OFDM, a high-rate symbol stream is fed into a serial-to-parallel converter, and the N low-rate data streams output are then sent simultaneously over N orthogonal carriers [19]. The data rate per carrier is a factor of N smaller then the original data rate, and hence bandwidth per carrier is only $(1/N)^{th}$ of the overall system bandwidth. As a result, each transmitted symbol (one per carrier) experiences a flat fade. This translates into simple receiver design and a system that avoids multipath.

In this chapter, we briefly review the OFDM concept, its transmitter and receiver design, its performance, and its limitations.

2.1 Introduction to the Transmitter and Receiver

OFDM system benefits include: (1) the ability to reduce the input of frequency selective fading, (2) large spectral efficiency, and (3) the ability to support very high-speed transmission. The generalized block diagram of the typical OFDM transmitter is shown in Figure 2.1. Referring to Figure 2.1, a high-rate input symbol stream is serial-to-parallel converted, and then each data symbol is modulated onto its own carrier. This carrier modulation is typically implemented via the Inverse Fast Fourier Transform (IFFT), making the transmitter easy to implement.

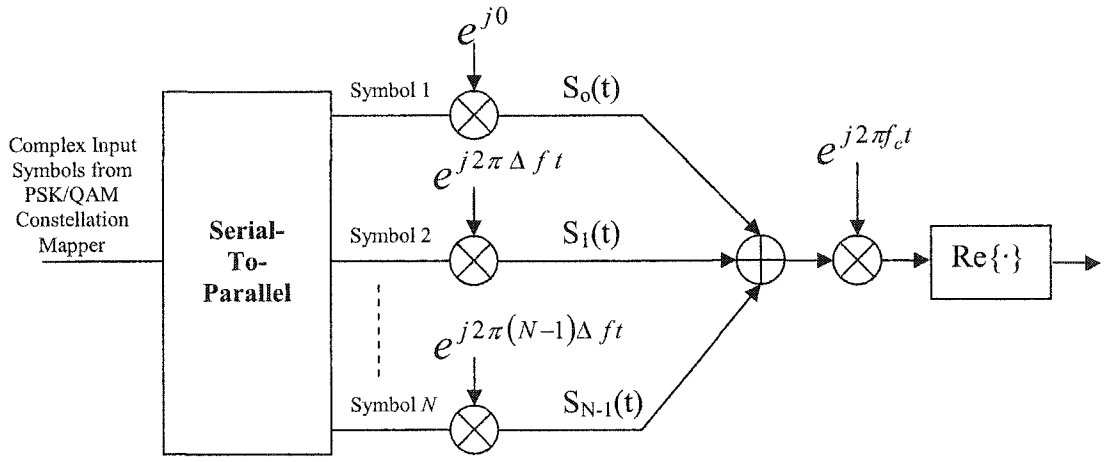

Figure 2.1: General OFDM Transmitter

The OFDM receiver is depicted in Figure 2.2, illustrating detection of the N transmitted symbols. It is important to note that Figure 2.2 is the generalized block

diagram of the receiver. Practical implementations use the FFT to perform much of the demodulation processes.

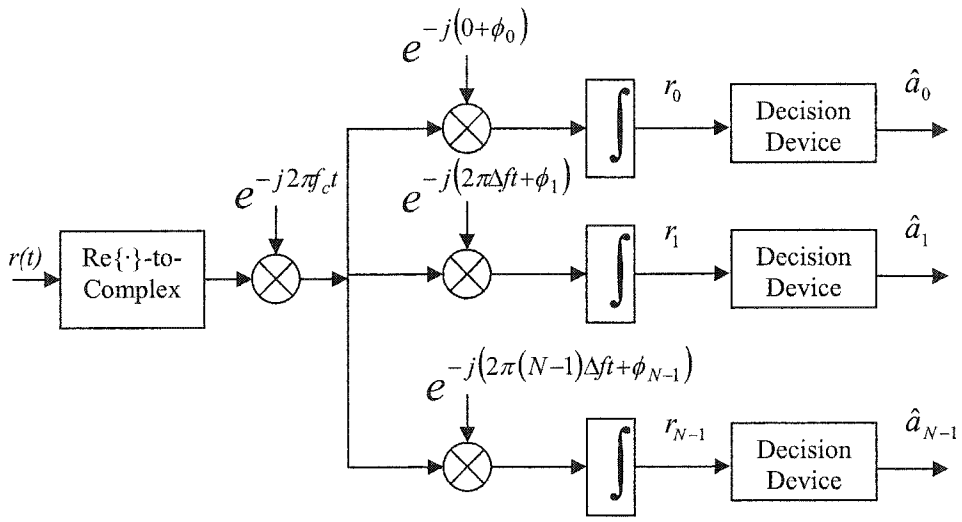

Figure 2.2: The OFDM receiver

2.2 OFDM Transmit and Receive Signals

Referring to Figure 2.1, the k^{th} symbol is placed on the k^{th} carrier leading to:

$$s_k(t) = a_k e^{j(2\pi k\Delta ft)} \tag{2.1}$$

where (1) a_k denotes the k^{th} symbol and is assumed to be +1 or –1 with equal probability (BPSK symbols are assumed throughout this chapter for ease in presentation); (2) $k\Delta f$ is the k^{th} carrier, and $\Delta f = 1/T_s$ (T_s is the symbol rate) to assure

orthogonality among carriers. Now, considering the entire block of N parallel symbols, the transmitted signal in OFDM is:

$$s(t) = \mathrm{Re}\left\{ \sum_{k=0}^{N-1} a_k e^{j(2\pi f_c t + 2\pi k \Delta f t)} \right\} \tag{2.2}$$

$$s(t) = \sum_{k=0}^{N-1} a_k \cos(2\pi f_c t + 2\pi k \Delta f t) \tag{2.3}$$

It is important to note that BPSK is assumed for ease in presentation, and it is understood that this is a low-bandwidth-efficiency example. Improved bandwidth efficiencies are observed with higher order PSK and QAM constellations. It is also important to note that we do not explicitly include the cyclic prefix in the OFDM transmission model because our analysis is per-OFDM block. However, in realistic scenarios of contiguous OFDM block transmission, a cyclic prefix is assumed between successive OFDM blocks (typical of traditional OFDM) [19].

The OFDM received signal, assuming the sent signal *s(t)* in (2.3), is mathematically characterized by the following equation:

$$r(t) = \sum_{k=0}^{N-1} \alpha_k a_k \cos(2\pi f_c t + 2\pi k \Delta f t + \phi_k) + n(t) \tag{2.4}$$

Here, α_k and ϕ_k are the fade parameter and phase offset, respectively, introduced into the k^{th} carrier by the frequency selective Rayleigh fading channel, and *n(t)* is a zero mean

Gaussian random variable with variance $N_0/2$ representing additive white Gaussian noise (AWGN).

At the OFDM receiver, referring to Figure 2.2, *r(t)* returns to baseband and is then separated into its N orthogonal carrier components (which includes channel phase correction). Carrier orthogonality leads to the received signal on the k^{th} carrier corresponding to $r_k = \alpha_k a_k + n_k$ (where $k \in [0,1,...,N-1]$). We have assumed perfect phase synchronization at the receiver, for reasons of ease in presentation. Finally, each of the N signals enter a hard decision device, outputting $\hat{a}_k$, the k^{th} decision.

2.3 OFDM Simulated Performance

Figure 2.3 illustrates the bit error rate (BER) versus signal to noise ratio for OFDM. The simulated system transmits $N = 32$ BPSK symbols over $N = 32$ orthogonal carriers. To model a realistic wireless environment, the Rayleigh fading channel employed in our simulation demonstrates frequency selectivity over the entire bandwidth, BW, but flat fading over each of the N narrowband carriers. Specifically, we assumed a channel model with 4-fold frequency diversity over the entire bandwidth. As a result, the fading gain (α_k's) in the 32 carriers are correlated according to [55]

$$R_{i,j} = \frac{1}{1+\left(\frac{\Delta f_{i,j}}{(\Delta f_c)}\right)^2} \tag{2.5}$$

where $R_{i,j}$ is the correlation between carrier i and carrier j, and $\Delta f_{i,j}$ is the frequency separation between these two carriers. Generation of correlated fades, for purposes of simulation, has been discussed in [56] and [57].

Referring to Figure 2.3, OFDM requires an SNR of approximately 23 dB to achieve a BER of 10^{-3}.

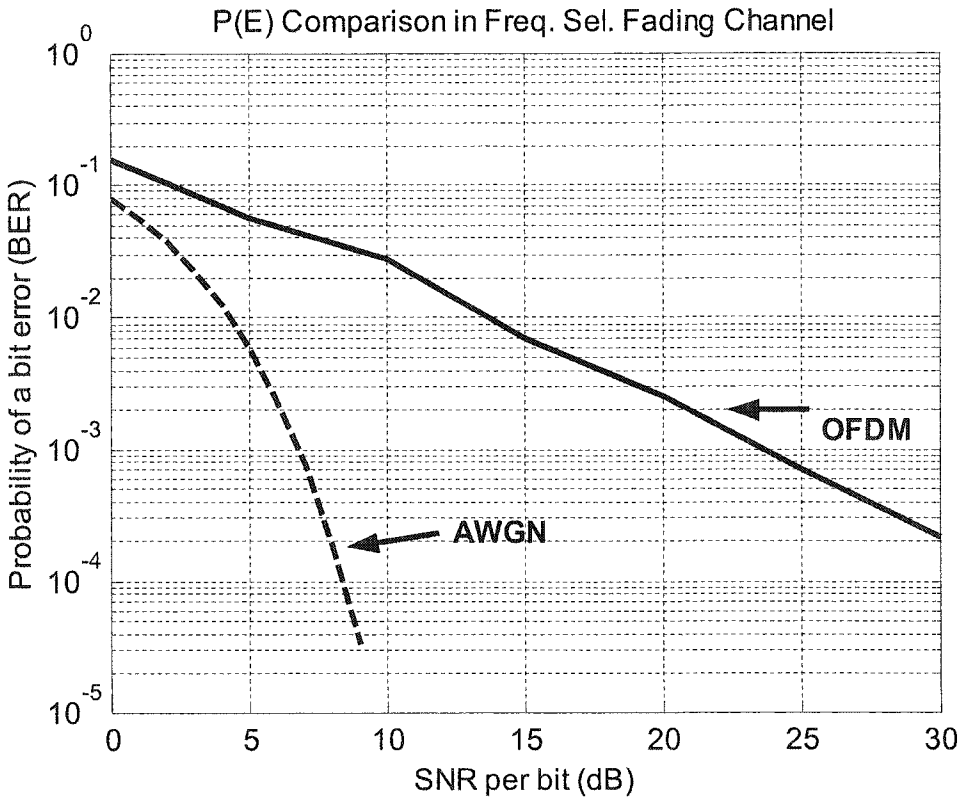

Figure 2.3: Simulated Performance of OFDM

2.4 OFDM's Limitations

OFDM is not without its disadvantages. Since each carrier undergoes a flat fade and reaches the receiver with a different amplitude, it is possible, even likely, that some of the N data symbols are completely lost due to deep fades. This is observed in the poor performance curve of Figure 2.3. To improve performance, Coded OFDM (COFDM) has been introduced in, e.g., [20-25].

In COFDM, incoming information symbols are channel coded prior to serial-to-parallel conversion by a rate m/n coder. The coded symbols are then interleaved, ensuring that adjacent coded symbols are transmitted via non-adjacent carriers. This coding strategy introduces a frequency diversity benefit in addition to the channel coding gain. The resulting performance curve (Figure 2.4) shows a system with reduced sensitivity to fading. The drawback is, of course, a lower throughput (by a factor of n/m).

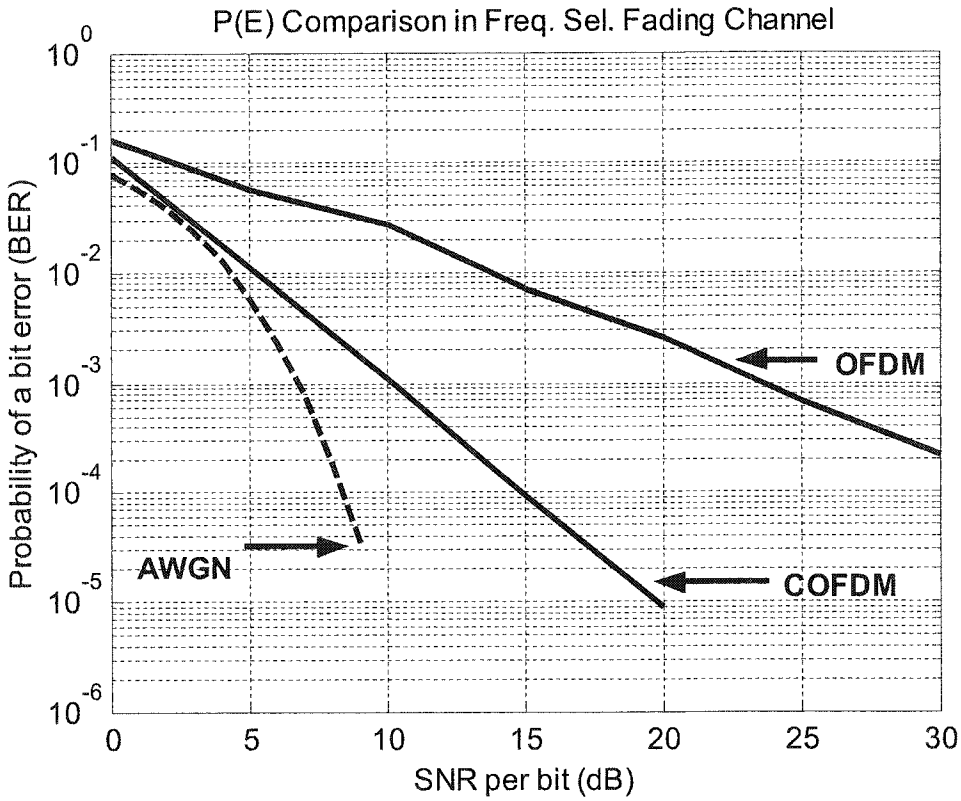

Figure 2.4: Performance of OFDM and COFDM

A further drawback of OFDM, and its method of orthogonal carrier transmission, is high (poor) PAPR (Peak-to-Average Power Ratio) [26]. Specifically, high peaks in power (up to N times the average) result from unstable envelopes, a consequence of using independently modulated carriers. This, in turn, pushes the transmit power amplifier into saturation whenever peaks in transmit power are observed. A number of solutions to OFDM's peak-to-average power ratio (PAPR) problem have been proposed in the literature (i.e., block coding [27], peak cancellation [28-29], partial transmit sequences [30], selective mapping [31], and clipping [32]), but, while reducing the PAPR, these methods typically increase system complexity.

PAPR is defined as the peak transmit power per OFDM block versus the average transmit power in that same block, i.e., mathematically:

$$PAPR = \frac{P_{\max}}{P_{\text{mean}}} = \frac{\max_{0<t<T_s} |s(t)|^2}{\text{mean}_{0<t<T_s} |s(t)|^2} \tag{2.6}$$

The average transmit power in OFDM is:

$$P_{\text{mean}} = NP_o \tag{2.7}$$

where P_o is the per-carrier power, i.e.,

$$\left(P_o = \frac{1}{2} A^2 \right) \tag{2.8}$$

The OFDM method of serial-to-parallel converting incoming information symbols and transmitting each symbol on its own unique carrier leads to the potential for high peak power (i.e., N times the average). This is a result of possible in-phase, coherent addition of all carriers. As the number of carriers (N) increases, so does the peak power's maximum level. In its worst case (WC), where the N carriers combine coherently, OFDM's peak transmit power is equal to:

$$P^{WC}_{(\max),OFDM\,(0<t<T_x)} = \frac{1}{2}\left(\sum_{i=1}^{N} A \right)^2 = \frac{1}{2}(NA)^2 = \frac{1}{2} N^2 A^2 \tag{10}$$

Figure 2.5 shows PAPR levels across 10,000 transmit symbols for OFDM with N = *32* carriers and random input of +1 and -1 (BPSK) symbols. Evident in Figure 2.5, spurious peaks with PAPR > 7.5 are quite common in OFDM transmissions (arising 2.5%

of the time), and peaks of 15 < PAPR < 20 result at select transmission times. On average, OFDM demonstrates a mean PAPR of 3.79 and a variance of 1.5.

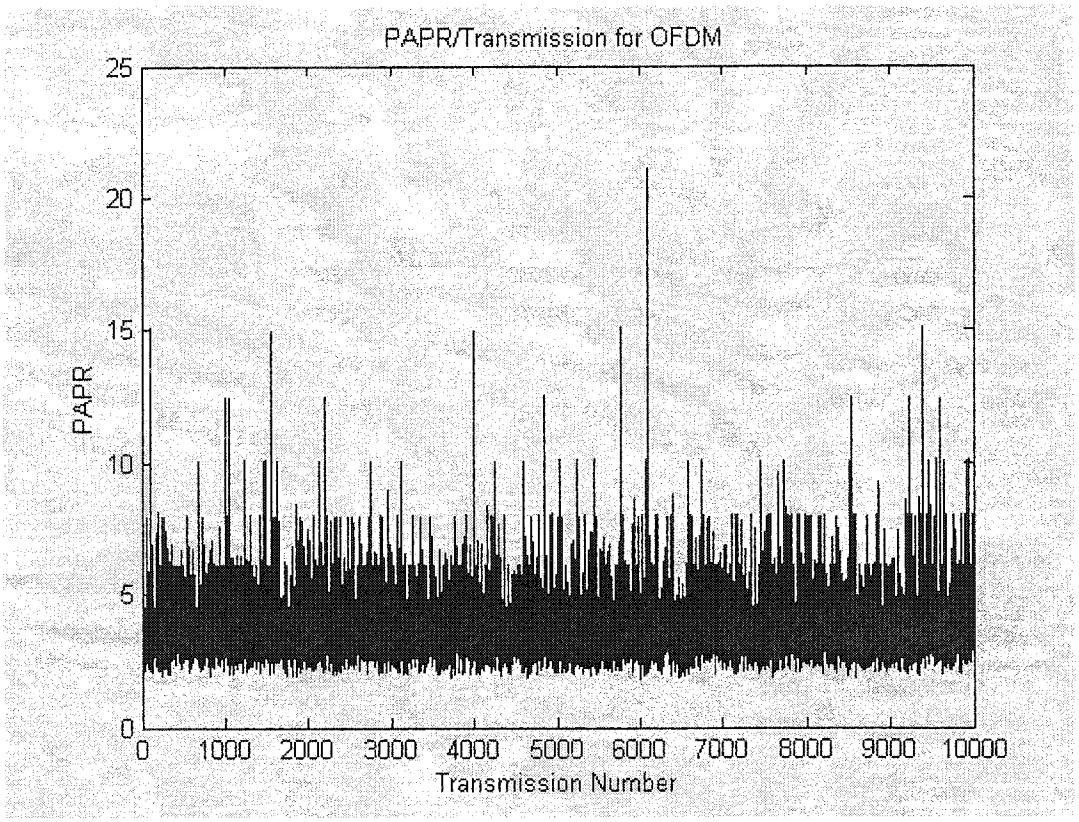

Figure 2.5: PAPR per Transmission of OFDM

Deliberate clipping of the OFDM signal is a low-complexity method for reducing the PAPR (e.g., [58][59]). With the clipping algorithm of [58] and [59] applied to OFDM, similar results are observed. Figure 2.6 displays the PAPR levels across 10,000 transmissions for the resulting 32-symbol (BPSK), 32-carrier clipped OFDM system. Here, a Clipping Ratio (CR) (as defined in [32]) of 1.4 was implemented. It is important to note that the clipping algorithm of [58][59] (implemented here for comparative purposes) is not a hard clipping (whereby any input above a threshold is clipped to the

threshold). Hard clipping creates large out-of-band distortions, and, wanting to avoid this side effect for the purposes of fair comparison, we compare to a 'soft-clipping:' Here, when an output exceeds a predefined threshold, the value is modified by a function which attempts to jointly (1) minimize the PAPR and (2) minimize the out-of-band distortion.

Referring to Figure 2.6, the clipping algorithm greatly reduces the number of times the PAPR exceeds a level of 7.5, but spurious levels are still prevalent. The mean and variance of PAPR with clipping are reduced to 3.2016 and 0.6917 respectively.

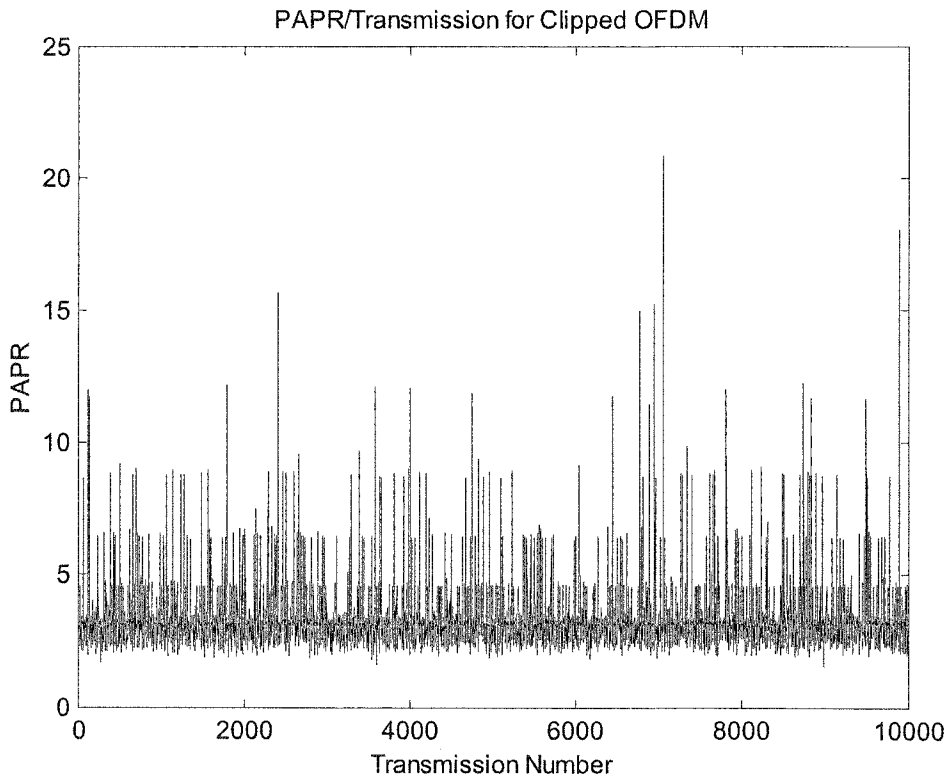

Figure 2.6: PAPR per Transmission of Clipped OFDM

2.5 Conclusions

In this chapter, we have briefly reviewed OFDM, explaining its transmitter structure, receiver structure, and performance. We also discussed the limitations that exist in OFDM, mainly performance issues and concerns surrounding PAPR. In the chapters to follow, we provide innovative methods for improving OFDM.

Part III:

CI/OFDM and PO-CI/OFDM

Chapter 3 OFDM with CI Spreading Codes: Transmission

This chapter introduces a novel OFDM architecture that utilizes Carrier Interferometry (CI) spreading codes to enhance performance (by exploiting frequency diversity) *without* bandwidth expansion or decreased data rate. This architecture also eliminates the high peaks in transmit power common in traditional OFDM, thereby eliminating Peak-to-Average Power Ratio (PAPR) concerns.

The idea underlying CI/OFDM is very similar to that in MC-CDMA systems [19]: In MC-CDMA, N users occupy N carriers simultaneously, but are separated by spreading codes applied across carriers. The spreading codes used in CI/OFDM correspond to those used to create user orthogonality in CI/MC-CDMA [19] [20] [21]. This paper brings the benefits of MC-CDMA spreading to OFDM systems (where spreading is not per user but rather per parallel data stream). (The concept of CI/OFDM is not unlike that of Spread OFDM (SOFDM) [15][16], where each data stream is spread over all the OFDM carriers via Hadamard Walsh codes. However, in SOFDM, spreading codes do little to eliminate PAPR concerns, whereas, in CI/OFDM, spreading codes are carefully selected to alleviate PAPR problems while simultaneously achieving spreading benefits.)

3.1 Introduction to CI Spreading Codes in OFDM Systems

OFDM systems, as discussed in Chapter 2, serial-to-parallel convert the high-rate input symbol stream into N low-rate symbol streams. Next, each low-rate symbol stream is modulated onto its own carrier and sent out over the channel. This OFDM process can be expressed as follows: the spreading code

$$c_k(t) = \sum_{i=0}^{N-1} \beta_k^i e^{j2\pi i \Delta f t} \tag{3.1}$$

is applied to symbol stream k, where

$$\beta_k^k = 1 \text{ and } \beta_k^j = 0 \ (j \neq k) \tag{3.2}$$

and i refers to the carrier. In other words, the code applied to the k^{th} symbol on the k^{th} carrier is 1, whereas the code applied to the k^{th} symbol on the j^{th} carrier ($j \neq k$) is 0, nulling it from all other carriers. Hence, should the k^{th} carrier become lost in a deep fade, the data symbol will be lost.

In this thesis, we apply spreading codes that enable *all* data symbols to be spread onto *all* carriers to exploit the frequency diversity available in the channel. That is, we

apply spreading codes that allow *all* data symbols to occupy *all* carriers at the same time. Specifically, the CI spreading code

$$c_k(t) = \sum_{i=0}^{N-1} \beta_k^i e^{j2\pi i \Delta f t} \tag{3.3}$$

is applied to the low-rate symbol stream k, where

$$\beta_k^i = e^{j\theta_k^i} \tag{3.4}$$

and θ_k^i is carefully selected to allow symbol stream k to be separable from the other symbols co-located on identical carriers.

Moreover, we introduce Pseudo-Orthogonal Carrier Interferometry (PO-CI) spreading sequences for application to OFDM systems. In Pseudo-Orthogonal Carrier Interferometry OFDM (PO-CI/OFDM), each low-rate (parallel) symbol stream is sent simultaneously over all N carriers by application of complex spreading sequences (applied in the frequency domain). By applying pseudo-orthogonal spreading sequences in frequency (over the N OFDM carriers), we support K ($K > N$) symbol streams with only the N carriers. Specifically, in the case of real signaling (e.g., BPSK), we double the number of information symbols (i.e., $K = 2N$) on the original number of carriers (i.e., N), *without* bandwidth expansion, and with minimal loss in performance.

We also demonstrate that Carrier Interferometry OFDM (CI/OFDM) and Pseudo-Orthogonal Carrier Interferometry OFDM (PO-CI/OFDM) eliminate the large peaks in transmit power, and, hence, most PAPR issues, without significant increase in system complexity. Specifically, while the average transmit power in CI/OFDM and PO-CI/OFDM is the same as that in OFDM, the peak values are much lower. This is because the spreading codes applied to the N carriers result in one symbol's power reaching a maximum, when the powers of the remaining symbols are at a minimum. In other words, CI/OFDM and PO-CI/OFDM demonstrate a stable envelope, and, therefore, a PAPR with an average and standard deviation far smaller than that of traditional OFDM.

3.2 Spreading Codes

The CI spreading sequence in the code equation (3), i.e.,

$$\left\{\beta_k^0, \beta_k^1, \ldots, \beta_k^{N-1}\right\} = \left\{e^{j\theta_k^0}, e^{j\theta_k^1}, \ldots, e^{j\theta_k^{N-1}}\right\} \tag{3.5}$$

is applied to symbol stream k to ensure orthogonality between $K = N$ transmitted symbol streams, even though symbol streams occupy the same carriers at the same time. These CI spreading sequences correspond to:

$$\left\{\beta_k^0, \beta_k^1, \ldots, \beta_k^{N-1}\right\} = \left\{e^{j\theta_k^0}, e^{j\theta_k^1}, \ldots, e^{j\theta_k^{N-1}}\right\} = \left\{e^{j\frac{2\pi}{N}\cdot 0\cdot k}, e^{j\frac{2\pi}{N}1\cdot k}, \ldots, e^{j\frac{2\pi}{N}(N-1)\cdot k}\right\} \tag{3.6}$$

One elegant feature of these CI codes, is their flexibility: orthogonal CI sequences can be defined for any length N, and are not limited to the $N = 2^m$ constraint (i.e., N is a power-of-two constraint) of the well-known HW (Hadamard-Walsh) codes. Also, CI codes help with PAPR considerations, as shown in Section 3.4.

To increase throughput in an OFDM system utilizing CI spreading sequences (allowing more than $K = N$ data streams to be sent simultaneously on the N carriers), we also determine a set of pseudo-orthogonal spreading sequences. That is, while the set of spreading sequences defined in equation (3.6) allows us to support $K = N$ symbol streams on N carriers (orthogonally), we seek pseudo-orthogonal spreading sequences that allow us to support $K = 2N$ symbol streams on N carriers. Specifically, we (1) allow the first N symbol streams' spreading sequences to be chosen according to equation (3.6); and (2) to the next set of N symbol streams $\left(k \in \{N, N+1, N+2, \ldots, 2N-1\}\right)$, the following spreading sequences are applied:

$$\left\{\beta_k^0, \beta_k^1, \ldots, \beta_k^{N-1}\right\} = \left\{e^{j\theta_k^0}, e^{j\theta_k^1}, \ldots, e^{j\theta_k^{N-1}}\right\} = \left\{e^{j\frac{2\pi}{N}\cdot 0\cdot k + 0\cdot\Delta\theta}, e^{j\frac{2\pi}{N}\cdot 1\cdot k + 1\cdot\Delta\theta}, \ldots, e^{j\frac{2\pi}{N}(N-1)k + (N-1)\Delta\theta}\right\} \tag{3.7}$$

The second set of N symbol streams has been assigned spreading sequences that allow them to be orthogonal to one another, but pseudo-orthogonal to the first set. Hence, our pseudo-orthogonal code selection is based on the combining of two orthogonal code sets, similar in form to the work of [27] where two sets of orthogonal Hadamard-Walsh codes layered with long codes were successfully combined to create a

new pseudo-orthogonal code set. We select $\Delta\theta$ such that we minimize the amount of inter-code interference between the two sets of orthogonal CI spreading codes. The intuitive solution is to select

$$\Delta\theta = \pi/N \tag{3.8}$$

This creates a second set of spreading sequences equidistant from the original set. In Appendix A, we prove (mathematically) that the selection of $\Delta\theta = \pi/N$ minimizes the average correlation between spreading code sets in the case of real signaling. Hence, the following is used as the second set of spreading codes:

$$\left\{\beta_k^0, \beta_k^1, \ldots, \beta_k^{N-1}\right\} = \left\{e^{j\frac{2\pi}{N}\cdot 0\cdot k + 0\cdot\frac{\pi}{N}}, e^{j\frac{2\pi}{N}\cdot 1\cdot k + 1\cdot\frac{\pi}{N}}, \ldots, e^{j\frac{2\pi}{N}(N-1)k + (N-1)\frac{\pi}{N}}\right\} \tag{3.9}$$

That is, for OFDM systems employing pseudo-orthogonal CI spreading codes, we support $K = 2N$ symbol streams on N carriers, referenced as symbol stream 0 to symbol stream $2N$-1, where each symbol stream is applied to all N carriers by the following spreading sequences:

$$\left\{\beta_k^0, \beta_k^1, \ldots, \beta_k^{N-1}\right\} = \left\{e^{j\frac{2\pi}{N}\cdot 0\cdot k + 0\cdot\Delta\theta_k}, e^{j\frac{2\pi}{N}\cdot 1\cdot k + 1\cdot\Delta\theta_k}, \ldots, e^{j\frac{2\pi}{N}(N-1)k + (N-1)\Delta\theta_k}\right\} \tag{3.10}$$

and

$$\Delta\theta_k = \begin{cases} 0, & k = 0,1,\ldots,N-1 \\ \dfrac{\pi}{N}, & k = N, N+1,\ldots,2N-1 \end{cases} \tag{3.11}$$

By applying these spreading sequences, we can support twice as many real symbol streams as traditional OFDM ($K = 2N$ vs. $K = N$), and, hence, support a doubling in throughput. Moreover, in OFDM with PO-CI codes, each symbol stream is spread onto all carriers (whereas in OFDM each stream remains on one carrier), leading to frequency diversity benefits.

3.3 OFDM with CI Spreading Codes: Transmit Signaling

The typical OFDM transmitter of Section 2.1 is shown in Figure 3.1(a), and the CI/OFDM transmitter (employing CI spreading codes) is depicted in Figures 3.1(b) and 3.1(c). In both OFDM and CI/OFDM, a high-rate input symbol stream is serial-to-parallel converted. However, unlike OFDM, where each symbol is modulated onto its own carrier, in CI/OFDM *each* symbol is modulated onto *all* the N carriers. To separate symbols located on identical carriers, we apply the unique spreading sequences of equation 3.6 across symbol k's carriers. Specifically, the spreading sequence applied to symbol k's carriers correspond to the set $\left\{e^{j\theta_k^0}, e^{j\theta_k^1}, \ldots, e^{j\theta_k^{N-1}}\right\}$, where $\theta_k^i = \left(\frac{2\pi}{N}\right) \cdot k \cdot i$, and is referred to as a CI (Carrier Interferometry) spreading code (Figure 3.1(c)).

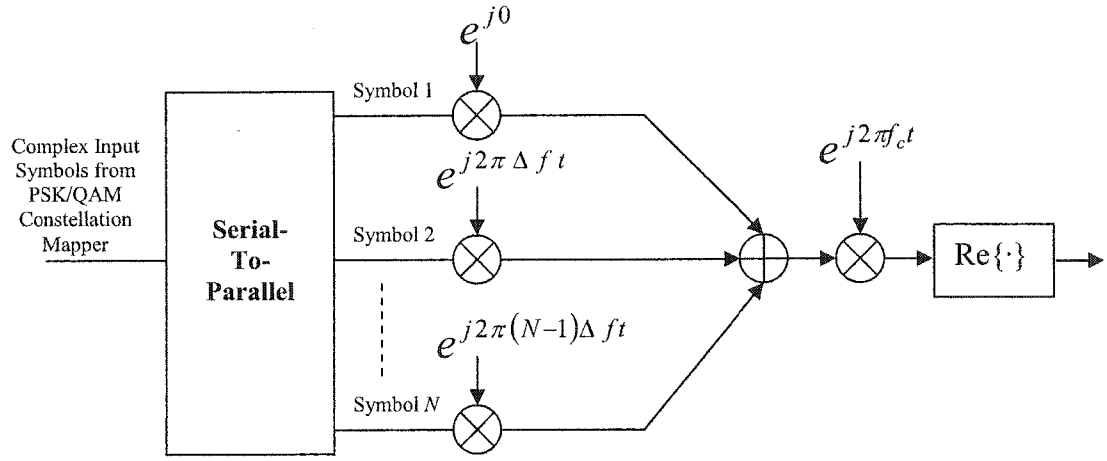

(a) OFDM

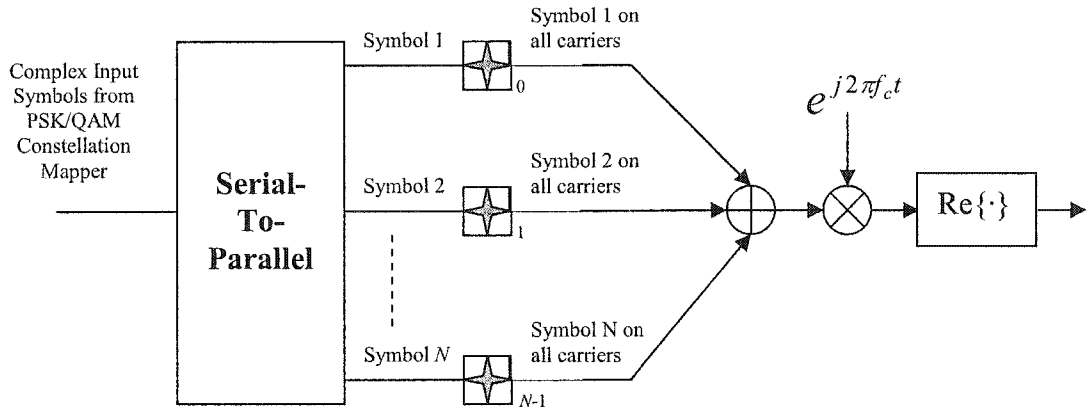

(b) CI/OFDM

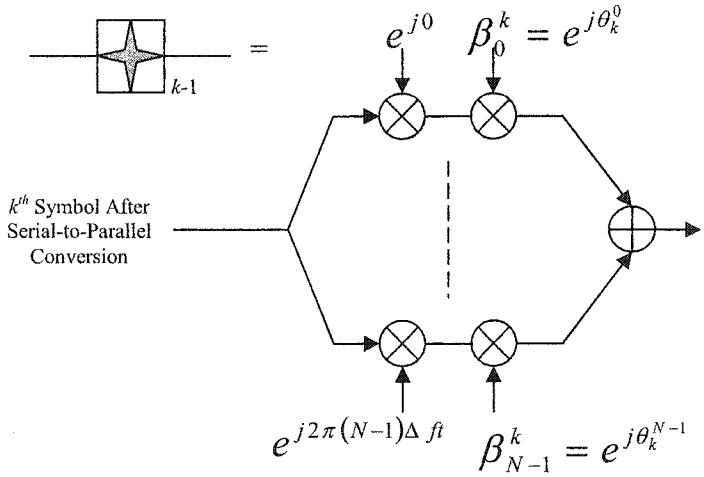

(c)

Figure 3.1: (a) General OFDM transmitter, (b) CI/OFDM transmitter, (c) Expansion of symbol k spreading to the N carriers from part (b)

The transmitted signal for the k^{th} symbol in a CI/OFDM system is thus:

$$s_k(t) = A \cdot \mathrm{Re}\left\{ \sum_{i=0}^{N-1} a_k^n e^{j\left(2\pi f_c t + 2\pi f_i t + \frac{2\pi}{N} k \cdot i\right)} \right\} \tag{3.12}$$

where (1) a_k^n is the n^{th} symbol in the k^{th} symbol stream and is assumed (in this chapter) to be +1 or −1 with equal probability (corresponding to the commonly used BPSK constellation, and ensuring real signaling); (2) $f_i = i\Delta f$, and $\Delta f = 1/T_s$ (T_s is the symbol rate) to assure orthogonality among carriers; (3) $\left(\frac{2\pi}{N}\right) \cdot k \cdot i$ is the phase offset used to generate symbol k's spreading code, and ensures orthogonality among the N symbols; and (4) A is a parameter used to establish the symbol energy. Now, over the entire block of N parallel symbols, the transmitted signal in CI/OFDM is:

$$s(t) = A \cdot \sum_{k=0}^{N-1} \sum_{i=0}^{N-1} a_k^n \cos\left(2\pi f_c t + 2\pi f_i t + \frac{2\pi}{N} \cdot k \cdot i\right) \tag{3.13}$$

It is important to note that BPSK is assumed for ease in presentation, and it is understood that this is a low-bandwidth-efficiency example. Improved bandwidth efficiencies are observed with higher order PSK and QAM constellations. CI spreading codes apply equally well to these scenarios, as seen in future chapters.

3.4 CI/OFDM Transmit Signal's PAPR

CI/OFDM's transmit signal dramatically improves PAPR. As discussed in Section 2.4, PAPR is defined as the peak transmit power per OFDM block versus the average transmit power in that same block, i.e., mathematically:

$$PAPR = \frac{P_{\max}}{P_{\text{mean}}} = \frac{\max_{0<t<T_s} |s(t)|^2}{\text{mean}_{0<t<T_s} |s(t)|^2} \tag{3.14}$$

The average transmit power in CI/OFDM and OFDM is:

$$P_{\text{mean}} = NP_o \tag{3.15}$$

where P_o is the per-carrier power, i.e.,

$$\left(P_o = \frac{1}{2} A^2 \right) \tag{3.16}$$

The OFDM method of serial-to-parallel converting incoming information symbols and transmitting each symbol on its own unique carrier leads to the potential for high peak power (i.e., N times the average). This is a result of possible in-phase, coherent addition of all carriers. As the number of carriers (N) increases, so does the peak power's maximum level. In its worst case (WC), where the N carriers combine coherently, OFDM's peak transmit power is equal to:

$$P^{WC}_{(\max),OFDM\,(0<t<T_s)} = \frac{1}{2}\left(\sum_{i=1}^{N} A\right)^2 = \frac{1}{2}(NA)^2 = \frac{1}{2}N^2A^2 \tag{3.17}$$

In CI/OFDM, as discussed in Section 3.2, all symbols are transmitted simultaneously over all carriers, and an appropriate spreading sequence (applied across carriers) makes symbols separable at the receiver. These carefully-selected spreading sequences also reduce peak transmit powers. Specifically, they ensure that when one symbol's carriers add coherently, other symbol's carriers do not add coherently. The maximum or peak transmit power from equation (2) is much less than the summation of maximum carrier powers in (3.17), because when $s_k(t)$ reaches its maximum (see Equation (3.12)), $s_j(t)$ (where $(j \neq k)$) is at a minimum.

This can be seen in Figures 3.2(a)-(c). Figure 3.2(a) represents the envelope of the first transmit data symbol after spreading over all carriers with CI codes (assuming N = 8); Figure 3.2(b) represents the envelope of the second transmit symbol after spreading; and Figure 3.2(c) overlays all the envelopes of all N = 8 data symbols (after spreading over the N = 8 carriers) in the time domain. The envelope of the composite signal (conceptually) is the linear combination of these N waveforms – a signal with a low PAPR.

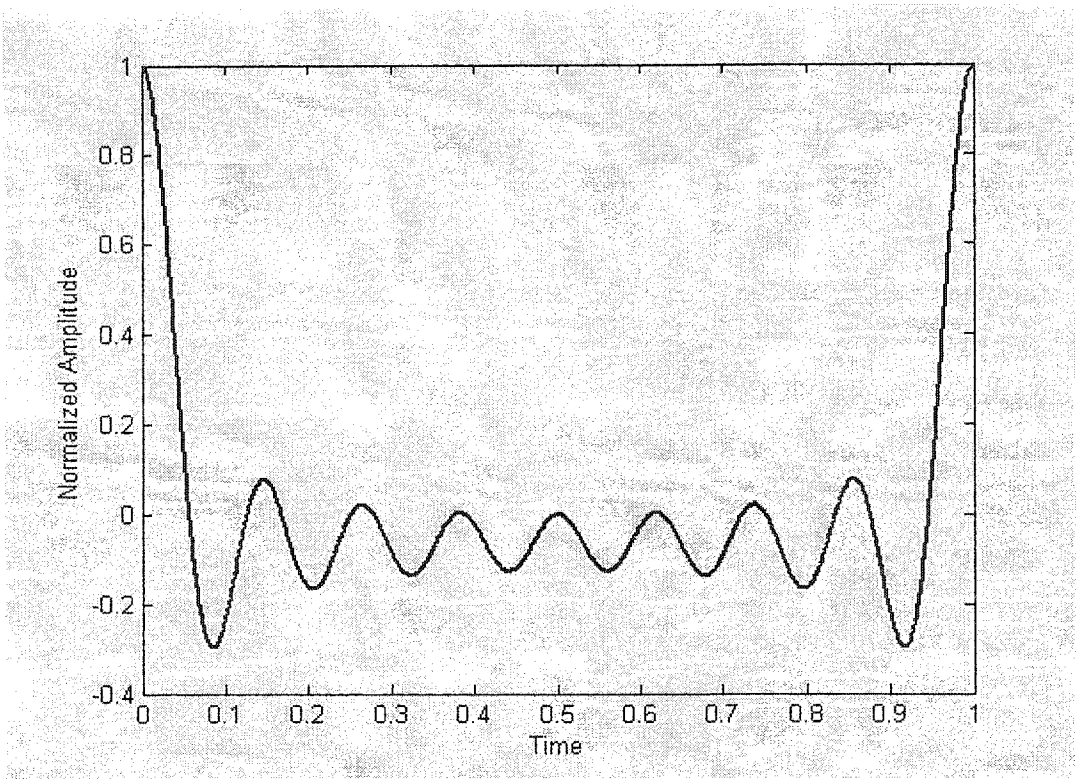

(a)

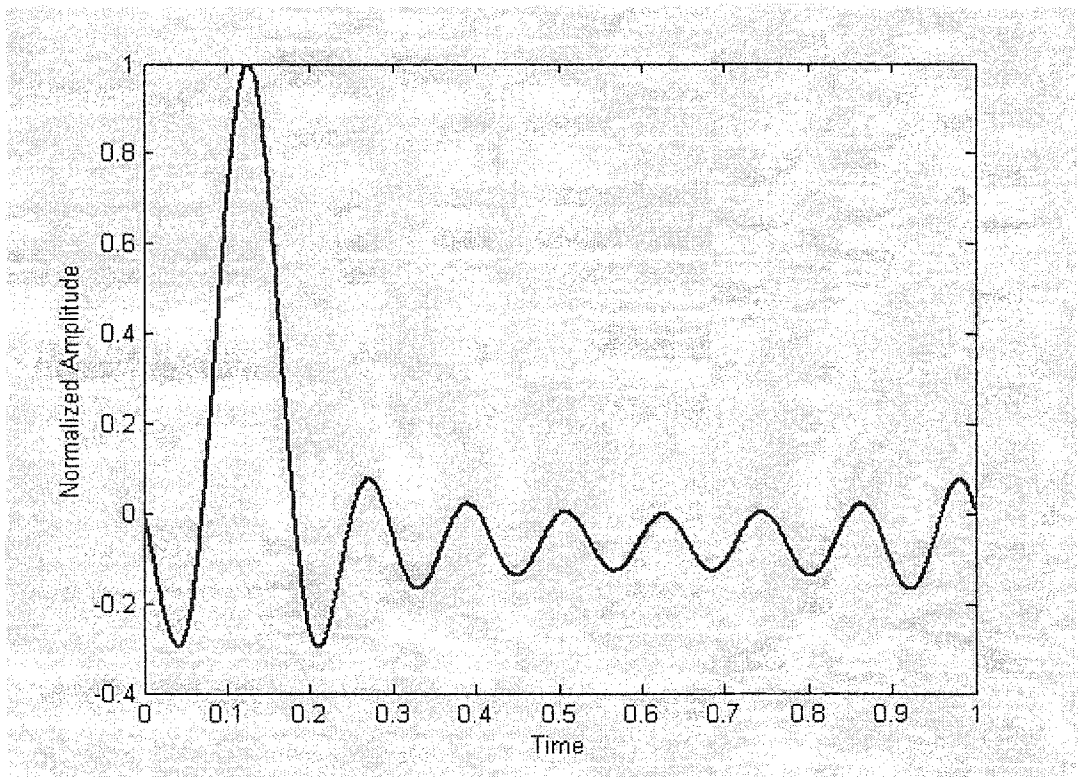

(b)

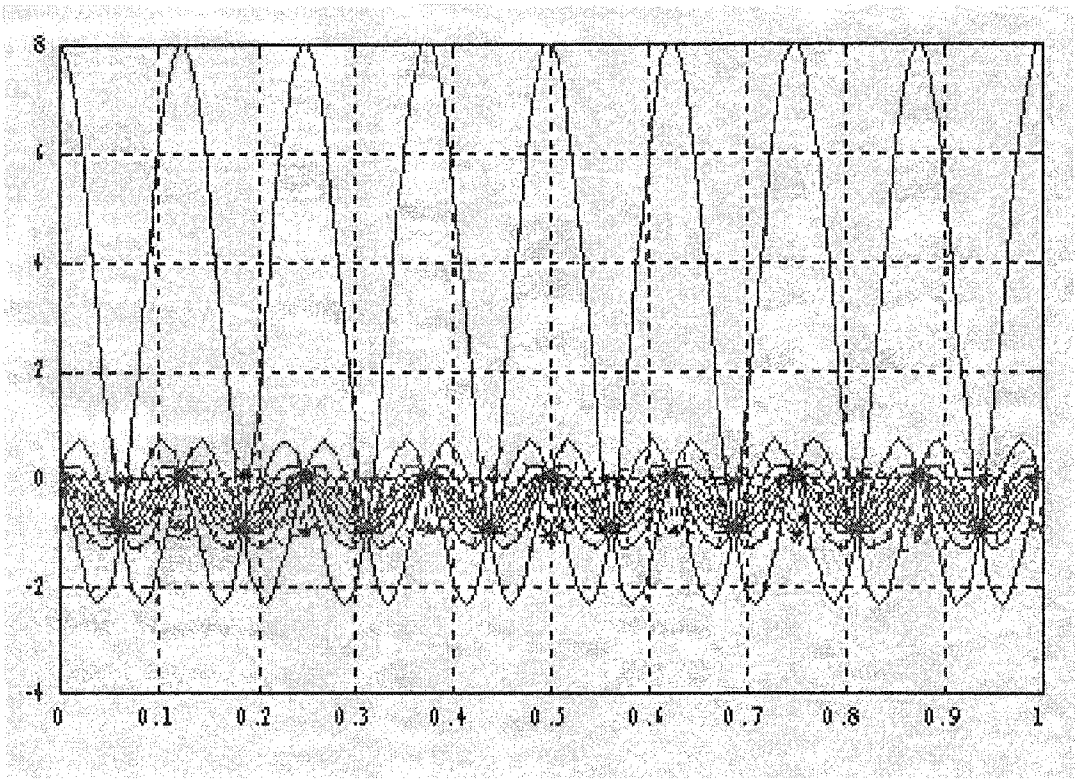

(c)

Figure 3.2: Transmit envelopes signal of CI/OFDM signals:
(a) Symbol 1, (b) Symbol 2, and (c) all N symbols

Figure 3.3 shows PAPR levels across 10,000 transmit symbols for both OFDM (Figure 3.3(a)) and CI/OFDM (Figure 3.3(b)), each with $N = 32$ carriers and BPSK data symbols. Evident in Figure 3.3, spurious peaks with PAPR > 7.5 are quite common in OFDM transmissions (arising 2.5% of the time), and peaks of 15 < PAPR < 20 result at select transmission times. CI/OFDM, on the other hand, displays *no* peaks with PAPR >

6.5, and displays PAPR < 5 at almost all times. On average, OFDM demonstrates an average PAPR of 3.79 while CI/OFDM's average PAPR is 3.41.

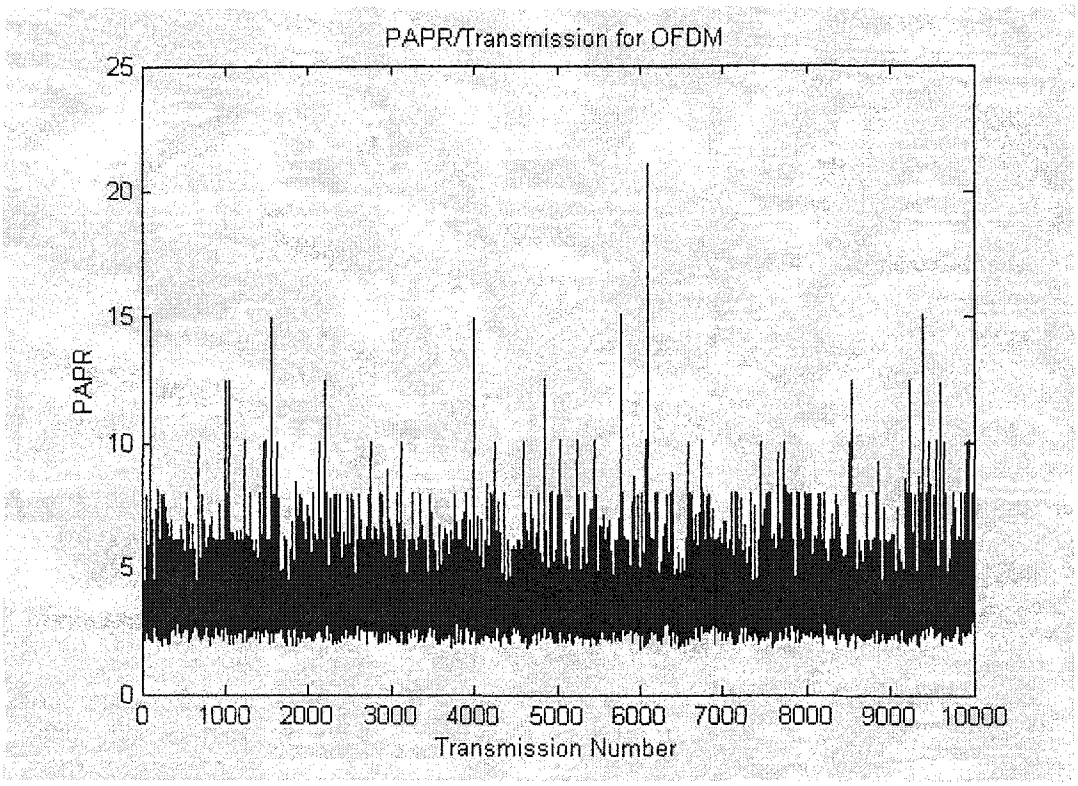

(a) PAPR per Transmitted OFDM Symbol

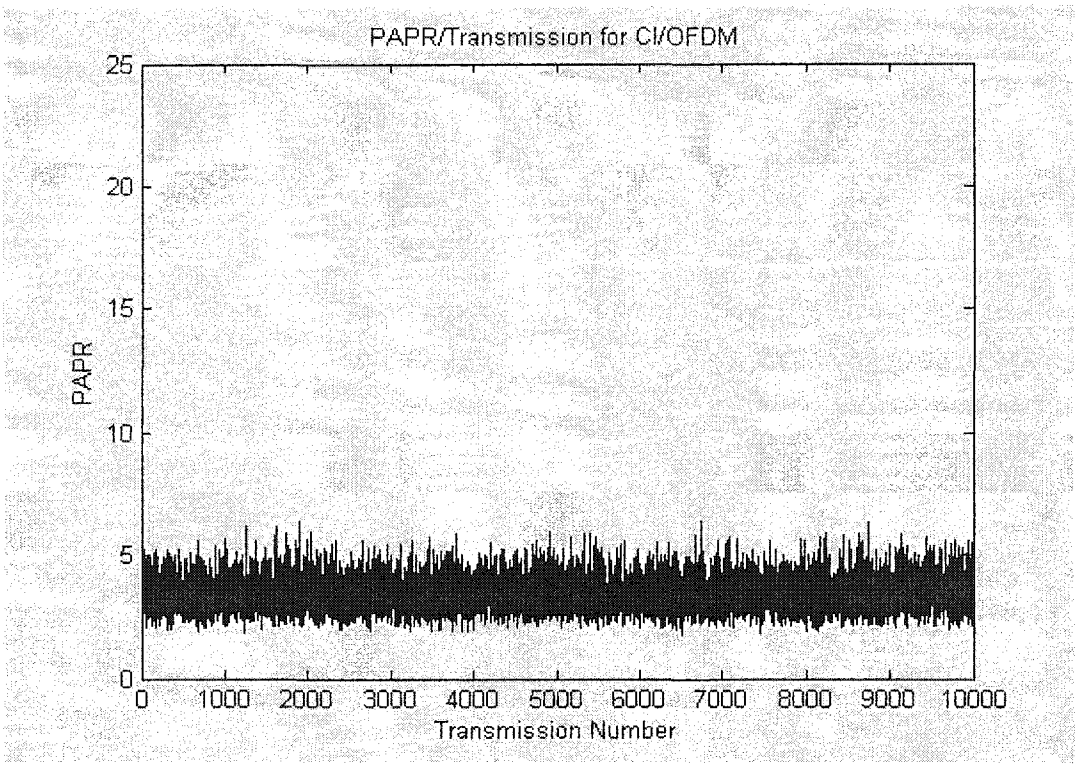

(b) PAPR per Transmitted CI/OFDM Symbol

Figure 3.3: PAPR per Transmission (a) OFDM and (b) CI/OFDM

Figure 3.4 demonstrates the standard deviation of the PAPR as a function of increasing number of carriers. For $N = 32$ carriers, OFDM's PAPR demonstrates a standard deviation of 1.23 (a variance of 1.5), while CI/OFDM's standard deviation is only 0.665 (a variance of 0.442).

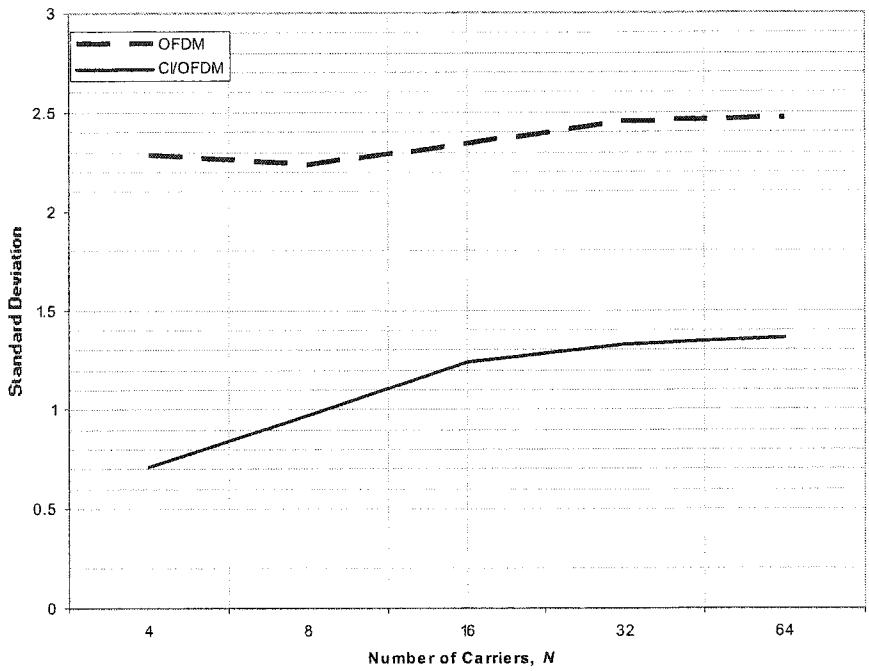

Figure 3.4: PAPR standard deviation for OFDM vs. CI/OFDM

Figures 3.5(a)-(c) plot the pdf (probability density function) of the PAPR (determined empirically over one million OFDM symbols). As it can be seen in Figure 3.5(a), the PAPR of traditional OFDM is spread over a large number of values, and is not well concentrated about the mean. Figure 3.5(b) shows clipping effectively concentrates the PAPR levels about the mean, but does little to contain the spurious peaks. This can be directly attributed to the in-band distortion caused by clipping. Finally, it can be seen from Figure 3.5(c) that CI/OFDM's PAPR remains close to the mean value.

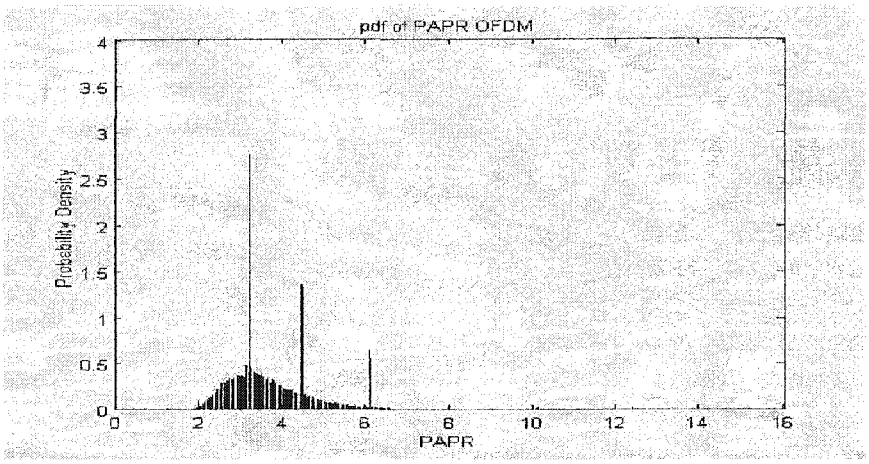

(a)

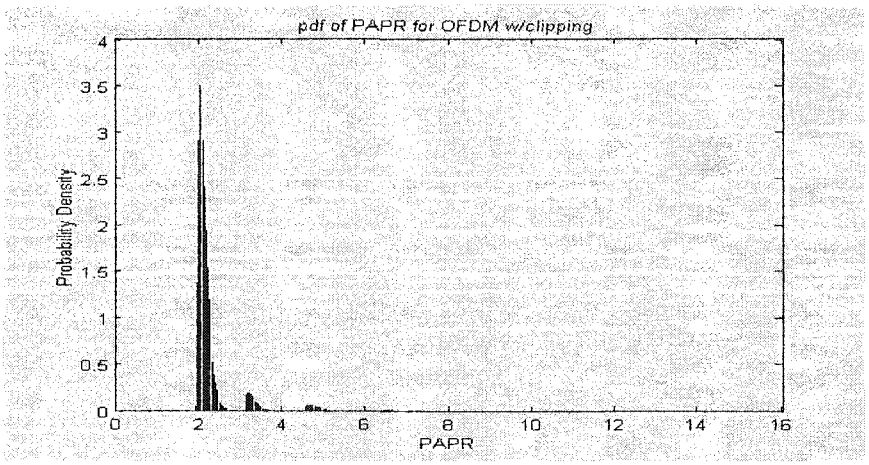

(b)

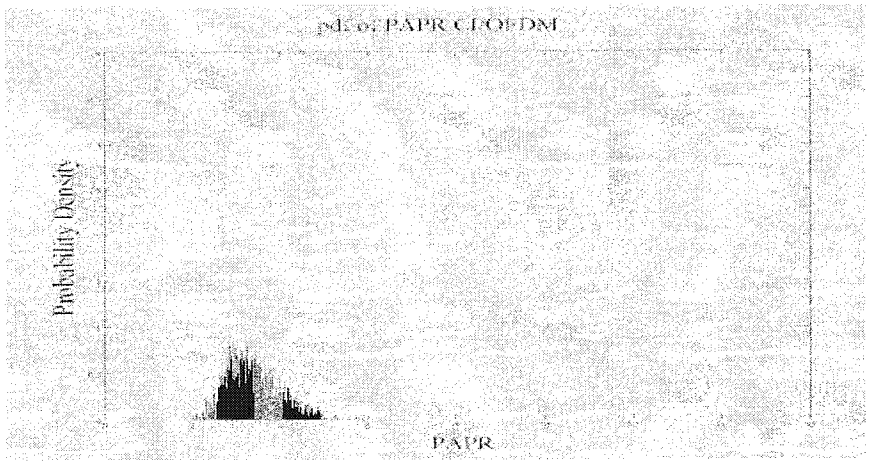

(c)

Figure 3.5: pdf of PAPR for (a) OFDM, (b) OFDM with clipping, and (c) CI/OFDM

Now, referring to Figure 3.6, 98% of the CI/OFDM transmissions demonstrate PAPR < 5, and all transmissions (100%) demonstrate PAPR < 6.5. Meanwhile, only 88% of the OFDM transmissions demonstrate PAPR < 5, and it is not until y = 32 that Pr(PAPR < y) = 100%. Clearly, the excellent PAPR characteristics of CI/OFDM allow transmit amplifiers to operate with greater power efficiency, since large peaks do not exist, and as such there is no risk of non-linear operation or out-of-band spectral growth.

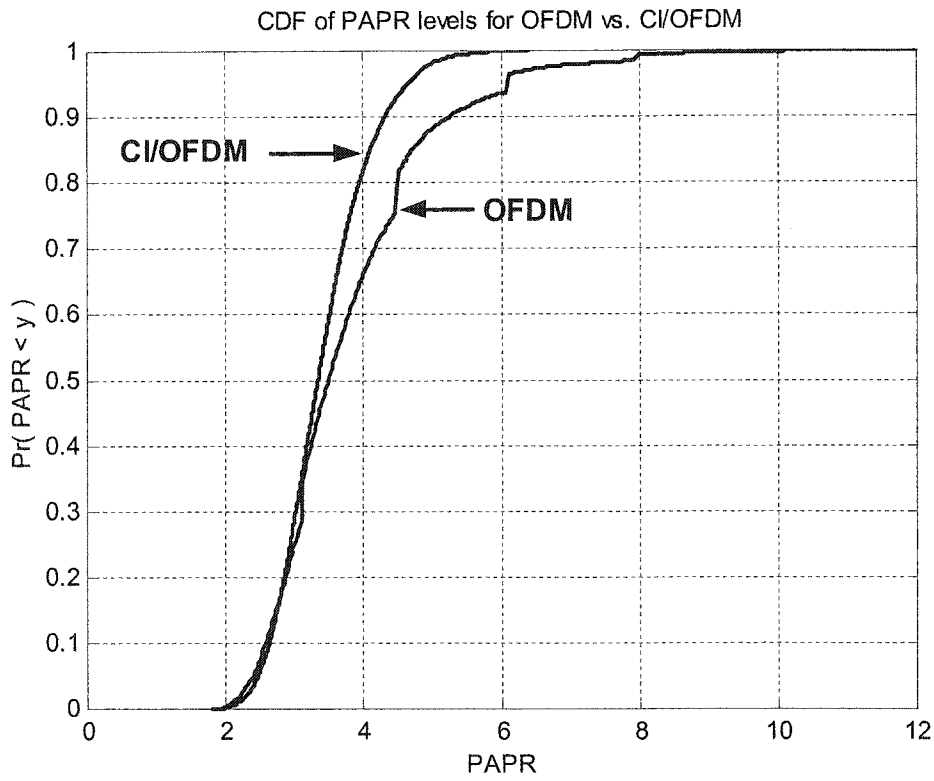

Figure 3.6: Cummulative Distribution Function for PAPR for OFDM and CI/OFDM ($N = 32$ carriers)

3.5 OFDM with Pseudo-Orthogonal CI Spreading Codes: Transmit Signaling

Similar to both OFDM and CI/OFDM of Figures 3.1(a) – 3.1(c), PO-CI/OFDM serial-to-parallel converts the high-rate input symbol stream. Next, in PO-CI/OFDM, *each* low-rate symbol stream is spread onto *all* of the N carriers, as in Figure 3.1(b) and

3.1(c). Specifically, the PO-CI spreading code $c_k(t) = \sum_{i=0}^{N-1} \beta_k^i e^{j2\pi i\Delta f t}$ is applied to symbol stream k, where $\beta_k^i = e^{j\theta_k^i}$, and θ_k^i is carefully selected as seen in equations (3.9) - (3.11).

By applying all $2N$ PO-CI spreading sequences, PO-CI/OFDM supports twice as many real symbol streams as traditional OFDM ($K = 2N$ vs. $K = N$), and, hence, PO-CI/OFDM supports a doubling in throughput.

The transmitted signal for the k^{th} symbol stream in PO-CI/OFDM is:

$$s_k(t) = A \cdot \mathrm{Re}\left\{ a_k^n c_k(t) e^{j2\pi f_c t} \right\} \tag{3.18}$$

$$s_k(t) = A \cdot \mathrm{Re}\left\{ a_k^n \sum_{i=0}^{N-1} e^{j\vartheta_k^i} e^{j2\pi i\Delta f t} e^{j2\pi f_c t} \right\} \tag{3.19}$$

$$s_k(t) = A \cdot \sum_{i=0}^{N-1} a_k^n \cos\left(2\pi f_c t + 2\pi f_i t + \frac{2\pi}{N} i \cdot k + i \cdot \Delta\theta_k \right) \tag{3.20}$$

where: (1) a_k^n is the n^{th} symbol in the k^{th} symbol stream and is assumed (in this chapter) to be +1 or −1 with equal probability (corresponding to the commonly used BPSK constellation, and ensuring real signaling); (2) $f_i = i\Delta f$, and $\Delta f = 1/T_S$ (T_S is the symbol rate after serial-to-parallel conversion) to assure orthogonality among carriers; (3) $\theta_k^i = \frac{2\pi}{N} i \cdot k + i \cdot \Delta\theta_k$ (where $\Delta\theta_k = 0$ for $k < N$, and $\Delta\theta_k = \frac{\pi}{N}$ otherwise) is the phase offset (associated with the i^{th} element of the spreading sequence) used to ensure

separability between symbol k and the (K-1) other symbols; and (4) A is a parameter used to establish the symbol energy. The PO-CI/OFDM transmitted signal, considering the $2N$ parallel symbol streams, is thus:

$$s(t) = \sum_{k=0}^{2N-1} s_k(t) \tag{3.21}$$

$$s(t) = A \cdot \sum_{k=0}^{2N-1} \sum_{i=0}^{N-1} a_k^n \cos\left(2\pi f_c t + 2\pi f_i t + \frac{2\pi}{N} i \cdot k + i \cdot \Delta\theta_k \right) \tag{3.22}$$

3.6 PO-CI/OFDM's Transmit Signal PAPR Benefit

In this section, we characterize the PAPR benefits of the proposed PO-CI/OFDM system. Consistent with the assumption throughout this chapter, we assume BPSK modulation in the discussion that follows (although PAPR benefits extend regardless of constellation as will be shown in Chapter 5). The PAPR equations (as defined in Section 2.4 and 3.4) are:

$$PAPR = \frac{P_{\max}}{P_{\text{mean}}} = \frac{\max_{0<t<T_s} |s(t)|^2}{\text{mean}_{0<t<T_s} |s(t)|^2} \tag{3.23}$$

The average power of both PO-CI/OFDM and OFDM is:

$$P_{\text{mean}} = NP_o \tag{3.24}$$

where P_o is the power of one carrier, i.e., assuming PSK modulation,

$$\left(P_o = \frac{1}{2}A^2\right) \tag{3.18}$$

In PO-CI/OFDM, as discussed in Section 3.5, *each* symbol is transmitted simultaneously over *all* carriers, and an appropriate spreading sequence makes symbols separable at the receiver. However, our selection of spreading sequences has a second benefit: it reduces peak power. Specifically, the spreading sequence selected $\left(i.e., \left\{\beta_k^0, \beta_k^1, \ldots, \beta_k^{N-1}\right\} = \left\{e^{j\frac{2\pi}{N}0\cdot k+0\cdot\Delta\theta_k}, e^{j\frac{2\pi}{N}1\cdot k+1\cdot\Delta\theta_k}, \ldots, e^{j\frac{2\pi}{N}(N-1)k+(N-1)\Delta\theta_k}\right\}\right)$ ensures that when one symbol's carriers add coherently, other symbol's carriers do not add coherently. This can be seen in Figures 3.7(a)-(c). Figure 3.7(a) represents the envelope of the first transmit data symbol after spreading over all carriers with CI codes (assuming N = 8); Figure 3.7(b) represents the envelope of the second transmit symbol after spreading; and Figure 3.7(c) overlays all the envelopes of all $2N$ = 16 data symbols (after spreading over the N = 8 carriers) in the time domain. The envelope of the composite signal (conceptually) is the linear combination of these $2N$ waveforms – a signal with a low PAPR.

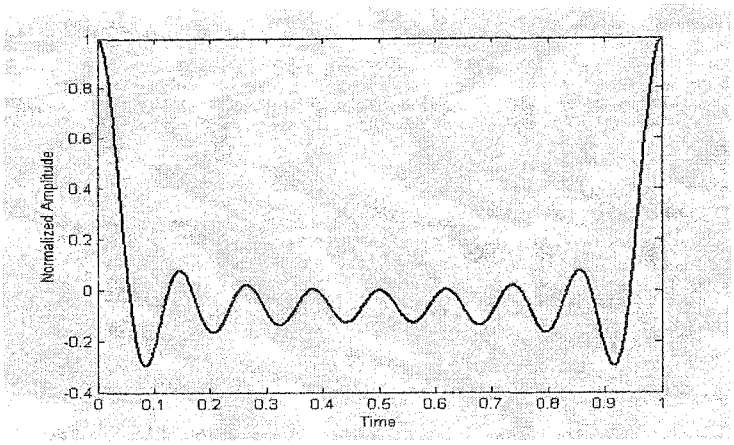

(a)

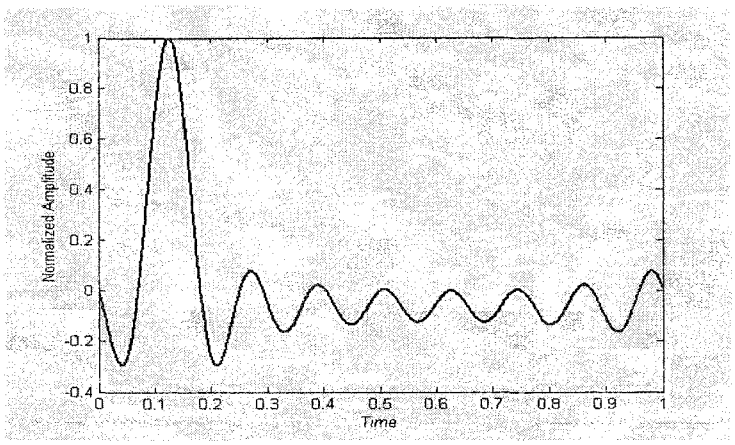

(b)

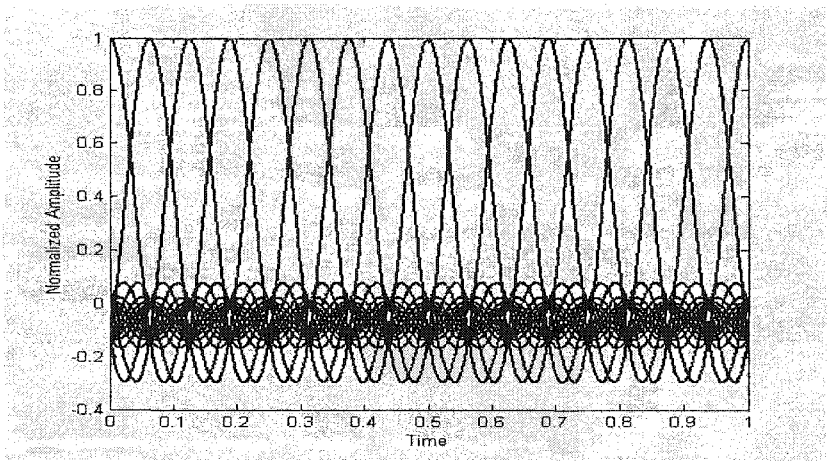

(c)

Figure 3.7: Transmit envelopes signal of PO-CI/OFDM signals: (a) Symbol 1, (b) Symbol 2, and (c) all *2N* symbols

Specifically, we observe from Figures 3.7(a)-(c) that when $S_k(t)$ reaches its maximum, $S_j(t)$ (where $(j \neq k)$) is at a minimum or a very low value (i.e., $P_j << P_o$). Hence, constructive combining of all N symbol energies at any one moment in time is not possible, because peaks in symbol energies are evenly spread over the OFDM symbol time (Figure 3.7). As a result, an excellent PAPR per PO-CI/OFDM symbol is observed. To confirm the anticipated PAPR for PO-CI/OFDM systems, the authors first conducted an exhaustive search over all possible symbols to determine the worst-case PAPR. While the exhaustive search is prohibitively large for large values of N, we were able to conduct these searches for N = 2, 4, and 8. The results are tabulated in Table 1, which demonstrate (1) the worst case PAPR values for PO-CI/OFDM are far smaller than that in a traditional OFDM system, and (2) the PO-CI/OFDM PAPR benefit relative to traditional OFDM (on a worst case basis) grows as a function of increasing N.

Number of Carriers (N)	OFDM Worst Case PAPR	PO-CI/OFDM Worst Case PAPR
2	2	1
4	4	1.2636
8	8	1.7275

Table 3.1: Exhaustive search, worst case PAPR values for OFDM vs. PO-CI/OFDM

Next, we present our empirical study characterizing the PAPR benefits via pdfs and cdfs assuming N = 32 carriers. Figure 3.8 illustrates PAPR levels across 1,000,000 transmissions for 32-symbol, 32-carrier OFDM (Figure 3.8(a)) and 64-symbol, 32-carrier PO-CI/OFDM (Figure 3.8(b)).

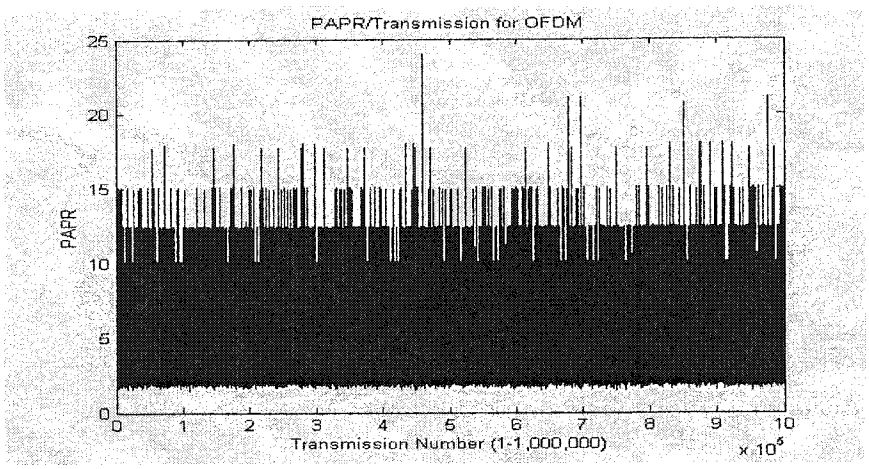

(a)

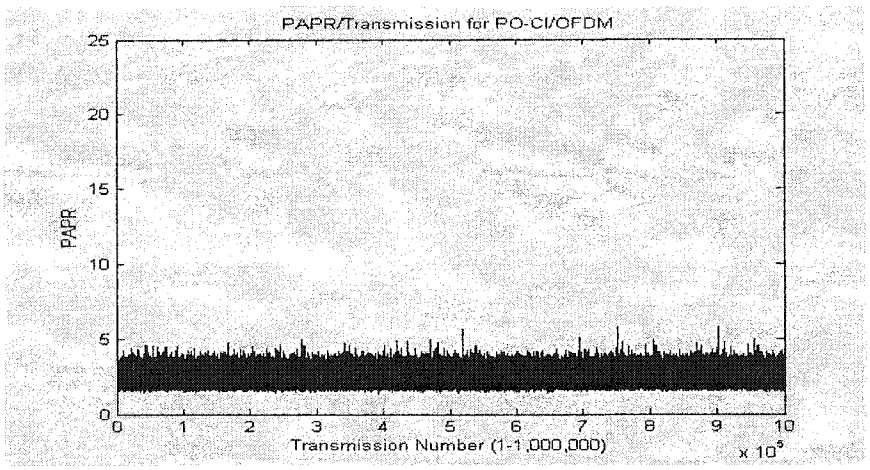

(b)

Figure 3.8: PAPR per Transmission for (a) OFDM and (b) PO-CI/OFDM

Referring to Figure 3.8, OFDM's PAPR can be characterized as erratic, displaying a mean PAPR of 3.8080, and consistently reaching levels exceeding 6 (5% of the time), with some PAPR values exceeding 20 and even 25. PO-CI/OFDM, on the other hand, displays no PAPR value above 5.82 and stays close to its mean PAPR level of 2.4546.

Figure 3.9 demonstrates the standard deviation of the PAPR as a function of increasing number of carriers per OFDM symbol (i.e., increasing N). As the number of carriers increases, the standard deviation of OFDM's PAPR also increases, but the opposite is true in PO-CI/OFDM: in PO-CI/OFDM, the standard deviation of the PAPR decreases with increasing number of carriers. For the 32-symbol, 32-carrier OFDM and 64-symbol, 32-carrier PO-CI/OFDM systems shown in Figure 3.8, OFDM's PAPR demonstrates a standard deviation of 1.23 (a variance of 1.5), while PO-CI/OFDM's standard deviation is only 0.355 (a variance of 0.125).

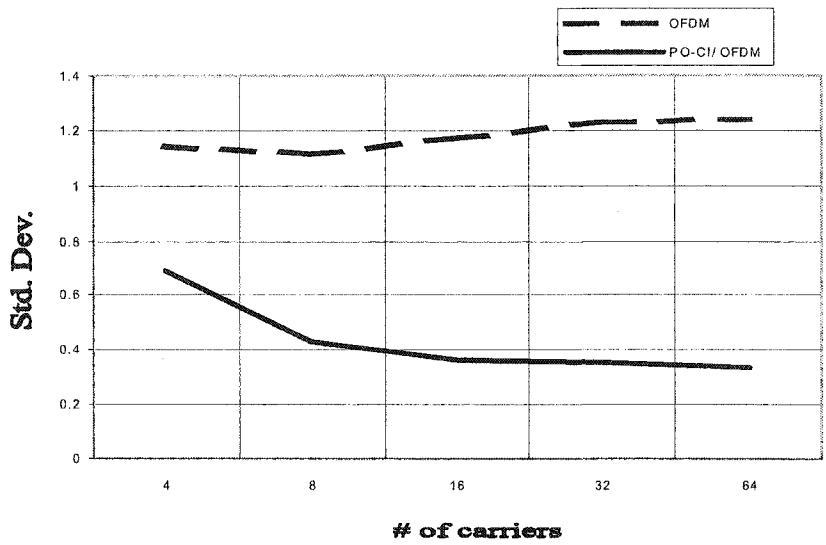

Figure 3.9: PAPR standard deviation for OFDM vs. PO-CI/OFDM

When compared to an OFDM system that has a clipping algorithm applied (i.e., [30][31]), similar results are observed. Figure 3.10(a) displays the PAPR levels across 1,000,000 transmissions for a 32-symbol, 32-carrier OFDM system with clipping, and

Figure 3.10(b) displays the 64-symbol, 32-carrier PO-CI/OFDM system. Here, a Clipping Ratio (CR) (as defined in [14]) of 1.4 was implemented. It is important to note that the clipping algorithm of [30][31] (implemented here for comparative purposes) is not a hard clipping (whereby any input above a threshold is clipped to the threshold). Hard clipping creates large out-of-band distortions, and, wanting to avoid this side effect for the purposes of fair comparison, we compare to a 'soft-clipping:' Here, when an output exceeds a predefined threshold, the value is modified by a function which attempts to jointly (1) minimize the PAPR and (2) minimize the out-of-band distortion.

Although hard to see with the 1,000,000 samples of Figure 3.10(a), the clipping algorithm greatly reduces the number of times the PAPR exceeds a level of 5, but spurious levels are still prevalent. The mean and standard deviation of PAPR with clipping are reduced to 2.3971 and 0.9733 respectively. Still, as evident from the figure, PO-CI/OFDM's PAPR is far better than that of clipped OFDM.

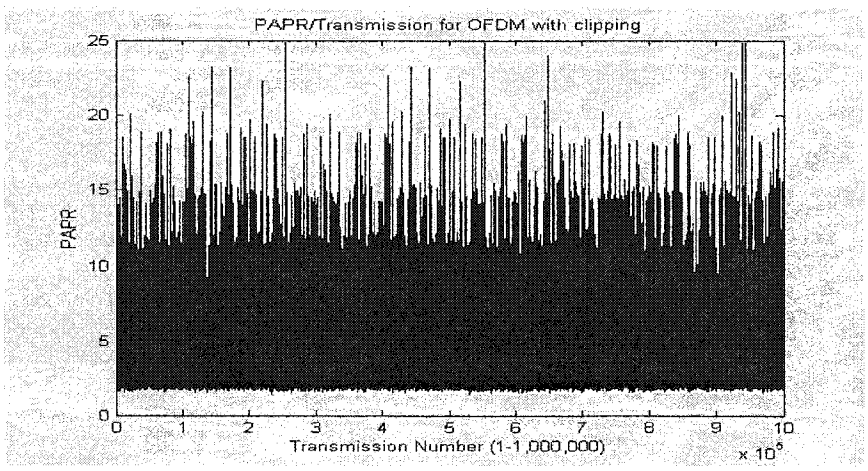

(a)

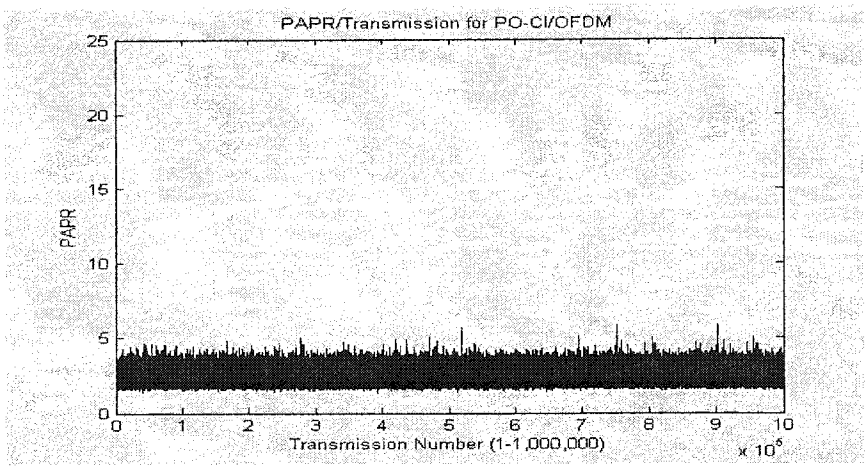

(b)

Figure 3.10: PAPR per Transmission (a) OFDM w/clippping, and (b) PO-CI/OFDM

Figures 3.11(a)-(c) plot the pdf (probability density function) of the PAPR (determined empirically over one million OFDM symbols). As it can be seen in Figure 3.11(a), the PAPR of traditional OFDM is spread over a large number of values, and is not well concentrated about the mean. Figure 3.11(b) shows clipping effectively concentrates the PAPR levels about the mean, but does little to contain the spurious peaks. This can be directly attributed to the in-band distortion caused by clipping. Finally, it can be seen from Figure 3.11(c) that PO-CI/OFDM's PAPR remains close to the mean value.

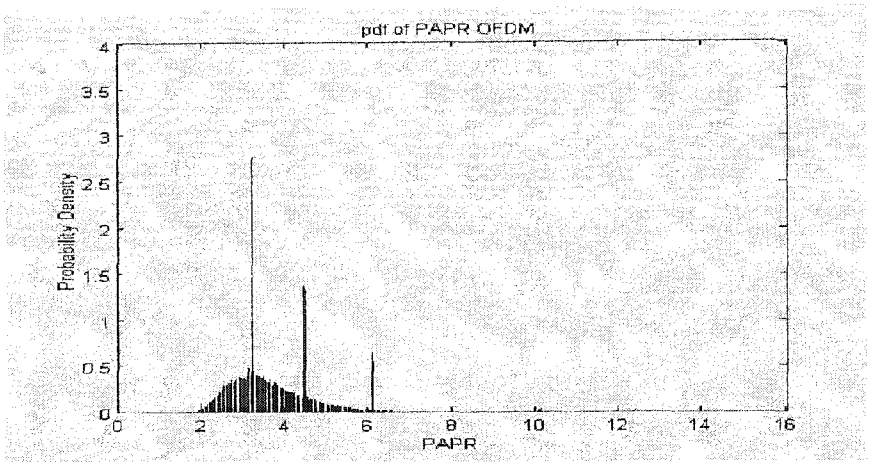

(a)

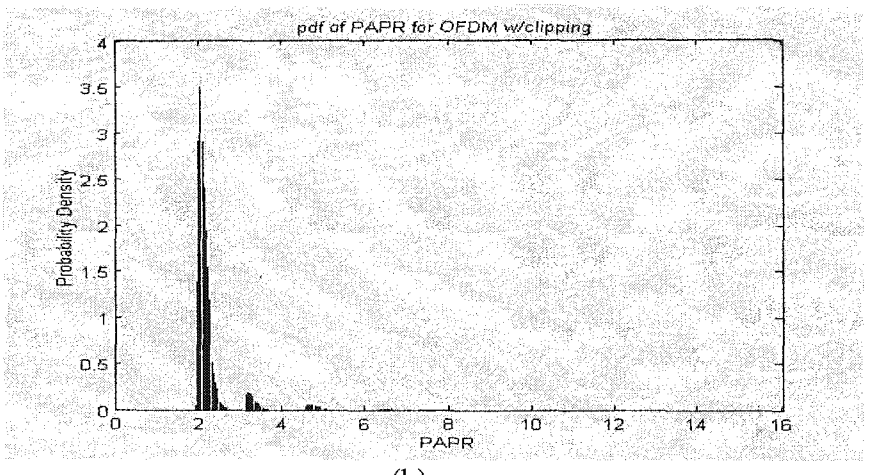

(b)

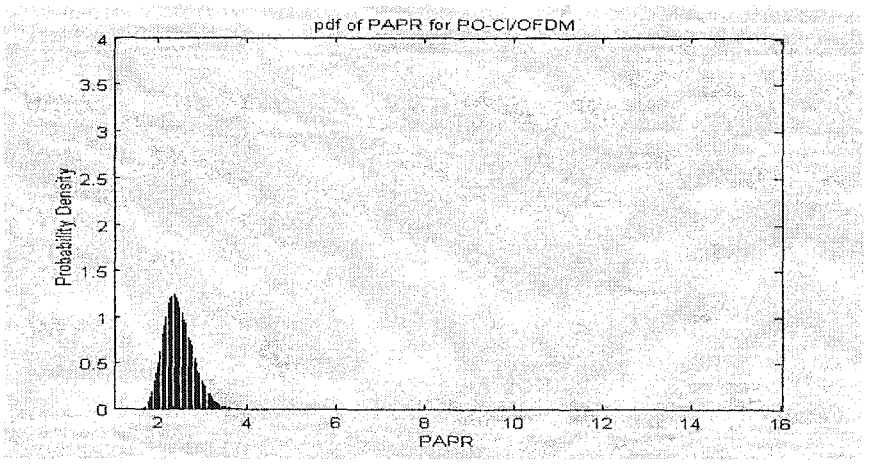

(c)

Figure 3.11: pdf of PAPR for (a) OFDM, (b) OFDM with clipping, and (c) PO-CI/OFDM

Figure 3.12 illustrates the cumulative distribution function (CDF) of the PAPR, again determined empirically over one million OFDM symbols. As seen in Figure 3.12, clipping improves the PAPR statistics of OFDM (mean 2.412 and standard deviation 1.053), but it is not until $y = 24.8$ that $\Pr(\text{PAPR} < y) = 100\%$. PO-CI/OFDM, on the other hand, demonstrates $\Pr(\text{PAPR} < y) = 100\%$ when $y = 5.82$.

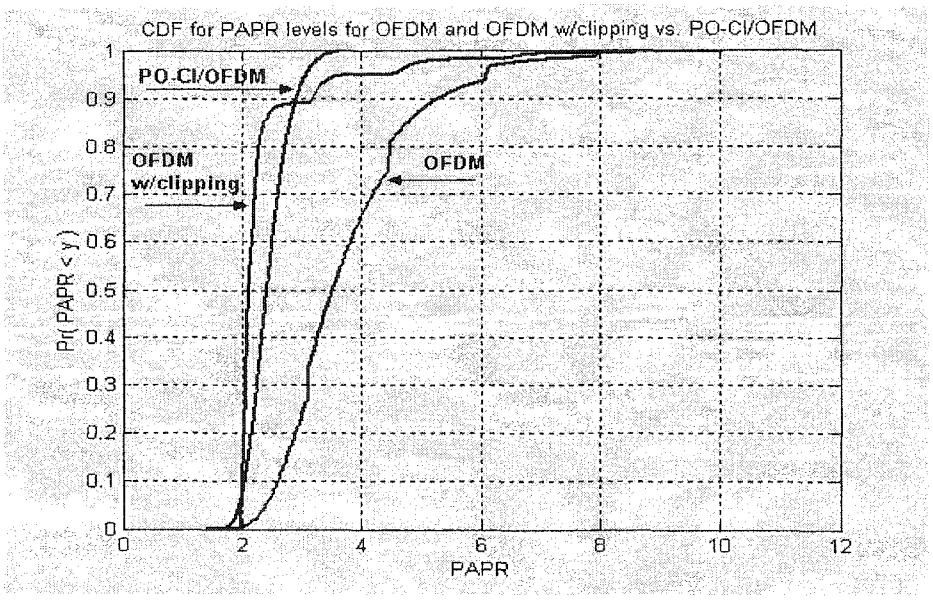

Figure 3.12: Cummulative Distribution Function for PAPR for Clipped OFDM vs. PO-CI/OFDM and OFDM

3.7 Conclusions

In this chapter, CI/OFDM and PO-CI/OFDM transmit signals and structures were introduced. Specifically, the CI and PO-CI spreading codes were defined and applied to the traditional OFDM transmitter architecture. In the resulting CI/OFDM and PO-CI/OFDM systems, *each* data symbol is spread across *all* of the N carriers in a manner that ensures PAPR benefits. Specifically, (1) whereas traditional OFDM often demonstrates PAPR levels above 7.5 for a 32-carrier system (even reaching levels as high as 32), CI/OFDM rarely exceed 5 (and *never* exceed 6.55); and (2) PO-CI/OFDM implementations of OFDM further eliminate PAPR problems.

The cost of added transmitter complexity (for spreading) in CI/OFDM and PO-CI/OFDM, relative to current OFDM, is minimal when compared to the substantial throughput (PO-CI/OFDM) and PAPR benefits (of both CI/OFDM and PO-CI/OFDM). (Specifically, it has been suggested by our corporate partners that the addition of a CI processing at transmitter and receiver will require (approximately) an additional 10% in complexity relative to the existing OFDM baseband architecture.) We believe this is a price well worth paying for the increase in throughput and the elimination of PAPR problems in traditional OFDM systems.

Chapter 4 Reception in CI/OFDM and PO-CI/OFDM Systems

As discussed in Chapter 2, OFDM and its method of orthogonal carrier transmission are not without drawback. One problem with OFDM lies in the fact that each carrier experiences a uniform flat fade, and hence each carrier reaches the receiver with a different amplitude. Even with very sensitive equalizers, data is lost in deep fades. Channel coding overcomes this problem by introducing redundancy and frequency diversity. The downside of such a coding is reduced throughput (by a factor of, e.g., 50% [20]).

In this chapter, we show how to construct the receiver for the proposed CI/OFDM system, and how this receiver creates significant performance gain without the loss in throughput experienced by Coded OFDM. Specifically, in this chapter, we present a novel OFDM receiving architecture which exploits frequency diversity to increase OFDM performance *without* bandwidth expansion or decreased data rate.

Beginning with the Carrier Interferometry OFDM (CI/OFDM) and the Pseudo-Orthogonal Carrier Interferometry OFDM (PO-CI/OFDM) transmitter discussed in Chapter 3, where *each* information symbol is *simultaneously* modulated onto *all* carriers (by means of unique CI spreading sequences) we now illustrate corresponding (novel) method for reception.

4.1 CI/OFDM and PO-CI/OFDM Receiver Structure

After transmission over a slow frequency-selective fading channel (typical of OFDM transmissions), each received carrier experiences a unique flat fade. The received signal for CI/OFDM, assuming the sent signal *s(t)* in (3.6), is mathematically characterized by the following equation:

$$r(t) = A \cdot \sum_{k=0}^{N-1} \sum_{i=0}^{N-1} \alpha_i a_k^n \cos\left(2\pi f_c t + 2\pi f_i t + i \cdot \frac{2\pi}{N} \cdot k + \phi_i \right) + n(t) \tag{4.1}$$

The received signal for PO-CI/OFDM, assuming the sent signal *s(t)* in (3.13), is mathematically characterized by the following equation:

$$r(t) = A \cdot \sum_{k=0}^{2N-1} \sum_{i=0}^{N-1} \alpha_i a_k^n \cos\left(2\pi f_c t + 2\pi f_i t + \frac{2\pi}{N} i \cdot k + i \cdot \Delta\theta_k + \phi_i \right) + n(t) \tag{4.2}$$

In (4.1) and (4.2), α_i and ϕ_i are the fade parameter and phase offset, respectively, introduced into the i^{th} carrier by the frequency selective Rayleigh fading channel, and *n(t)* is additive white Gaussian noise (AWGN). We will assume perfect phase synchronization, for reasons of ease in presentation.

Figure 4.1 depicts the CI/OFDM and PO-CI/OFDM receiver for detection of the k^{th} symbol stream. The receiver (1) down converts the incoming signal *r(t)* (represented

in the figure as a real-to-complex block followed by a complex down conversion, but implemented practically with a cosine and sine (I and Q) mixer and integrator), (2) separates the resulting complex baseband signal (generated from *r(t)*) into its *N* orthogonal carriers (typically implemented as an FFT), (3) compensates for the channel phase effect, then (4) removes the k^{th} symbol stream's phase offset (due to spreading) from each carrier.

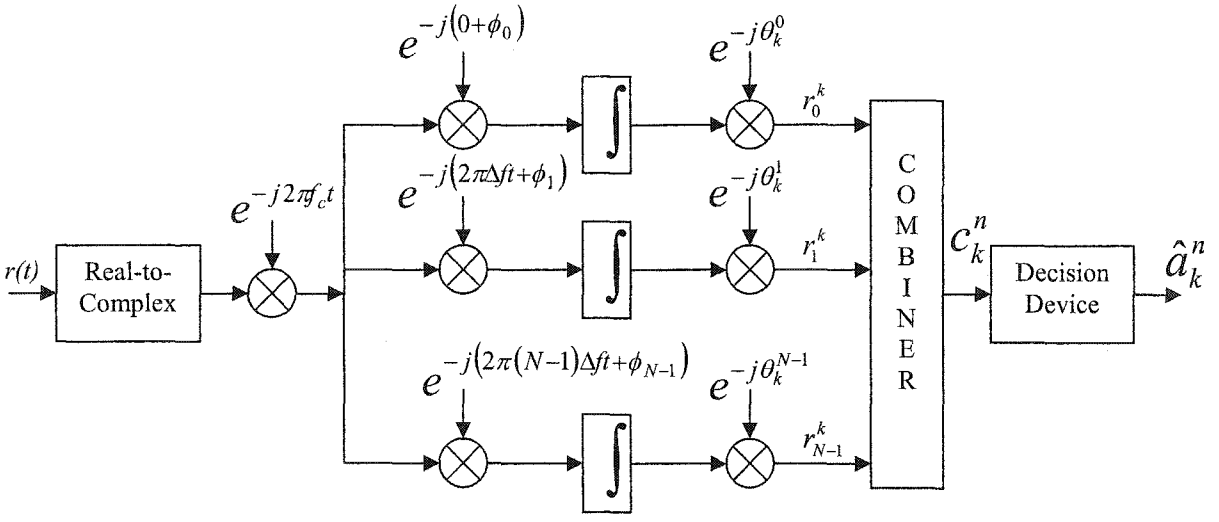

Figure 4.1: The CI/OFDM receiver for the k^{th} symbol

This results in the decision vector

$$\underline{r}_k^n = \left(r_k^n(0), r_k^n(1), \ldots, r_k^n(N-1)\right) \tag{4.3}$$

For CI/OFDM, the decision variable becomes

$$r_k^n(i) = A \cdot \alpha_i a_k^n + A \cdot \sum_{j=0, j\neq k}^{N-1} \alpha_i a_j^n e^{j\left(i\left(\frac{2\pi}{N}\cdot k - \frac{2\pi}{N}\cdot j\right)\right)} + n_i \tag{4.4}$$

For PO-CI/OFDM, the decision variable is

$$r_k^n(i) = A \cdot \alpha_i a_k^n + A \cdot \sum_{j=0, j\neq k}^{2N-1} \alpha_i a_j^n e^{j\left(i\left(\frac{2\pi}{N}k + \Delta\theta_k - \left(\frac{2\pi}{N}j + \Delta\theta_j\right)\right)\right)} + n_i \tag{4.5}$$

Now, since data symbol a_k^n is assumed real, it suffices to consider only the real component of the decision statistic.

That is, the decision statistic for CI/OFDM is

$$r_k^n(i) = A \cdot \alpha_i a_k^n + A \cdot \sum_{j=0, j\neq k}^{N-1} \alpha_i a_j^n \cos\left(i\left(\frac{2\pi}{N} \cdot k - \frac{2\pi}{N} \cdot j\right)\right) + n_i \tag{4.6}$$

and the decision statistic for PO-CI/OFDM is

$$r_k^n(i) = A \cdot \alpha_i a_k^n + A \cdot \sum_{j=0, j\neq k}^{2N-1} \alpha_i a_j^n \cos\left(i\left(\frac{2\pi}{N}k + \Delta\theta_k - \left(\frac{2\pi}{N}j + \Delta\theta_j\right)\right)\right) + n_i \tag{4.7}$$

The first term in both (4.6) and (4.7) represents a faded replica of the desired signal; the third term is a zero mean Gaussian random variable with mean 0 and variance $N_0/2$, expressing the impact of the AWGN; and the second term represents the presence of the *(N – 1)* interfering symbols in CI/OFDM and in the presence of the (*2N*-1) interfering symbols in PO-CI/OFDM -- that is, it represents *inter-symbol interference* (ISI).

A combining strategy is then employed to help restore orthogonality between symbol streams, maximize frequency diversity benefits, and/or minimize noise. In an AWGN or flat fading channel, i.e., whenever $\alpha_1 = \alpha_2 = \cdots = \alpha_N$, the optimal combining is equal gain combining (EGC). That is, $C_k^n = \sum_{i=0}^{N-1} r_k^n(i)$, restores orthogonality between codes, minimizes correlation between pseudo-orthogonal codes, and minimizes noise. The equal gain combining across decision vector components $r_k^n(i)$, however, is not an optimal strategy in a frequency selective channel (due to the carrier dependent fade, α_i). In such channels, the MC-CDMA literature (e.g., [60]) has shown that a minimum mean square error combining (MMSEC) offers a performance close to that of optimal ML (Maximum Likelihood) methods. Specifically, MMSEC jointly minimizes interference from other spreading codes and noise, while exploiting frequency diversity. Employing MMSE combining in the receiver leads to the decision variable:

$$C_k^n = \sum_{i=0}^{N-1} r_k^n(i) \cdot \left[\frac{\alpha_i}{N p_i \alpha_i^2 + N_0/2} \right] \tag{4.8}$$

where p_i is a known constant for carrier i and corresponds to

$$p_i = \begin{cases} 1, & i = 0, \dfrac{N}{2} \\ \dfrac{1}{2}, & else \end{cases} \tag{4.9}$$

for up to N parallel symbol transmissions (CI/OFDM), and

$$p_i = \begin{cases} \frac{1}{2}, & i \neq 0 \\ 1, & i = 0 \end{cases} \tag{4.10}$$

when $N+1$ to $2N$ parallel symbol transmissions occupy the system (PO-CI/OFDM).

Finally, the CI/OFDM or PO-CI/OFDM decision variable C_k^n enters a hard decision device, outputting $\hat{a}_k^n$.

The complexity of employing an MMSE cross-carrier combining in CI/OFDM is larger than that of the usual OFDM frequency equalization. However, (1) the MMSEC requires only per-carrier gains and phase offset estimates (as well as estimates of the signal-to-noise ratio) which is similar to the estimates required in OFDM systems; and (2) because a number of the weights and/or weighted terms can be shared by multiple symbols, the total increase in receiver complexity has been shown to correspond to (approximately) a 10% increase in number of gates. We believe this is a price well worth paying for the gains in performance illustrated in the forthcoming sections.

4.2 Simulation Results for CI/OFDM and PO-CI/OFDM

The following section illustrates the performance of an $N = 32$ carrier CI/OFDM and PO-CI/OFDM system. The following channel models are employed: (1) AWGN

channels (which form a bench mark for comparison), and (2) a frequency selective wireless channel, where selectivity exists over the entire bandwidth, BW, but flat fading is present over each of the $N = 32$ narrowband carriers. Specifically, we assumed both 2-fold and 4-fold frequency diversity over the entire bandwidth. As a result, the fading gain ($\alpha_i's$) in the 32 carriers are correlated according to [55]

$$R_{i,j} = \frac{1}{1+\left(\frac{\Delta f_{i,j}}{(\Delta f_c)}\right)^2} \tag{4.11}$$

where $R_{i,j}$ is the correlation between carrier *i's* fade and carrier *j's* fade, $\Delta f_{i,j}$ is the frequency separation between these two carriers, and $(\Delta f)_c$ is the coherence bandwidth (frequency range over which correlation is above 0.5) [56-57].

Figure 4.2 illustrates the bit error rate (BER) versus signal to noise ratio for OFDM and CI/OFDM in all three channels (AWGN, 2-fold, and 4-fold frequency diversity). Each system transmits $N = 32$ BPSK symbols over $N = 32$ orthogonal carriers.

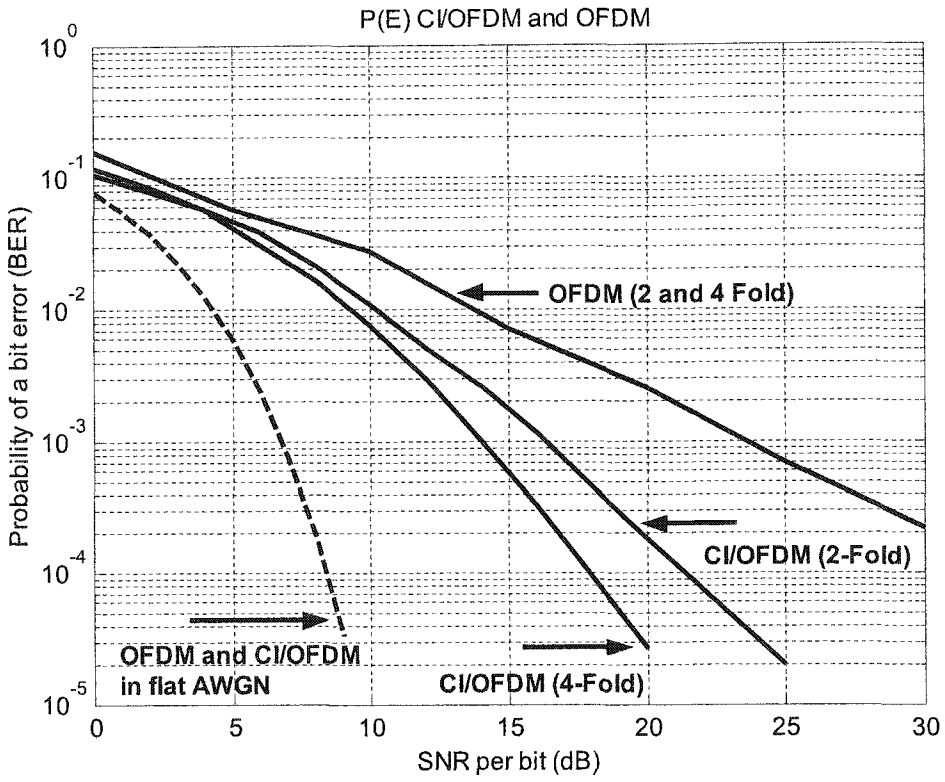

Figure 4.2: BER results of CI/OFDM and OFDM

In transitioning from the flat fading AWGN case to the 2-fold or 4-fold frequency diversity channel, the OFDM system loses approximately 17 dB of performance at a BER of 10^{-3}. Referring to the 4-fold frequency diversity case, the CI/OFDM system offers 10 dB performance gain over OFDM at a BER of 10^{-3}. When the diversity gain is reduced to 2-fold frequency diversity, the CI/OFDM system offers a performance gain of approximately 7 dB at a BER of 10^{-3}. These gains are due to the frequency diversity benefit in the CI/OFDM system. It is apparent that the intersymbol interference due to the second term in (4.6) (reduced by the combining in (4.8)) is more then compensated for by the gain achieved via frequency diversity (sending the same symbol over the $N = 32$ carriers). The performance gain is even larger at lower BER's:

for example, at BER of 10^{-4}, an 18 dB gain is available for the 4-fold frequency diversity case. It is also key to note that as the level of frequency diversity increases in the channel, the CI/OFDM system will continue to outperform OFDM by larger amounts. Again, this can be directly attributed to CI/OFDM's ability to exploit the frequency diversity available in the channel, whereas the OFDM system cannot.

Figures 4.3, 4.4, and 4.5 illustrate the bit error rate (BER) versus signal to noise ratio (SNR) for OFDM and PO-CI/OFDM for 4-fold frequency diversity, 2-fold frequency diversity, and AWGN channels. In all cases, BPSK modulation is assumed, N = 32 carriers are employed. The OFDM system transmits K = 32 symbol streams over the N = 32 carriers. In the PO-CI/OFDM system, by application of pseudo-orthogonal codes to each symbol, $K = 2N = 64$ symbol streams are sent over $N = 32$ carriers.

Referring to Figure 4.3, the increased capacity 64-symbol, 32-carrier PO-CI/OFDM system offers 8 dB gain over a 32-symbol, 32-carrier OFDM system at a BER of 10^{-3}. While offering an 8 dB gain over the 32-symbol, 32-carrier OFDM system, it also offers two times the throughput (64 BPSK symbols over the 32 carriers).

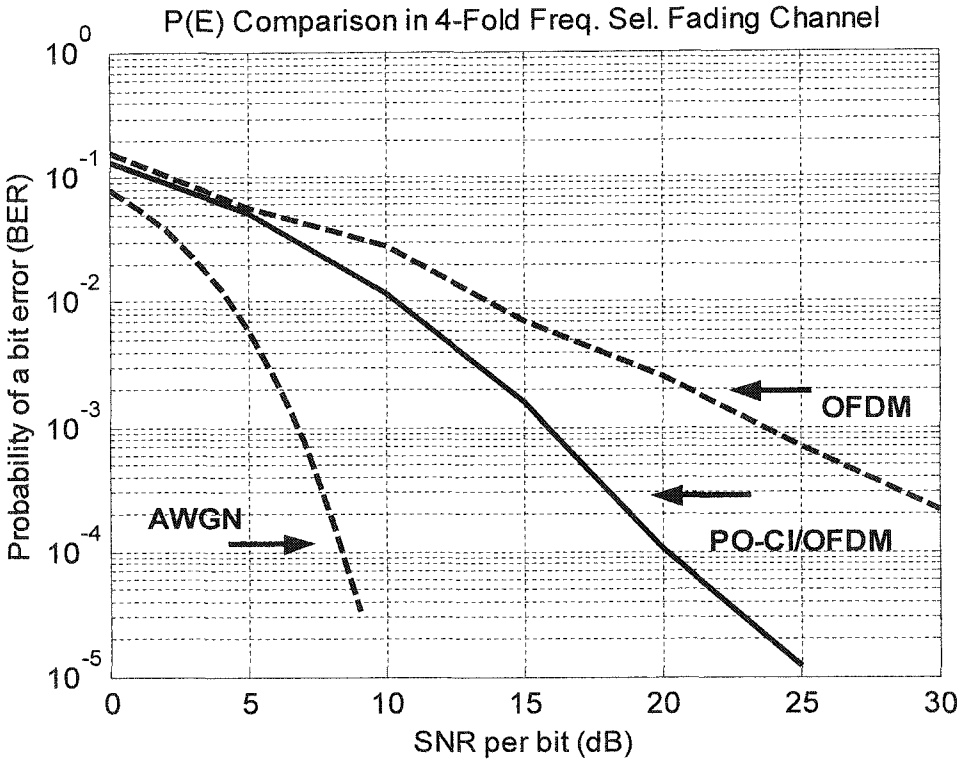

Figure 4.3: Performance results for PO-CI/OFDM vs. OFDM
(4-Fold Frequency Selectivity)

Figure 4.4 illustrates the diminishing performance benefit of PO-CI/OFDM as a function of reduced channel diversity. The PO-CI/OFDM system relies on the diversity gain (due to spreading) to overcome the impact of pseudo-orthogonal spreading. When the diversity gain shrinks from a 4-fold to a 2-fold gain, the PO-CI/OFDM system experiences degradation from its 4-fold performance. Specifically: the 8 dB performance gain of PO-CI/OFDM over OFDM at BER = 10^{-3} in Figure 4.3 is reduced to a 6 dB gain in Figure 4.4.

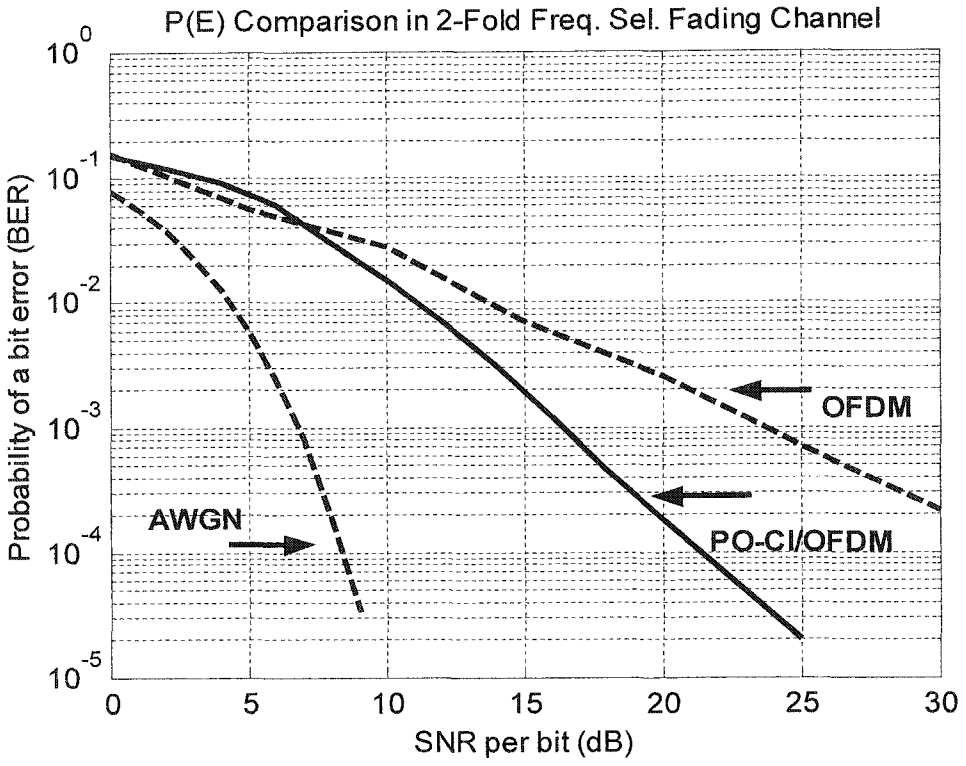

Figure 4.4: Performance results for PO-CI/OFDM vs. OFDM (2-Fold Frequency Selectivity)

Figure 4.5 illustrates the extreme case of an AWGN channel where no diversity gain is available. While unrealistic in most WLAN and cellular OFDM applications (present and future), Figure 4.5 shows PO-CI/OFDM's reliance on the diversity of its spreading code to outperform OFDM.

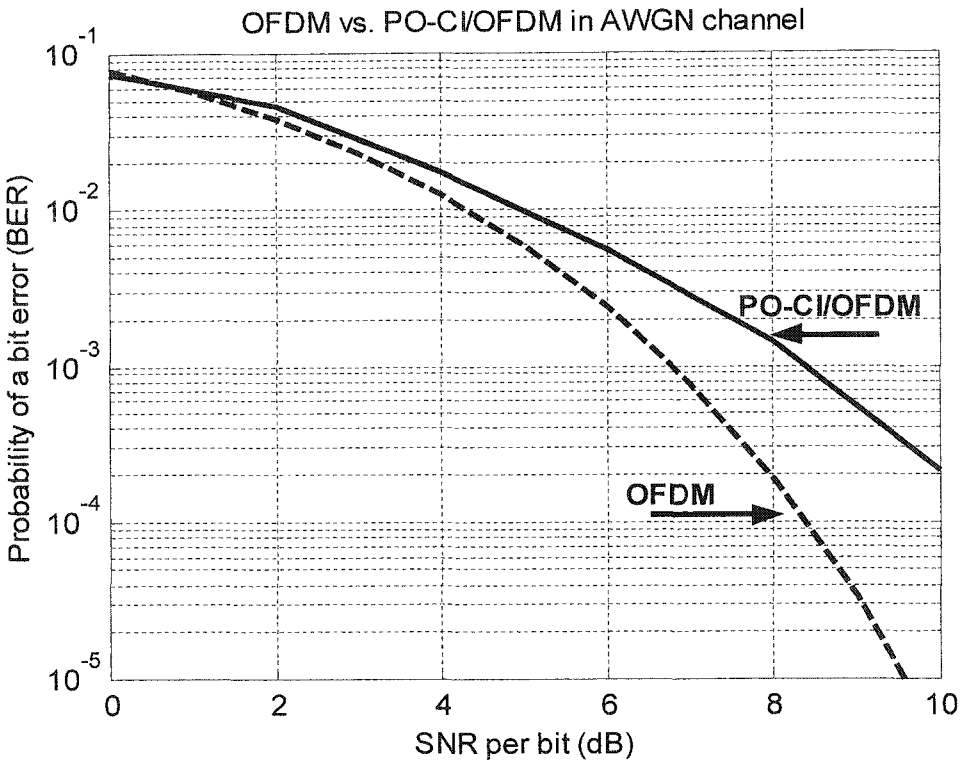

Figure 4.5: Performance results for PO-CI/OFDM vs. OFDM (AWGN Channel)

With no diversity available over the channel, the pseudo-orthogonal spreading of PO-CI/OFDM causes it to experience a performance loss relative to OFDM. That is, in an AWGN channel, the benefit of a doubling in throughput comes at a cost of some performance degradation. As diversity becomes available to the system, PO-CI/OFDM performance gains at a rapid rate.

4.3 Conclusions

In this chapter, the CI/OFDM and PO-CI/OFDM receivers and performances are illustrated. In typical fading environments, CI/OFDM outperforms OFDM by 10 dB at a BER of 10^{-3} without any cost in throughput, and with little cost in complexity. This dramatic gain is a result of CI/OFDM's inherent ability to exploit frequency diversity benefit via spreading.

Finally, in a frequency selective fading channel, 64-symbol, 32-carrier BPSK PO-CI/OFDM was shown to outperform OFDM by 8 dB at a BER of 10^{-3}, with little added complexity. This gain is a result of PO-CI/OFDM's inherent ability to exploit frequency diversity.

Chapter 5 Application of Channel Coding to CI/OFDM and PO-CI/OFDM

5.1 Introduction, Transmit Structure, and Receive Structure

OFDM systems typically include channel coding. The generalized block diagram of the COFDM (Coded OFDM) transmitter is shown in Figure 5.1. Referring to Figure 5.1, traditional COFDM systems take m input bits (e.g., $m = 1$) and channel code them to n output bits (e.g., $n = 2$). The output channel coded bits are then interleaved to ensure that adjacent coded bits reside upon non-adjacent carriers. Following interleaving, the interleaved, channel coded bits are mapped to PSK/QAM symbols, and finally fed into the OFDM modulator (Figure 2.1). Then, in the same serial to parallel manner, each bit (now coded on a symbol) is transmitted on its own carrier for a total of, e.g., $N/2$ information bits sent on N carriers. In this way, information bits are effectively sent on multiple carriers, enabling frequency diversity benefits (in addition to channel coding gain) at a cost of decreased throughput.

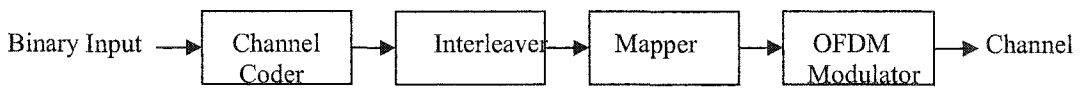

Figure 5.1: Simplified PHY Transmission Train for COFDM

In our proposed Coded CI/OFDM (CI/COFDM) system, each set of m input bits are similarly coded to n output bits (e.g., 1 bit to 2 bits), interleaved, and mapped to PSK/QAM symbols prior to entering the CI/OFDM modulator (Figure 3.1(b) and 3.1(c)). Now, since CI/OFDM already spreads each bit (coded on a symbol) onto all N carriers (exploiting the full frequency diversity benefit), each set of coded bits is time interleaved to create a time diversity benefit. The block diagram of the CI/COFDM system with a rate ½ coder, inclusive of this time interleaving, is illustrated in Figure 5.2.

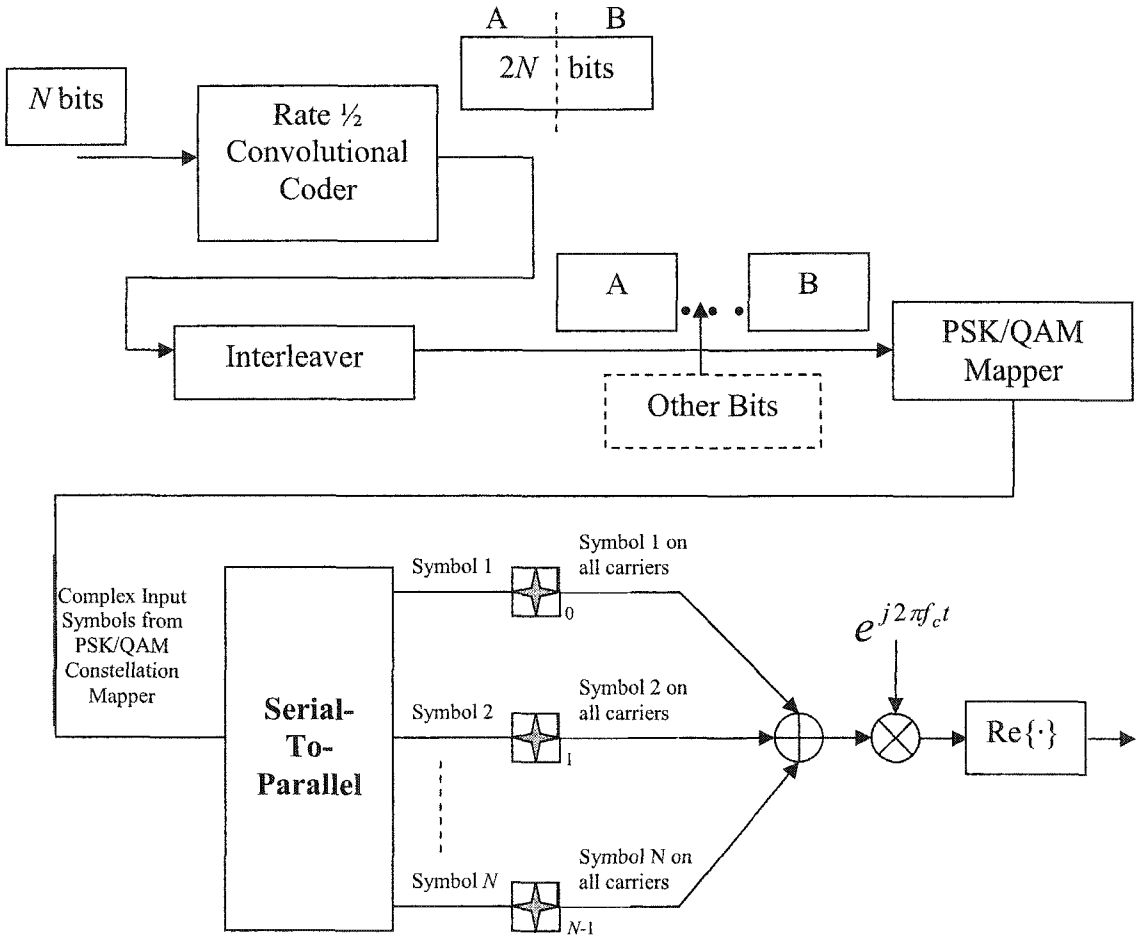

Figure 5.2: CI/COFDM

Referring to Figure 5.2, it can be seen that for a rate ½ convolutional coder, one bit is input and two coded bits are output, creating "coded output bit 1" (denoted in Figure 5.2 as A) and "coded output bit 2" (denoted in Figure 5.2 as B). These coded output bits are then time interleaved onto two different CI/OFDM symbols such that one CI/OFDM symbol contains N "coded output 1 bits" and another CI/OFDM symbol contains the second N "coded output 2 bits." In this way, CI/COFDM has the same degree of redundancy (i.e. same throughput) as COFDM, but instead of redundant bits being transmitted on the carriers at the same time, they are time interleaved. CI/COFDM then, offers the same frequency diversity benefit of CI/OFDM, and adds a time diversity benefit in addition to channel coding gain (while maintaining the same throughput of a COFDM system).

When channel coding is applied to PO-CI/OFDM, leading to PO-CI/Coded OFDM (PO-CI/COFDM), the transmitter operates as follows (Figure 5.3): (1) each m input bits (e.g., $m = 1$) are first channel coded to n output bits (e.g., $n = 2$); (2) interleaving follows where the n coded bits are interleaved such that they are sent at different OFDM symbol times (with a time separation selected to create a time diversity benefit); (3) next is bit-to-constellation mapping; (4) followed by serial-to-parallel conversation and spreading of the parallel data streams. Hence, PO-CI/COFDM benefits from (1) coding gain, (2) time diversity benefit, and (3) frequency diversity gain via the spreading.

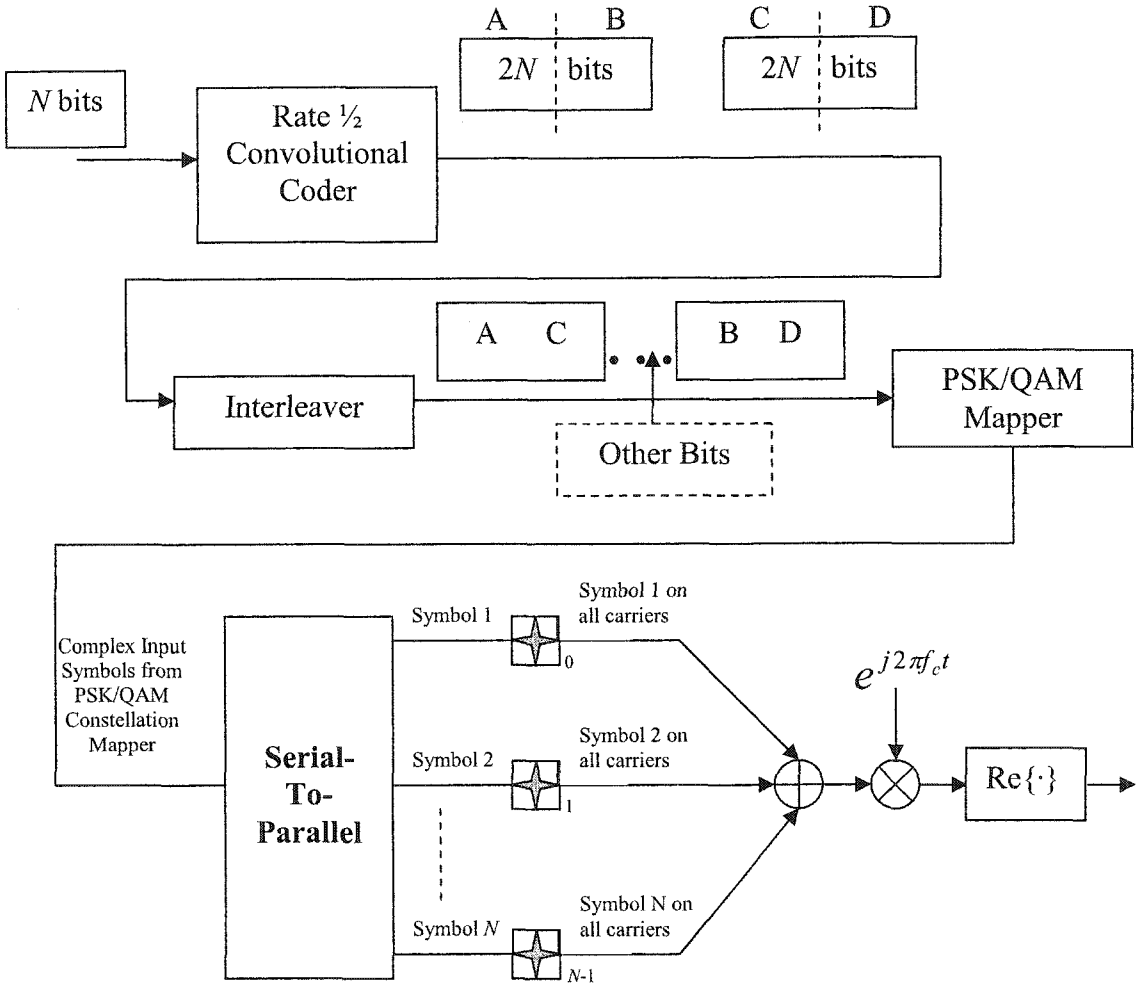

Figure 5.3: PO-CI/COFDM

At the receiver, the CI/OFDM and PO-CI/OFDM decision variable C_k^n (of equation 4.8) is input into a deinterleaver, followed by a soft decision decoding Viterbi Algorithm (VA), which performs channel decoding (rather than merely entering a decision device as with the uncoded CI/OFDM and PO-CI/OFDM systems). This can be seen in Figure 5.4.

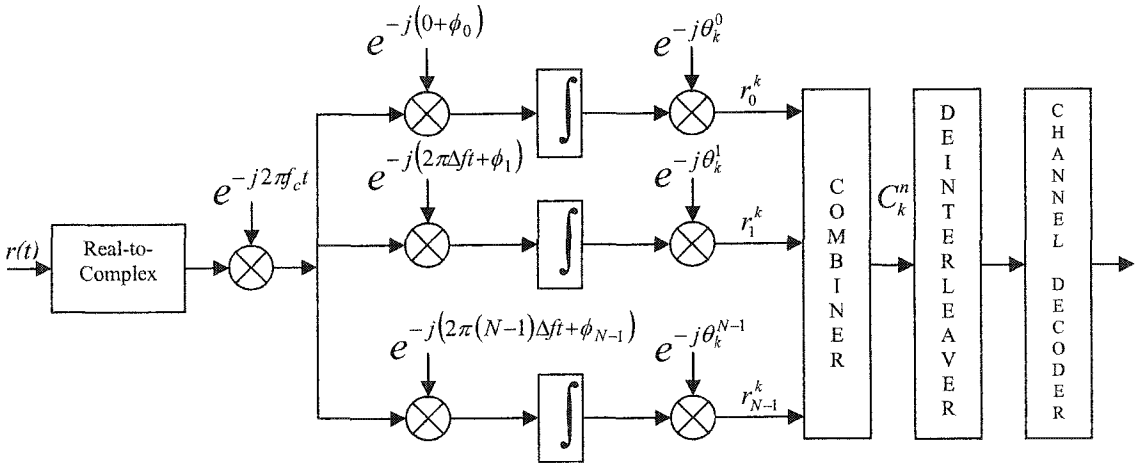

Figure 5.4: CI/COFDM and PO-CI/COFDM receiver

5.2 Simulation Results for CI/COFDM and PO-CI/COFDM

Figure 5.5 illustrates the bit error rate (BER) versus signal to noise ratio for OFDM, COFDM, CI/OFDM, and CI/COFDM. Each system transmits $N = 32$ BPSK symbols over $N = 32$ orthogonal carriers. In all cases, channel coding refers to rate ½ convolutional coding with constraint length 3, characterized by the generator polynomials $(5, 7)_8$ at the transmitter and use of the Viterbi algorithm (VA) at the receiver (channel decoder of Figure 5.4) [67]. Again, to model a realistic wireless environment, the Rayleigh fading channel employed in our simulation demonstrates frequency selectivity over the total bandwidth, BW, but flat fading over each of the N

narrowband carriers. Specifically, we assume the channel model with 4-fold frequency diversity over the entire bandwidth (as defined in equation 4.11).

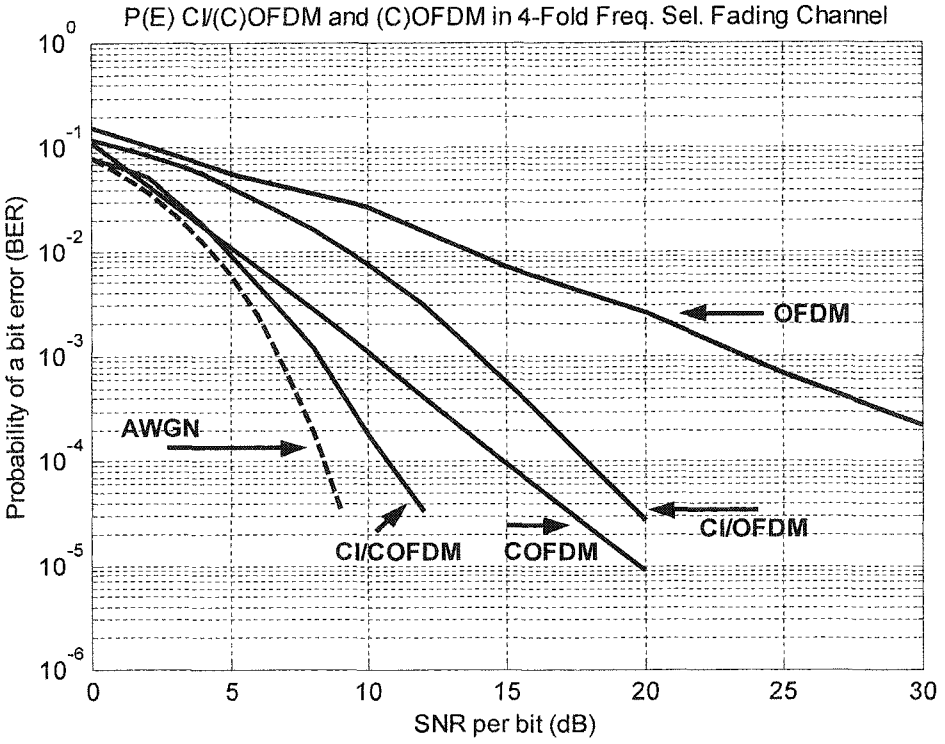

Figure 5.5: CI/(C)OFDM and (C)OFDM Performance

Referring to Figure 5.5, it is observed that the traditional COFDM system gains approximately 14 dB over OFDM at BER of 10^{-3}. The substantial benefits of channel coding, in terms of both redundancy and frequency diversity benefit, are apparent, but the cost is high -- in this case a factor of 2 degradation in throughput. Without any coding or loss in throughput, CI/OFDM offers 10 of COFDM's 14 dB gain. Moreover, with only a 4 dB performance loss relative to COFDM, CI/OFDM is available without the complexity of a soft decision decoding VA at its receiver.

When the identical rate ½ convolutional coding scheme is applied to the CI/OFDM system, creating CI/COFDM, 16 dB gain is achieved over OFDM, and a 2 dB gain is available over COFDM at BER of 10^{-3}. By BER of 10^{-4}, 23 dB gains are observed in relation to OFDM and 3 dB gains are achieved relative to COFDM. The performance benefits are observed because, not only is frequency diversity exploited, but in addition, (1) a time diversity benefit is achieved via symbol interleaving the channel coded symbols, and (2) convolutional decoding using a VA offers well-documented benefits.

Among the performance benefits of CI based OFDM systems, we consider the ability of CI/OFDM to achieve close to the performance of COFDM the most significant. This benefit suggests that (1) 100% gains in throughput can be achieved by CI/OFDM relative to COFDM (i.e., the throughput of uncoded OFDM can be achieved) and (2) the cost for this throughput gain is only a 4 dB degradation.

Referring now to Figure 5.6, the increased capacity 64-BPSK symbol, 32-carrier PO-CI/OFDM system offers 8 dB gain over a 32-BPSK symbol, 32-carrier OFDM system at a BER of 10^{-3}. While it loses 5 dB relative to the 16-information symbol, 32-carrier COFDM system, PO-CI/OFDM has four times the throughput relative to COFDM over the same 32 carriers (and a less complex receiver design). In Figure 5.6, the 32-information symbol, 32-carrier PO-CI/COFDM system demonstrates a 2 dB gain over the 16-information symbol, 32-carrier COFDM system, and hence 14 dB over typical OFDM at a BER of 10^{-3}. This means that the interference due to spreading sequences in PO-

CI/COFDM is more than compensated for by the gain achieved via the full frequency diversity (sending the same symbol over the $N = 32$ carriers), the time diversity (induced in time interleaving) and the VA convolutional decoding. These benefits allow the 32-information symbol, 32-carrier PO-CI/COFDM system to slightly outperform its 16-information symbol, 32-carrier COFDM counterpart. Hence, we can conservatively state that BPSK PO-CI/COFDM achieves the performance of COFDM, with the same throughput as OFDM. The cost, of course, is transmitter and receiver complexity.

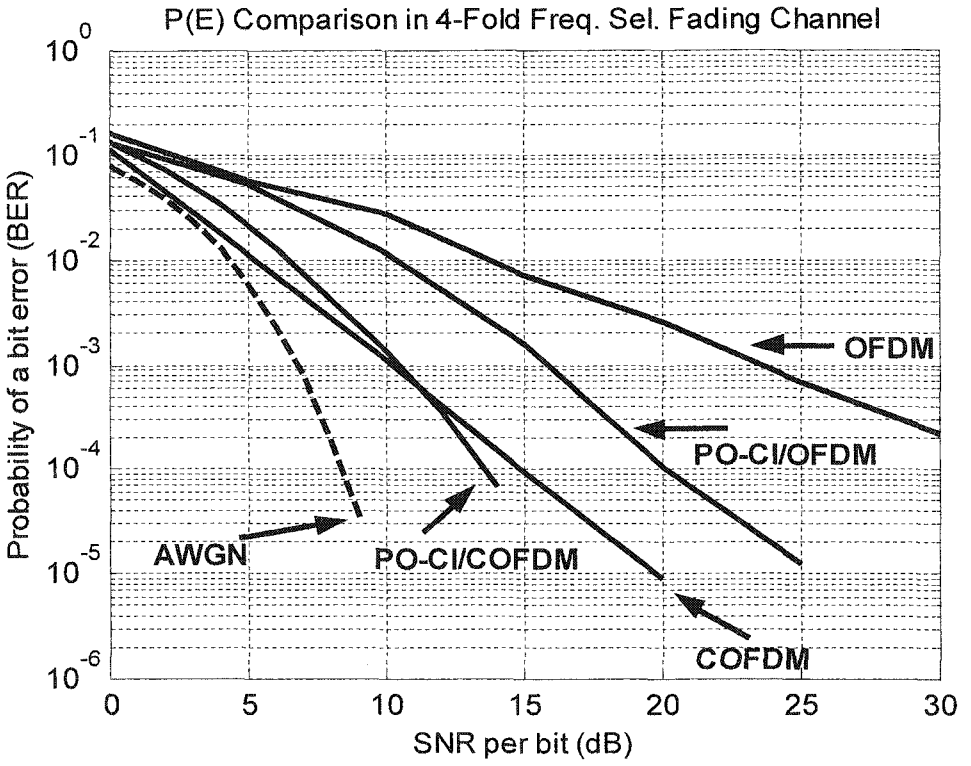

Figure 5.6: PO-CI/(C)OFDM and (C)OFDM Performance

When comparing system performances at a BER of 10^{-5} (typical of the performance requirement in, e.g., an OFDM WLAN operating at a 10% PER), the

performance of PO-CI/COFDM outperforms COFDM by approximately 5 dB. Here, gains in diversity and channel coding far exceed the losses from pseudo-orthogonal spreading.

5.3 Conclusions

In this chapter, the CI/COFDM and PO-CI/COFDM receivers and performances are illustrated. We first demonstrated that while traditional COFDM produces a dramatic gain in performance, CI/OFDM (without coding) offers close to the same performance as COFDM at a BER of 10^{-3}, while avoiding the cost in decreased throughput (by a factor of 2) and the cost of increased receiver complexity (to implement a VA). Moreover, we demonstrated that a coded version of CI/OFDM, namely CI/COFDM, which outperforms its COFDM counterpart. This results because CI/COFDM benefits from frequency diversity, time diversity, and channel coding. Furthermore, we have presented the coded BPSK PO-CI/COFDM system, which equals the performance of its COFDM counterpart while demonstrating the throughput of OFDM. This results because the benefits of frequency diversity, time diversity, and channel coding, evident in the PO-CI/COFDM architecture, outweigh the cost of interference due to pseudo-orthogonal spreading.

Chapter 6 CI/OFDM with Higher Order Constellations

In earlier chapters, we showed how Carrier Interferometry (CI) codes may be used to spread OFDM symbols over all N subcarriers to exploit frequency diversity without loss in throughput. We also showed how the carefully selected CI codes enable a stable transmit envelope, thereby eliminating PAPR problems. However, only BPSK was detailed. In this chapter, we extend the proposed CI/OFDM (Carrier Interferometry with OFDM) system by updating it for application with QAM modulation schemes. (For example, Minimized Mean Square Error Combining (MMSEC) is derived for CI/OFDM with QAM modulation schemes.) Simulated performance results over multi-path fading channels, as well as PAPR analysis, are presented for the higher-order modulations.

6.1 Introduction to CI with Higher Order Constellations

One of the benefits of OFDM is its spectral efficiency, and in order to achieve high-data rates while maintaining this efficiency, most OFDM archictectures utilize higher order modulations (e.g., 16 and 64 QAM). In earlier chapters, only BPSK modulation was considered. For higher modulation schemes, e.g., 16QAM or 64QAM, it

is possible that the increased MAI (multiple access interference) in CI/OFDM may cancel some of the performance benefits achieved via frequency diversity.

In this chapter, we extend the proposed CI/OFDM architecture to study its operation with 16QAM and 64QAM constellations. Optimal Minimized Mean Square Error Combining (MMSEC) schemes for both modulation formats are presented. Performance analysis and simulation results show that, even with QAM modulation schemes, CI/OFDM still significantly outperforms OFDM, gaining 5-7 dB at a fixed $BER = 10^{-3}$.

We also analyze the PAPR benefits of CI codes in higher-order constellation OFDM systems (QPSK, 16-QAM, and 64-QAM OFDM). This chapter confirms that the proposed technique (of spreading the data symbols onto all carriers) ensures the elimination of high peaks in the signal envelope (thereby eliminating the PAPR problem): It is further shown that the choice of constellation size does little to change the PAPR benefits of the CI spreading technique.

6.2 QAM CI/OFDM Transmitter and Receiver Structures

A typical OFDM transmitter (as discussed in Chapter 2 and 3) is shown in Figure 6.1(a), and the CI/OFDM transmitter is depicted in Figures 6.1(b) and 6.1(c). (Although previously discussed in earlier chapters, we re-present the architectures here in order to define the unique features when using QAM.) In both OFDM and CI/OFDM, input bits are serial to parallel converted. In OFDM, each information symbol is modulated onto a single (unique) carrier; in CI/OFDM, *each* information symbol is modulated onto *all* of the N carriers. To ensure the separation of information symbols at the receiver side, the transmitter applies a unique orthogonal spreading code to each information symbol (where spreading is applied in the frequency domain, i.e., across carriers (Figure 6.1(c))). In CI/OFDM, orthogonal Carrier Interferometry (CI) codes are applied to ensure the orthogonality among all transmitted information symbols. These spreading codes correspond to the application of (to the k^{th} symbol)

$$c^{(k)}(t) = \sum_{i=0}^{N-1} \beta_i^{(k)} e^{j2\pi i \Delta f t} \cdot g(t) \tag{6.1}$$

where (1) Δf is the carrier separation ($\Delta f = 1/T_s$ to ensure carrier orthogonality); (2) $g(t)$ is a rectangular pulse shape of duration T_s (where T_s is OFDM symbol length); and (3) $\left\{\beta_i^{(k)}, i = 0,1,\cdots,N-1\right\}$ refers to k^{th} symbol's spreading sequence characterized by

$$\left\{\beta_0^{(k)},\beta_1^{(k)},\cdots,\beta_{N-1}^{(k)}\right\}=\left\{e^{j\frac{2\pi}{N}\cdot k\cdot 0},e^{j\frac{2\pi}{N}\cdot k\cdot 1},\cdots e^{j\frac{2\pi}{N}\cdot k\cdot(N-1)}\right\} \tag{6.2}$$

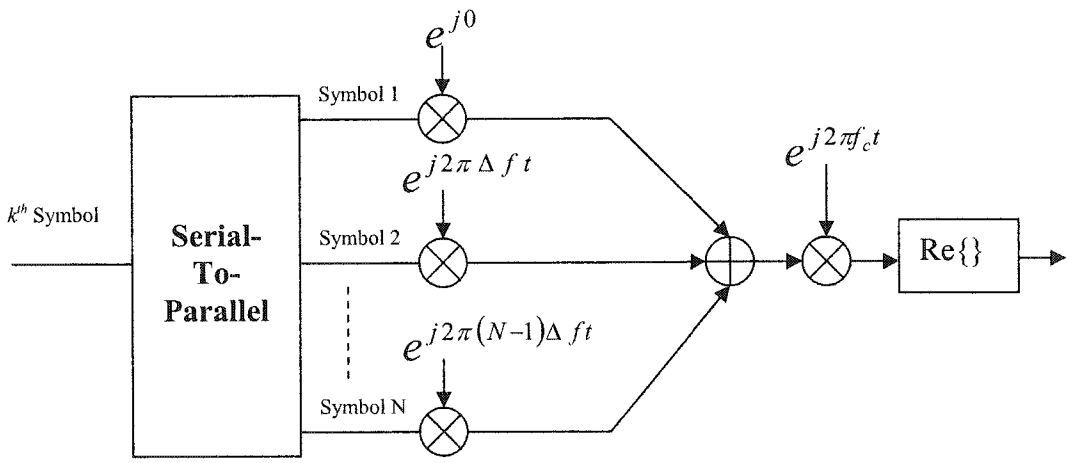

(a) OFDM Transmitter

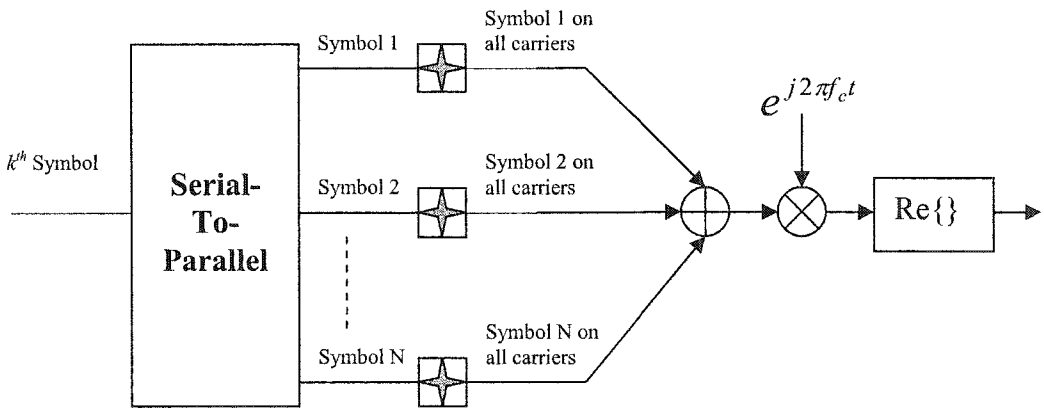

(b) CI/OFDM Transmitter

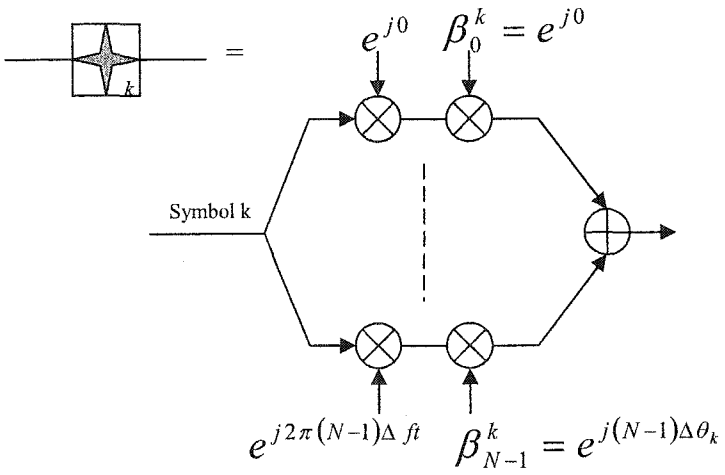

(c) CI/OFDM Transmitter for k^{th} symbol

Fig. 6.1 (a) OFDM Transmitter, (b) CI/OFDM Transmitter, detailing the Spreading Operation in CI/OFDM

The transmitted signal for the k^{th} symbol in CI/OFDM system is

$$s^{(k)}(t) = \mathrm{Re}\left[A \cdot s^{(k)} \cdot c^{(k)}(t) \cdot e^{j2\pi f_c t}\right] \tag{6.3}$$

$$s^{(k)}(t) = \mathrm{Re}\left[\sum_{i=0}^{N-1} A \cdot s^{(k)} \cdot e^{j(2\pi \cdot i \cdot \Delta ft)} \cdot e^{j\frac{2\pi}{N} \cdot k \cdot i} \cdot e^{j2\pi f_c t} \cdot g(t)\right] \tag{6.4}$$

In equation (6.4), A is a constant that ensures bit energy of unity (i.e, $A = \frac{1}{\sqrt{N}}$ for BPSK, $A = \frac{1}{\sqrt{5 \cdot N}}$ for 16QAM , and $A = \frac{1}{\sqrt{21 \cdot N}}$ for 64QAM), and $s^{(k)}$ is the k^{th} information symbol, and corresponds to

$$s^{(k)} = s_I^{(k)} + j s_Q^{(k)} \tag{6.5}$$

where $s_I^{(k)}$ is the so-called in-phase component of $s^{(k)}$ and $s_Q^{(k)}$ is the quadrature component. For BPSK modulation, $s_I^{(k)} \in \{-1,+1\}$ and $s_Q^{(k)} = 0$. For 16QAM, $s_{I,Q}^{(k)} \in \{-3,-1,+1,+3\}$. For 64QAM, $s_{I,Q}^{(k)} \in \{-7,-5,-3,-1,+1,+3,+5,+7\}$. Also in equation (6.4), f_c is the carrier frequency.

The total transmitted signal for one entire CI/OFDM symbol (considering all N transmit symbols) corresponds to

$$S(t) = \mathrm{Re}\left[\sum_{k=0}^{N-1}\sum_{i=0}^{N-1} A \cdot s^{(k)} \cdot e^{j(2\pi \cdot i \cdot \Delta f t)} \cdot e^{j\frac{2\pi}{N} \cdot k \cdot i} \cdot e^{j2\pi f_c t} \cdot g(t)\right] \tag{6.6}$$

$$\begin{aligned} S(t) &= S_I(t) + S_Q(t) \\ &= \sum_{k=0}^{N-1}\sum_{i=0}^{N-1} A \cdot s_I^{(k)} \cdot \cos(2\pi f_c t + 2\pi i \Delta f t + \frac{2\pi}{N} \cdot k \cdot i) \cdot g(t) \\ &- \sum_{k=0}^{N-1}\sum_{i=0}^{N-1} A \cdot s_Q^{(k)} \cdot \sin(2\pi f_c t + 2\pi i \Delta f t + \frac{2\pi}{N} \cdot k \cdot i) \cdot g(t) \end{aligned} \tag{6.7}$$

where $S_I(t)$ is the in-phase component of the transmit signal and $S_Q(t)$ is the quadrature component. Similarly, after transmission over a frequency-selective fading channel, the received CI/OFDM signal, assuming the transmit signal in (6.7), corresponds to

$$\begin{aligned} r(t) &= r_I(t) + r_Q(t) \\ &= \sum_{k=0}^{N-1} \sum_{i=0}^{N-1} A \cdot \alpha_i \cdot s_I^{(k)} \cdot \cos(2\pi f_c t + 2\pi i \Delta f t + \frac{2\pi}{N} \cdot k \cdot i + \phi_i) \cdot g(t) \\ &- \sum_{k=0}^{N-1} \sum_{i=0}^{N-1} A \cdot \alpha_i \cdot s_Q^{(k)} \cdot \sin(2\pi f_c t + 2\pi i \Delta f t + \frac{2\pi}{N} \cdot k \cdot i + \phi_i) \cdot g(t) + n(t) \end{aligned} \tag{6.8}$$

where (1) α_i and ϕ_i are the fading gain and phase offset, respectively, introduced into the i^{th} carrier by the frequency selective Rayleigh fading channel, and (2) *n(t)* is additive white Gaussian noise (AWGN). We assume perfect phase synchronization for ease in presentation.

The receiver structure for the k^{th} symbol in CI/OFDM (with a QAM constellation) is illustrated conceptually in Figure 6.2. Here, both the in-phase and quadrature components of the received signal are decomposed into their N carrier components and recombined to minimize the interference from other symbols (inter-symbol interference) and the noise. A hard decision devices follows to create the symbol estimation $\hat{s}_I^{(k)}$ and $\hat{s}_Q^{(k)}$. In practice, the frequency decomposition is better implemented (i.e., implemented at a reduced cost) by application of a single FFT.

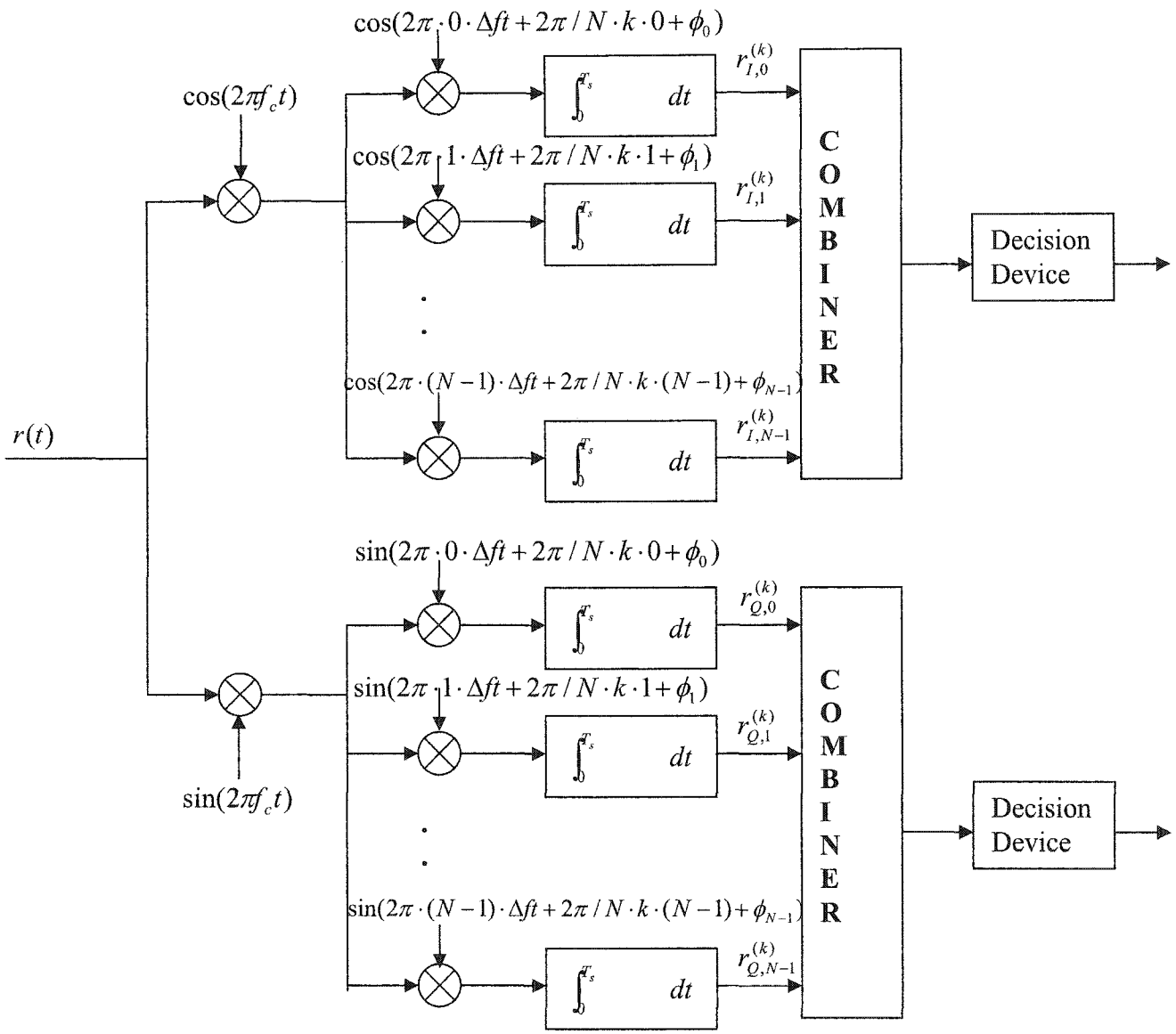

Figure 6.2. Receiver for CI/OFDM with QAM

6.3 Minimized Mean Square Error Combining for CI/OFDM with QAM

We will present the combiner (see Figure 6.2) for the in-phase component of the received signal (the presentation is analogous for the quadrature component combining). Considering the in-phase component, the decision statistics correspond to (Figure 6.2)

$$\vec{r}_I^{(k)} = (r_{I,0}^{(k)}, r_{I,1}^{(k)}, \cdots, r_{I,N-1}^{(k)}) \tag{6.9}$$

where

$$r_{I,i}^{(k)} = A\alpha_i s_{I,i}^{(k)} + \sum_{\substack{l=0 \\ l\neq k}}^{N-1} A\alpha_i s_I^{(l)} \cos(\frac{2\pi}{N}\cdot k\cdot i - \frac{2\pi}{N}\cdot l\cdot i) + \sum_{\substack{l=0 \\ l\neq k}}^{N-1} A\alpha_i s_Q^{(l)} \sin(\frac{2\pi}{N}\cdot k\cdot i - \frac{2\pi}{N}\cdot l\cdot i) + n_i \tag{6.10}$$

In equation (6.10), the first term represents the desired signal on the i^{th} carrier, the second and the third terms represent inter-symbol interference from the remaining *N-1* symbols, and the fourth term (a zero mean Gaussian random variable with variance $N_0/2$) represents the contribution of additive Gaussian noise. In an AWGN or a flat fading channel, i.e., $\alpha_i = C$ where C is a constant, a simple equal gain combining across carriers (index i) causes the second and third terms (ISI terms) to sum to zero (due to the orthogonality between CI spreading codes)). However, in a frequency selective fading channel, a carefully designed combiner (across carriers) needs to be employed to counter the loss of orthogonality between CI spreading codes (due to the carrier dependent gain, α_i). The general form of the combiner corresponds to

$$R_I^{(k)} = \sum_{i=0}^{N-1} W_i \cdot r_{I,i}^{(k)} \tag{6.11}$$

We propose the design of weights W_i based on Minimized Mean Square Error Combining (MMSEC) since this scheme has been shown (in the MC-CDMA literatures e.g., [60]) (1) to exploit the frequency diversity available in a frequency-selective fading channel and (2) to jointly minimize the inter-symbol interference (the second and third terms in (6.10)) and the additive noise (the fourth term in (6.10)).

It is easy to show that the i^{th} combining weight, derived via the MMSE criteria, corresponds to

$$W_i = \frac{A\alpha_i}{E\left[(r_{I,i}^{(k)})^2\right]} = \frac{A\alpha_i}{NA^2\alpha_i^2 E\left[(s_I^{(l)})^2\right] + \frac{N_0}{2}} \tag{6.12}$$

It is obvious that for 16QAM

$$E\left[(s_I^{(l)})^2\right] = 0.5 \cdot (1)^2 + 0.5 \cdot (3)^2 = 5 \tag{6.13}$$

and for 64QAM

$$E\left[(s_I^{(l)})^2\right] = 0.25 \cdot (1)^2 + 0.25 \cdot (3)^2 + 0.25 \cdot (5)^2 + 0.25 \cdot (7)^2 = 21 \tag{6.14}$$

Hence, the MMSEC weight for CI/OFDM with 16QAM is

$$W_i = \frac{\frac{1}{\sqrt{5N}}\alpha_i}{N \cdot \frac{1}{5N}\alpha_i^2 \cdot 5 + \frac{N_0}{2}} = \frac{\alpha_i}{\sqrt{5N}(\alpha_i^2 + \frac{N_0}{2})} \tag{6.15}$$

and for CI/OFDM with 64QAM is

$$W_i = \frac{\frac{1}{\sqrt{21N}}\alpha_i}{N \cdot \frac{1}{21N}\alpha_i^2 \cdot 21 + \frac{N_0}{2}} = \frac{\alpha_i}{\sqrt{21N}(\alpha_i^2 + \frac{N_0}{2})} \tag{6.16}$$

6.4 Channel Model and Simulated Performance Results

In this section, we test the performance of the CI/OFDM system with QAM modulation schemes and compare these with the performance of traditional OFDM systems. Here, simulations are performed over frequency selective Rayleigh fading channels, where both CI/OFDM and OFDM systems employ N=48 carriers to transmit 48 data bearing symbols.

To model realistic wireless environments, the Rayleigh fading channel employed in our simulation demonstrates frequency selectivity over the entire bandwidth, BW, but

flat fading over each of the N carriers. Specifically, we assumed a channel model with coherence bandwidth, $(\Delta f)_c$, characterized by

$$(\Delta f)_c / BW = 0.07 \tag{6.17}$$

which is common for OFDM based Wireless LAN (WLAN) systems. As a result, the α_i's in the 48 carriers are correlated according to

$$\rho_{i,j} = \frac{1}{1+((f_i - f_j)/(\Delta f)_c)^2} \tag{6.18}$$

where $\rho_{i,j}$, is the correlation between the i^{th} carrier and the j^{th} carrier, and $(f_i - f_j)$ is the frequency separation between these two carriers. Generation of correlated fades, for purposes of simulation, has been discussed in [56-57].

Figure 6.3 illustrates the bit error rate (BER) versus signal to noise ratio (SNR) results for OFDM and CI/OFDM with 16QAM and Figure 6.4 plots the same axis for 64QAM. In both figures, the curve marked with circles represents the performance of OFDM, while the curve marked with stars represents the performance of the proposed CI/OFDM. It is evident from these figures that CI/OFDM significantly outperforms OFDM in both cases. Specifically, for a 16QAM modulation scheme and a $BER = 10^{-3}$, we observe a 7 dB gain for CI/OFDM relative to OFDM. With 64QAM at $BER = 10^{-3}$, we observe a 5 dB gain for CI/OFDM relative to OFDM. The performance benefits of CI/OFDM over traditional OFDM (evident in from Figures 6.3 and 6.4) are a direct

consequence of the sprcading of each information symbol over all N carriers. The frequency domain spreading via orthogonal CI codes brings frequency diversity benefits to CI/OFDM systems, providing gain over traditional OFDM systems (where no frequency diversity is achieved).

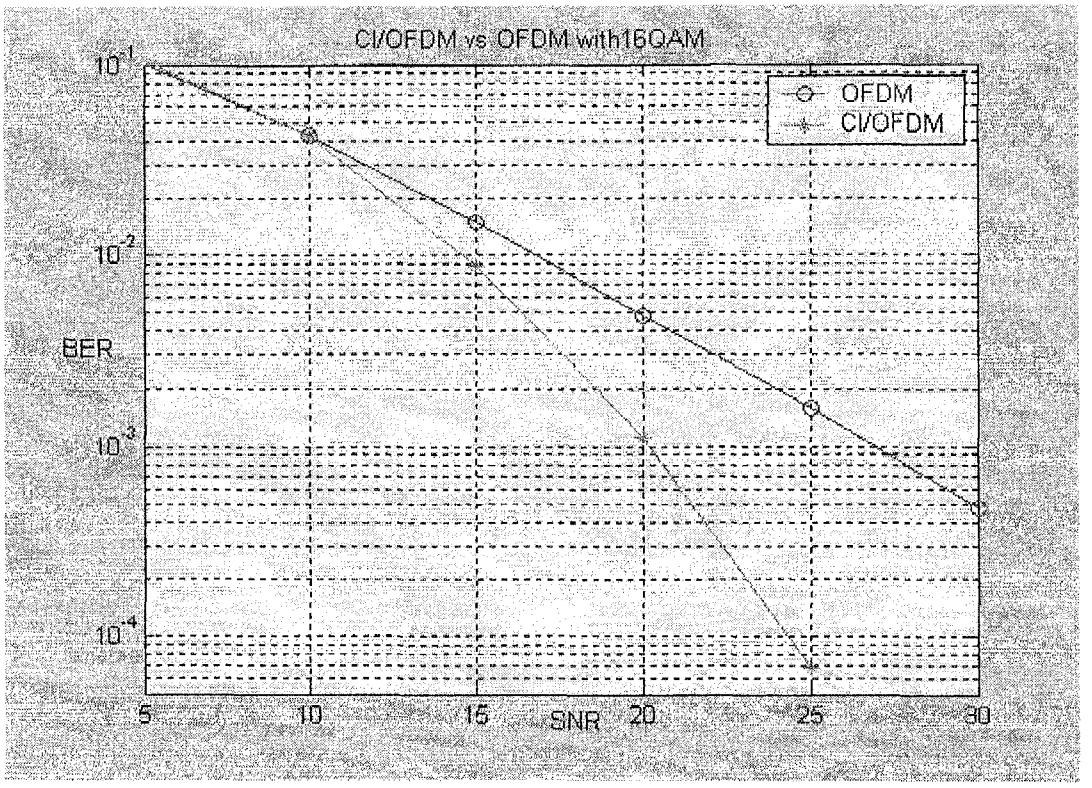

Figure 6.3. Simulation Results for CI/OFDM with 16QAM

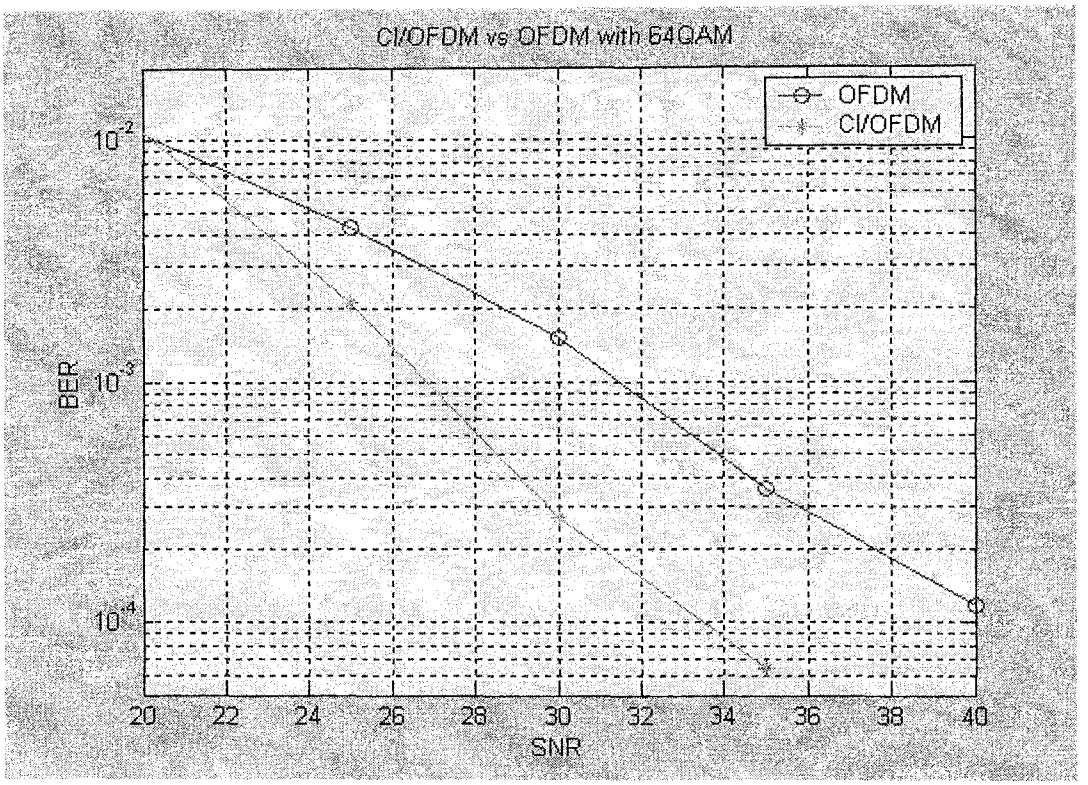

Figure 6.4. Simulation Results for CI/OFDM with 64QAM

6.5 CI/OFDM with Higher Order Constellations: PAPR Benefit

PAPR, as defined in Chapter 2 and 4, is the peak power per OFDM symbol versus the average power in that same symbol, i.e., mathematically:

$$PAPR = \frac{P_{\max}}{P_{\text{mean}}} = \frac{\max_{0<t<T_s} |s(t)|^2}{\text{mean}_{0<t<T_s} |s(t)|^2} \tag{6.19}$$

The average power in both OFDM and CI/OFDM is:

$$P_{mean} = NP_o \tag{6.20}$$

where P_o is the single-carrier power

$$\left(P_o = \frac{1}{2} A^2 \right) \tag{6.21}$$

The OFDM method of serial-to-parallel converting incoming information symbols and transmitting each symbol on its own unique carrier leads to the potential for high peak power. In the worst case (WC), an in-phase coherent addition of all N carriers leads to a P_{max} value of:

$$P_{\max}^{WC} = \frac{1}{2}\left(\sum_{i=1}^{N} A \right)^2 = \frac{1}{2}(NA)^2 = \frac{1}{2} N^2 A^2 \tag{6.22}$$

In CI/OFDM, presented in Chapter 3, *each* symbol is transmitted simultaneously over *all* carriers, and an appropriate spreading sequence ensures symbol separability at the receiver. However, our selection of spreading sequences has a second benefit: it reduces peak power. Specifically, the spreading sequence selected $\left(i.e., \left\{ \beta_k^0, \beta_k^1, \ldots, \beta_k^{N-1} \right\} = \left\{ e^{j\frac{2\pi}{N}0 \cdot k}, e^{j\frac{2\pi}{N}1 \cdot k}, \ldots, e^{j\frac{2\pi}{N}(N-1)k} \right\} \right)$ ensures that when one symbol's carriers add coherently, other symbol's carriers do not add coherently.

The PAPR benefit of CI/OFDM is best explained conceptually via the illustration of Figure 6.5. Figure 6.5 plots the envelope for each of the N transmit signals in an N-carrier CI/OFDM system (where $N = 8$ in Figure 6.5). That is, each of the $N = 8$ solid lines in Figure 6.5 represent the envelope of one data symbol (after spreading) in the time domain. (In presenting Figure 6.5, we have assumed all transmit signals correspond to constellation points with maximum amplitude.) The envelope of the composite signal (conceptually) is the linear combination of these N waveforms – a signal with a low PAPR.

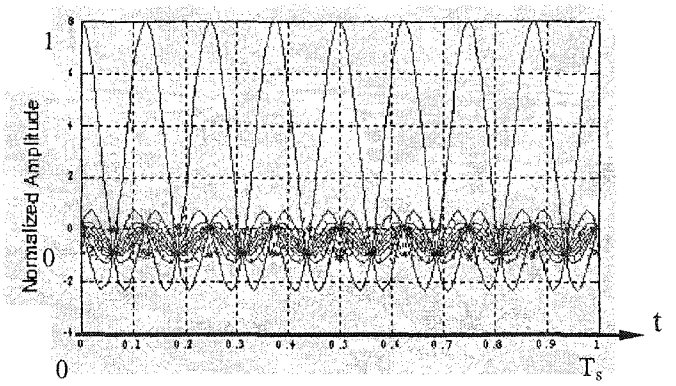

Figure 6.5: Representative transmitted signal of CI/OFDM

When $S^{(k)}(t)$ (in equation (6.4)) reaches its maximum, $S^{(j)}(t)$ (where $(j \neq k)$), is zero. Therefore, we argue that $P_{\max(PO-CI/OFDM)}$ is much less than $P_{\max(OFDM)}$ in almost all OFDM symbols, and considering worst case scenarios:

$$PAPR_{WC(OFDM)} = \frac{N^2 P_o}{NP_o} = N \tag{6.23}$$

and

$$PAPR_{WC(CI/OFDM)} = \frac{\frac{1}{2}\left(\max_{0<t<T_s}|s(t)|\right)^2}{NP_o} << N \tag{6.24}$$

One way in which we can understand how the spreading codes succeed in reducing PAPR (i.e., one way we can confirm the validity of equation (6.24) is to understand the spreading codes as a DFT (FFT) operation, which counters the PAPR problems of the IFFT (mapping one symbol per carrier). That is, the spreading codes selected undo the IFFT operation (resolving the PAPR problem), all the while being easily implemented into the OFDM architecture, and enabling frequency domain processing at the transmitter and receiver. In other words, these spreading codes map the usual OFDM system into a system analogous to the single-carrier frequency domain equalization of [68].

This conceptual presentation of the PAPR benefit of CI/OFDM is confirmed in the simulation of the remaining section.

6.6 CI/OFDM with Higher Order Modulations: Simulated PAPR Benefit

Figures 6.6(a), 6.7(a), and 6.8(a) illustrate typical PAPR values across 10,000 transmissions for a 48-symbol, 48-carrier OFDM system, and Figures 6.6(b)-6.8(b) plot the corresponding PAPR values for a 48-symbol, 48-carrier CI/OFDM system. (We select $N = 48$ carriers as this maintains consistency with the IEEE 802.11a WLAN standard.) Specifically, Figure 6.6 is a plot of PAPR values in QPSK OFDM, Figure 6.7 is a plot for 16-QAM, and Figure 6.8 details the 64-QAM scenario. Referring to Figures 6.6(a), 6.7(a), and 6.8(a), OFDM's PAPR can be characterized as erratic.

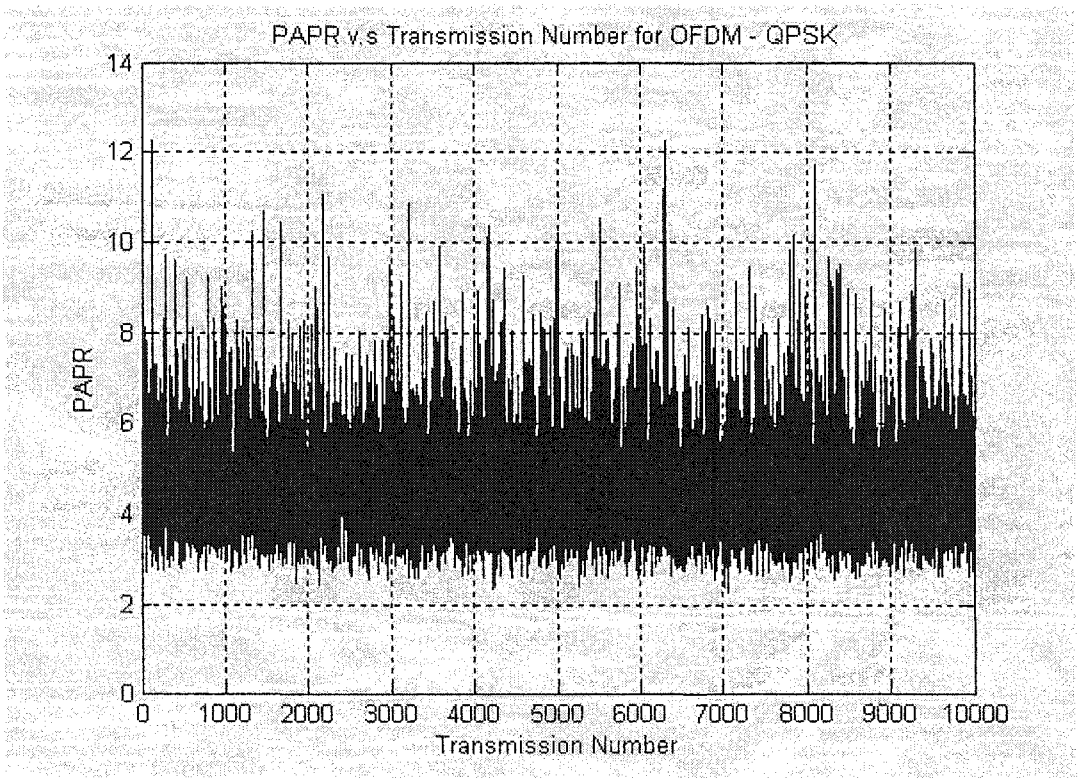

(a)

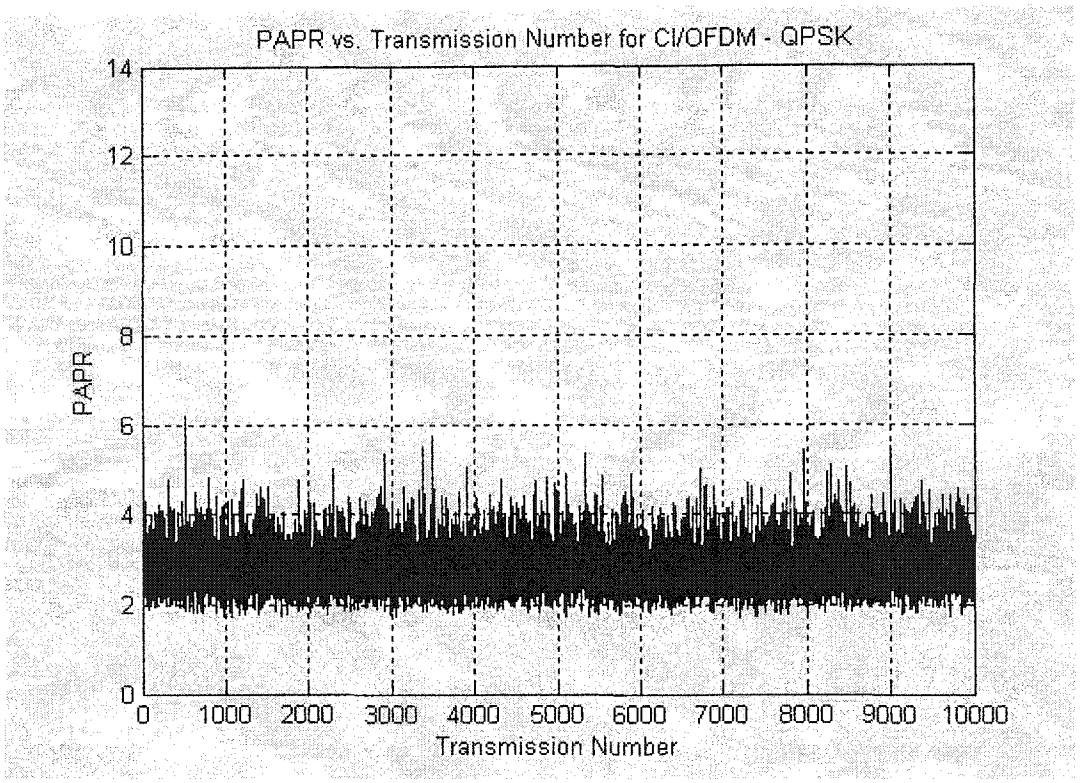

(b)

Figure 6.6: PAPR per Transmission for (a) OFDM–QPSK, (b) CI/OFDM–QPSK

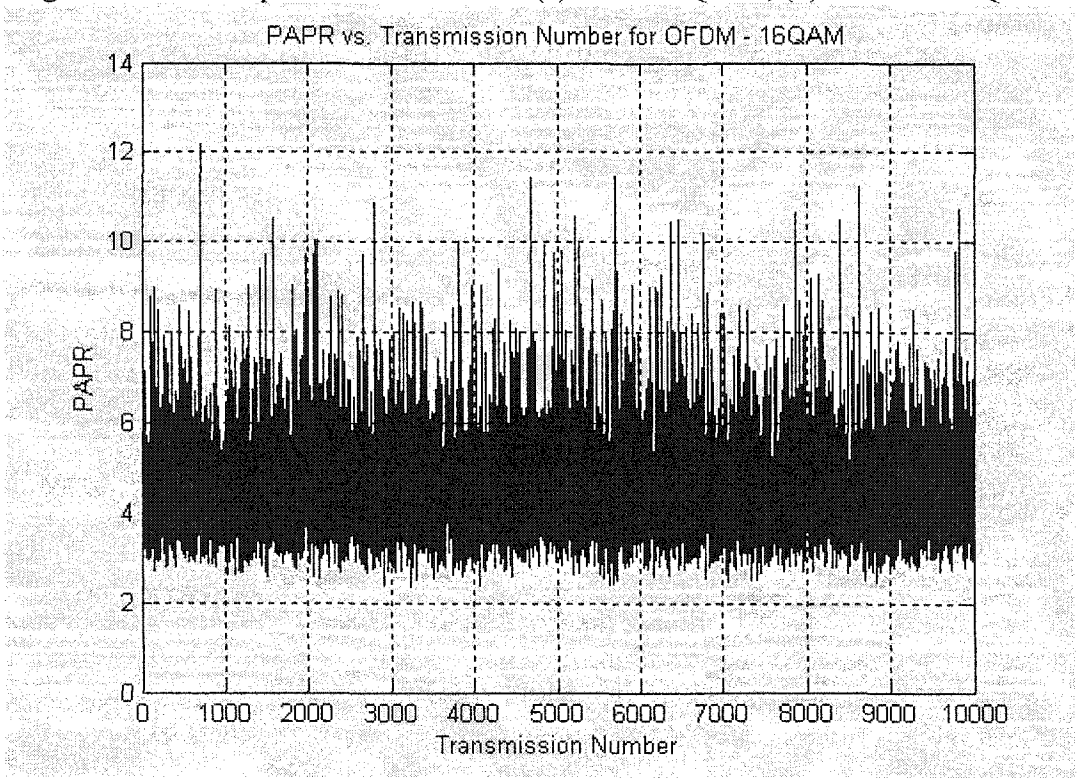

(a)

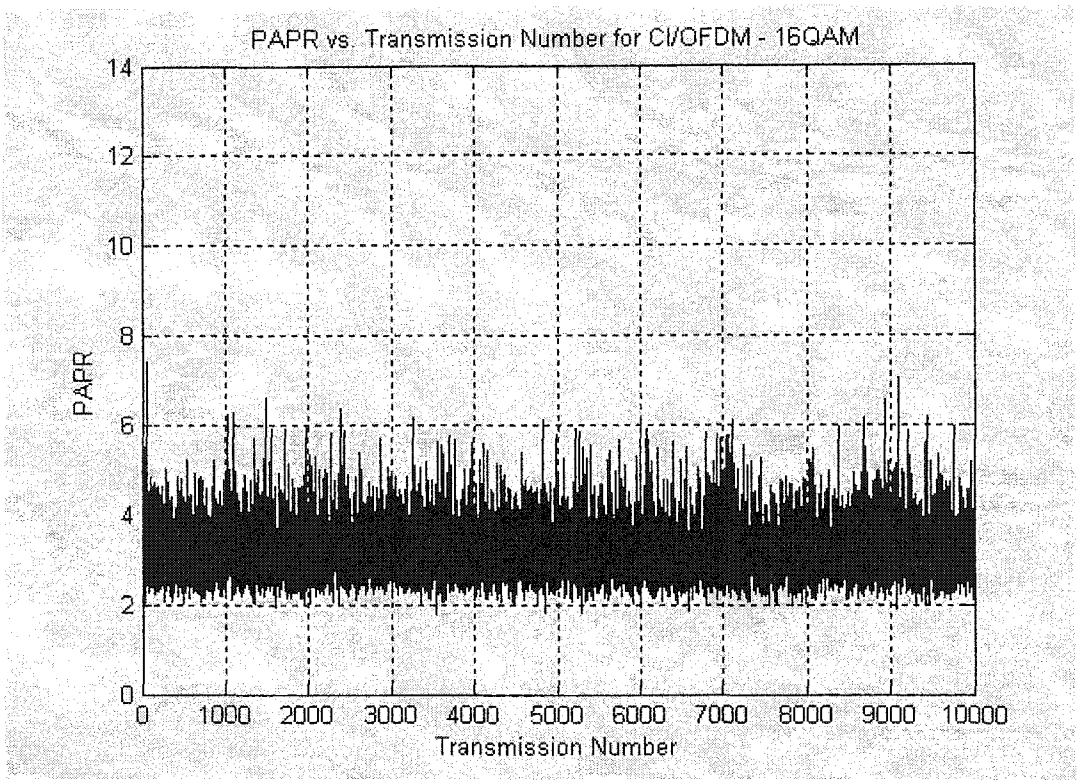

(b)

Figure 6.7: PAPR per Transmission OFDM vs. CI/OFDM – 16-QAM

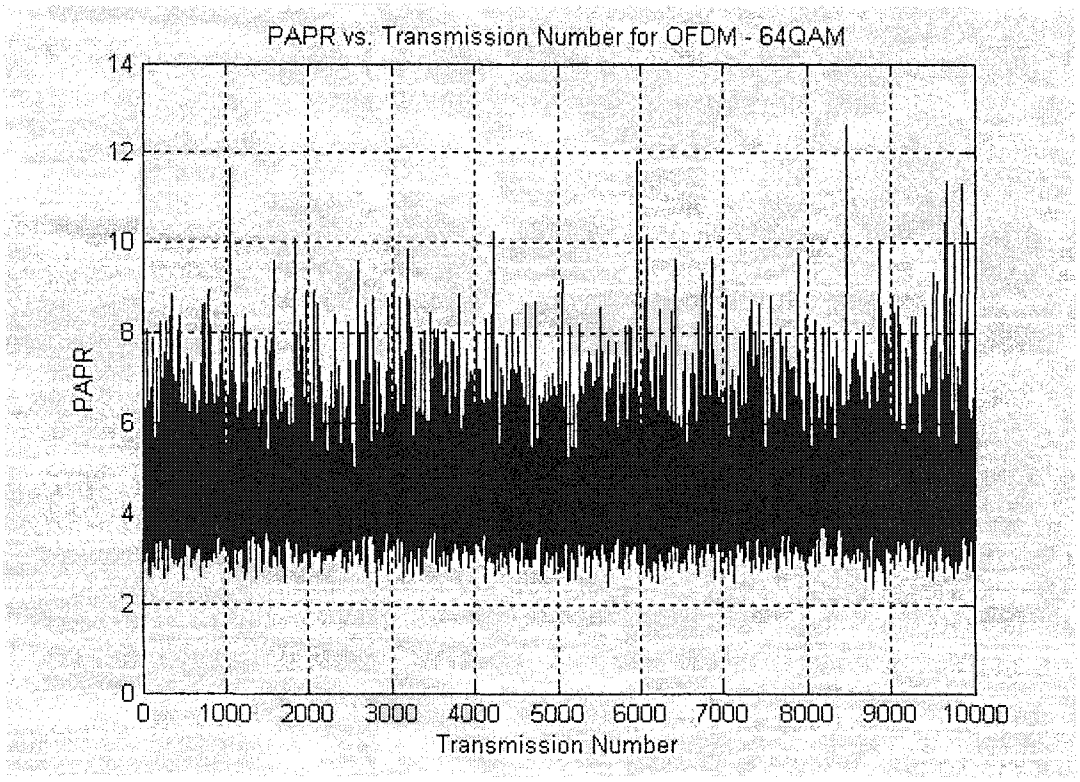

(a)

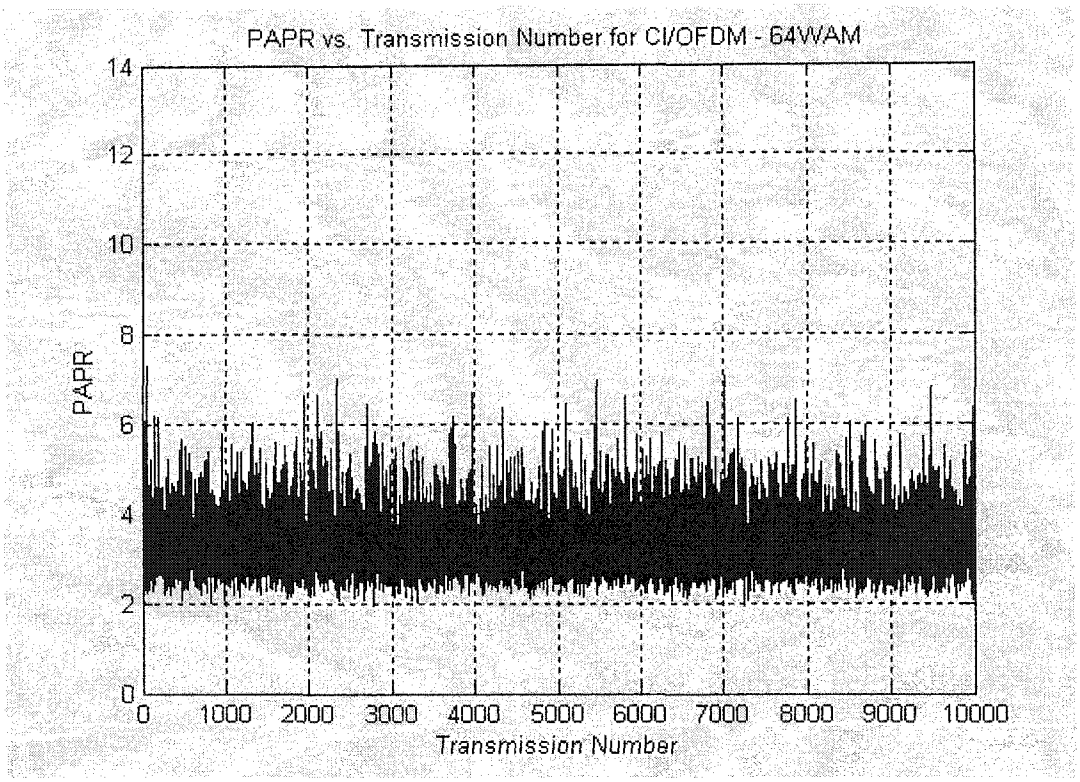

(b)

Figure 6.8: PAPR per Transmission OFDM vs. CI/OFDM – 64-QAM

Tables 6.1, 6.2, and 6.3 provide comparative values of means, variances, and peak values in OFDM vs. CI/OFDM systems. From Tables 6.1-6.3, OFDM displays means of 4.557 (QPSK), 4.532 (16-QAM), and 4.5516 (64-QAM), while CI/OFDM demonstrates means of 2.7927 (QPSK), 3.19 (16-QAM), and 3.3166 (64-QAM).

	OFDM	**CI/OFDM**
Average PAPR	4.5577	2.7927
Variance of PAPR	1.2715	0.2679
Max PAPR	12.2760	6.2046

TABLE 6.1: PAPR per Transmission OFDM vs. CI/OFDM – QPSK

	OFDM	CI/OFDM
Average PAPR	4.5320	3.19
Variance of PAPR	1.2413	0.3996
Max PAPR	12.1826	7.4230

TABLE 6.2: PAPR per Transmission OFDM vs. CI/OFDM – 16-QAM

	OFDM	CI/OFDM
Average PAPR	4.5516	3.3166
Variance of PAPR	1.2317	0.4343
Max PAPR	12.6422	7.3028

TABLE 6.3: PAPR per Transmission OFDM vs. CI/OFDM – 64-QAM

The more dramatic benefits of CI/OFDM, in terms of PAPR, come when comparing both the variance of PAPR and the peak PAPR values. Both variance and peak values are of far greater importance when considering operation within the transmit power amplifier's linear range.

Referring once again to Tables 6.1-6.3, OFDM displays variances of 1.2725 (QPSK), 1.2413 (16-QAM), and 1.2317 (64-QAM), whereas CI/OFDM displays variances of 0.2679 (QPSK), 0.3996 (16-QAM), and 0.4343 (64-QAM). In all three constellation formats, the OFDM variances are roughly a factor of 3 higher than in the proposed CI/OFDM system: The range of values a transmit amplifier must accommodate are far fewer in a CI/OFDM system. Moreover, the peak PAPR values (over a typical

10,000 symbol transmission) in the CI/OFDM system are approximately half of those experienced in the traditional OFDM system (~ 6 for CI/OFDM vs. ~ 12 for OFDM in all three constellation formats).

Figures 6.9, 6.10, and 6.11 compare the cumulative distribution function (CDF) of the PAPR for QPSK, 16-QAM, and 64-QAM respectively (OFDM vs. CI/OFDM), while Table 6.3 displays the 90% and 99% values from Figures 6.9-6.11. Referring to Figures 6.9-6.11, CI/OFDM systems demonstrate a far more desirable CDF than that of OFDM systems, regardless of transmit constellation size or type.

The PAPR benefit of CI/OFDM can translate to an increase in transmission range. Specifically, assume that clipping (due to saturation of the transmit power amplifier) must occur no more than 10% of the time. In this case, referring to Table 6.4, we must not clip any OFDM symbols with PAPR ≤ 6 (any OFDM symbol with PAPR > 6 may be clipped). Therefore, assuming a peak (max) power of 100 mW, the average power = peak power/6 = 16.67 mW.

For CI/OFDM systems (with clipping permitted no more than 10% of the time), a CI/OFDM symbol with PAPR ≤ 4 must experience no clipping (any CI/OFDM symbol with PAPR > 4 may be clipped). Therefore, (again assuming a peak (max) power = 100 mW) the average power = peak power/4 = 25 mW. By direct comparison, we observe that, at a fixed clipping percentage of 10%, a CI/OFDM system may operate with an

average power of 25 mW, whereas an OFDM system must operate at 16.67 mW. That is, CI/OFDM enjoys a 2 dB gain in transmit power.

Continuing the above discussion, the transmit signal in CI/OFDM systems will be received at a signal power of 2 dB more than that of OFDM. Therefore, if we consider that power decreases as a function of r^2, i.e., as a function of 20log(r), additional range equates 20log(r) = 2, i.e., CI/OFDM offers a range-increase-factor of 1.26. If OFDM demonstrates a range of 60 ft., CI/OFDM demonstrates a range of ~76 ft. If OFDM can operate at 90 ft., CI/OFDM operates at ~113 ft.

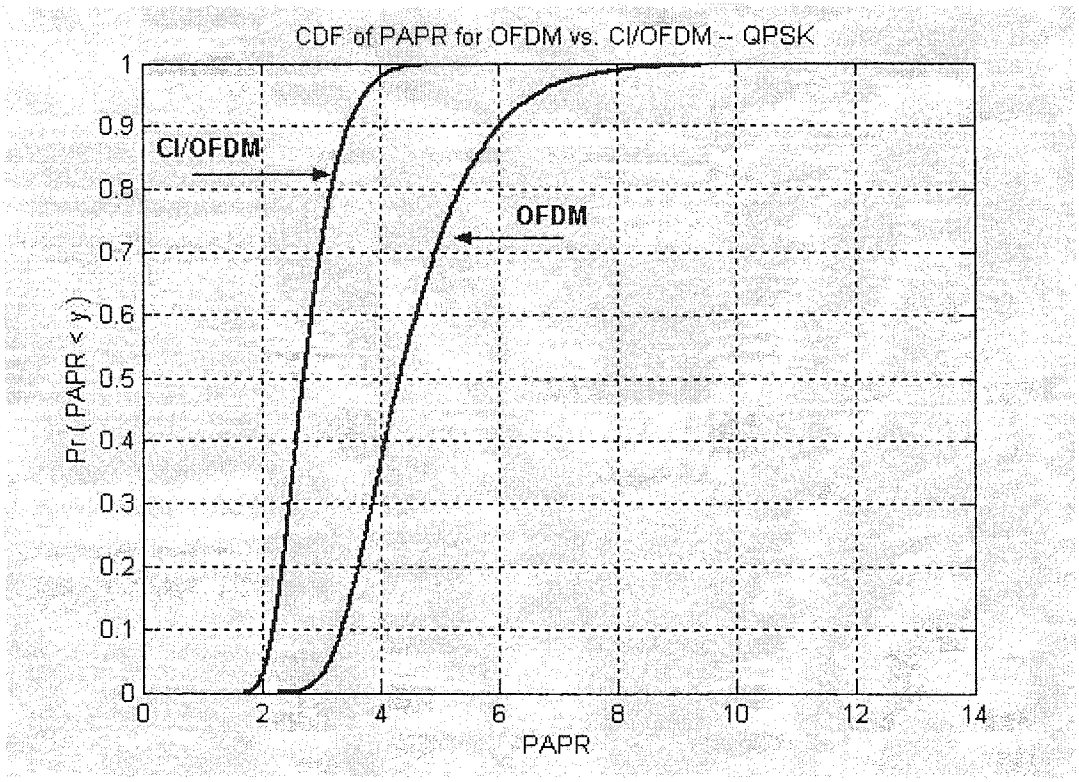

Figure 6.9: Cummulative Distribution Function for PAPR
OFDM vs. CI/OFDM – QPSK

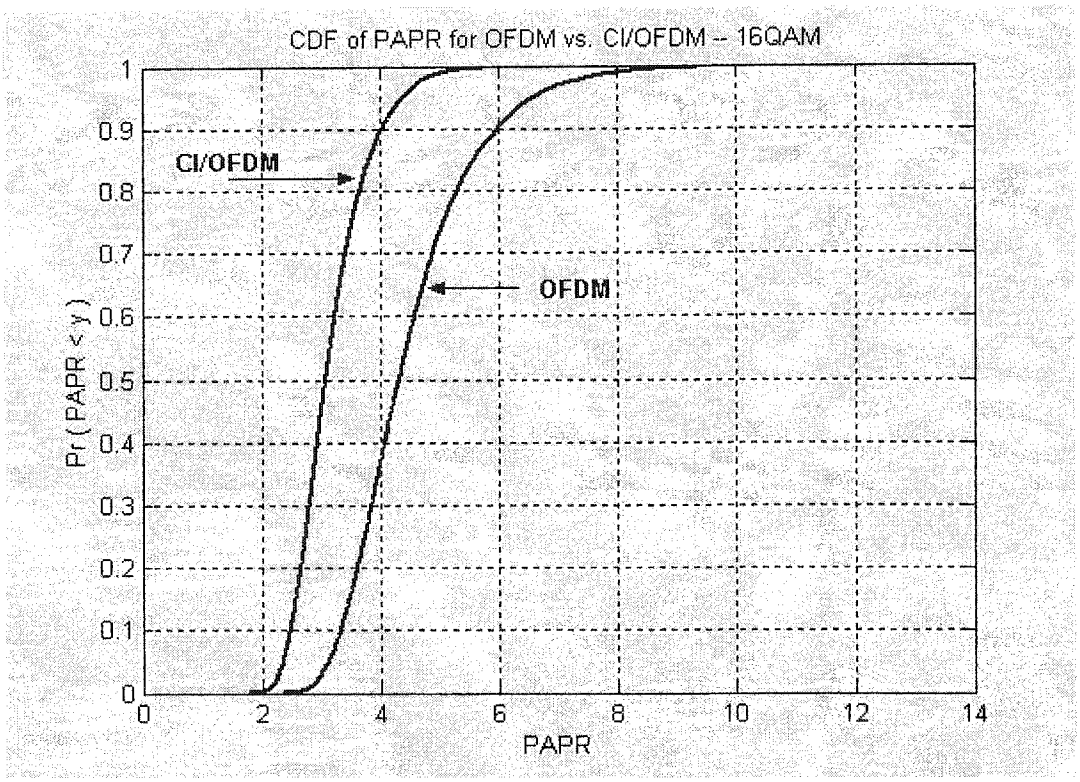

Figure 6.10: Cummulative Distribution Function for PAPR
OFDM vs. CI/OFDM – 16-QAM

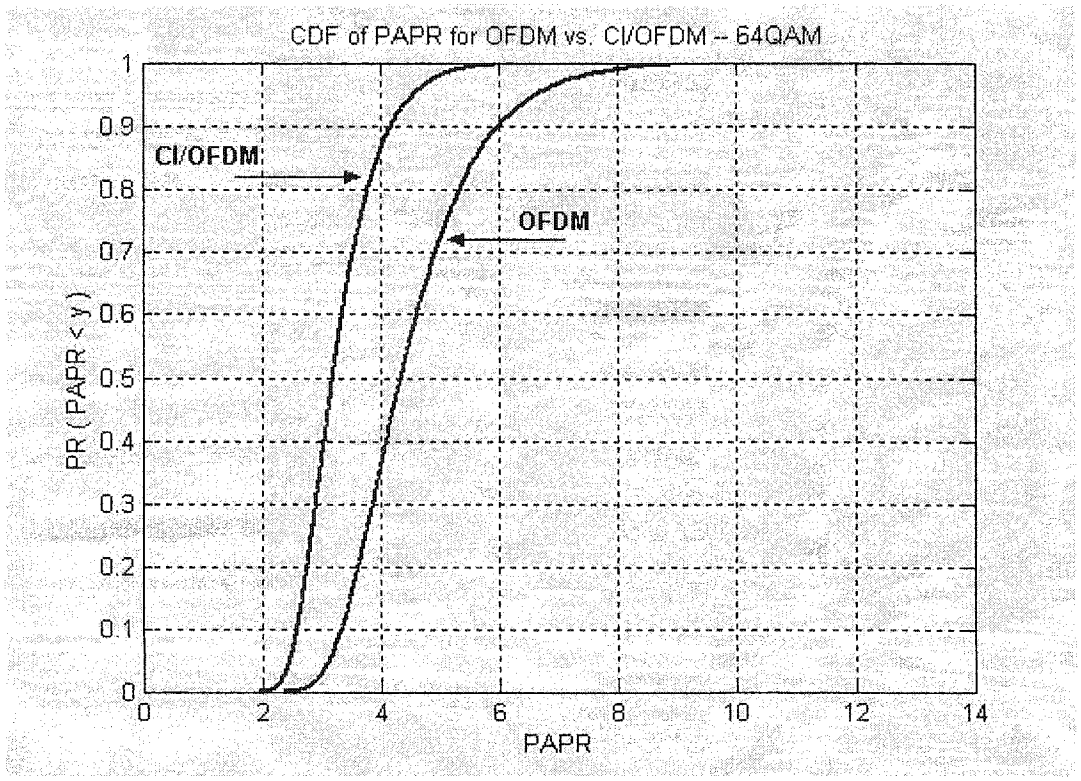

Figure 6.11: Cummulative Distribution Function for PAPR
OFDM vs. CI/OFDM – 64-QAM

		QPSK	16-QAM	64-QAM
90%				
	OFDM	6.0143	5.9953	6.0001
	CI/OFDM	3.4872	4.0379	4.0379
99%				
	OFDM	8.2132	8.115	8.096
	CI/OFDM	4.2932	5.079	5.3824

TABLE 6.4: CDF PAPR Relations for OFDM vs. CI/OFDM

6.7 Conclusions

In this chapter, the performance of CI/OFDM with QAM modulation schemes is analyzed. In frequency selective fading channels, CI/OFDM outperforms OFDM by, e.g., 7 dB (for 16QAM) and 5 dB (for 64QAM) at a BER of 10^{-3} (without any cost in throughput, and with little cost in complexity). This is a direct consequence of CI/OFDM's inherent ability to exploit the frequency diversity available in frequency-selective channels. It also proves that the increased interference created in multiple constellation symbols per carrier is more than compensated for via the CI technique of exploiting the frequency diversity of the channel.

We also demonstrated that the PAPR benefits of the CI/OFDM architecture extend to multiple higher-order constellations. We observe that regardless of constellation size (2, 4, 16 or 64) or type (PSK or QAM), CI spreading codes eliminate

high peaks in transmit power by careful creation of the per-symbol envelopes. Problems associated with large PAPR (in terms of complexity, e.g., coding, or out-of-band distortion, e.g., clipping) are eliminated. In short, excellent transmit PAPR is available via CI codes regardless of constellation size or type.

Part IV:

CI/OFDM RF Testing

Chapter 7 Application of CI/OFDM to IEEE 802.11a,g WLAN: Emulation and RF Testing

The emerging Wireless Local Area Networks (WLANs) represent tether-less broadband networks capable of supporting a variety of multimedia applications. These networks promise to bridge the gap between the dependable high-throughput wired world and the convenience of the wireless world.

Intense research in the area of Wireless Local Area Networks (WLANs) has been ongoing for the past decade (e.g., [69-73]). Coupling the research efforts with a standardization effort, the IEEE 802.11a 5 GHz WLAN standard [17] has emerged. Under IEEE 802.11a Physical Layer (PHY) specifications [74], Orthogonal Frequency Division Multiplexing (OFDM) is the modulation scheme of choice. OFDM is selected because of its well-known ability to avoid multipath effects while supporting high data rates: By serial-to-parallel converting one high-rate symbol stream into N low rate symbol streams, and transmitting each parallel stream over its own orthogonal carrier, the data rate in OFDM (per carrier) is effectively reduced by a factor of N from the original data rate. Hence, the bandwidth per carrier is only $(1/N)^{th}$ of the overall system bandwidth and, as a result, each carrier now experiences a flat fade upon transmission

[19]. Utilizing this OFDM strategy in WLAN minimizes the impact of multipath in frequency selective channels.

7.1 Introduction to CI/OFDM in IEEE 802.11a WLAN

One concern in OFDM, and therefore IEEE 802.11a, is that each carrier experiences a flat fade, and, hence, each carrier arrives at the receiver with a different amplitude. Even in the presence of very sensitive equalizers, data is lost in deep fades. WLAN systems combat this problem via the addition of redundancy, incorporating Forward Error Correction (FEC) convolutional coding (of rate $1/n$) into the PHY prior to OFDM modulation and transmission, effectively allowing each symbol to be sent over n distinct frequencies. This introduction of redundancy and frequency diversity overcomes much of the signal degradation due to fading. The downside of such a coding is reduced throughput (by a factor of n).

As presented in Chapters 2-6, many of OFDM's shortcomings may be overcome by the introduction of Carrier Interferometry (CI) spreading codes, which dramatically improve the performance of OFDM and COFDM. In the so-called CI/OFDM, *each* of the N low rate parallel symbol streams is *simultaneously* modulated onto *all* N carriers by application of a unique orthogonal complex spreading sequence (applied in the frequency

domain). This creates frequency diversity benefits for each symbol stream, leading to high performances *without* a decrease in throughput.

In this chapter, we apply Carrier-Interferometry OFDM to WLAN, creating CI-WLAN. We demonstrate how, in an indoor office test environment at a probability of error of 10^{-3}, our CI-WLAN gains 3 dB in performance over WLAN.

7.2 IEEE 802.11a Physical Layer

Figure 7.1 illustrates the main transmission blocks for WLAN as specified by IEEE 802.11a [74]. Referring to the "channel coder" block, channel coding is derived from a rate ½, constraint length 7 convolutional code utilizing 133 and 171 generator polynomials. Rates ⅔ and ¾ are available through puncturing. The "interleaver" block of Figure 6.1 serves a two-fold purpose: First, it ensures adjacent, coded bits are sent on non-adjacent carriers, and second, it alternates assignment of the adjacent, coded bits to constellation bits of greater and lesser importance. Following the interleaver is the "mapper," where, the carrier modulation scheme (BPSK, QPSK, 16QAM, or 64QAM) is employed. Situation dependent data rates of 6, 9, 12, 18, 24, 36, 48, and 54 Mbits/s are possible through appropriate choice of channel coding rate and symbol modulation ("mapper") scheme. The "OFDM modulator" block represents a 52 carrier OFDM

modulation scheme (i.e., the OFDM transmitter of Chapter 2, Figure 2.1), operating in the 5 GHz frequency band: 48 of the 52 carriers are information bearing and the remaining 4 contain pilot information necessary for phase tracking in coherent detection. Carrier spacing (Δf) is 312.5 kHz.

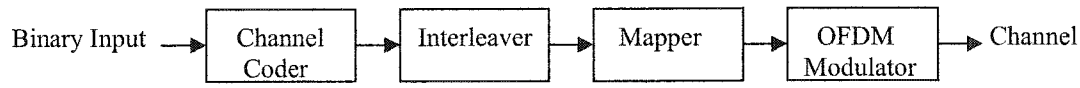

Figure 7.1: Simplified PHY Transmission Train for WLAN

7.3 CI-WLAN Transmitter Architecture

The usual OFDM modulator in WLAN is shown in Figure 7.2(a), whereas the proposed CI/OFDM modulator structure for CI-WLAN is shown in Figures 7.2(b) and 7.2(c). To review, both OFDM and CI/OFDM serial-to-parallel convert the high-rate input symbol stream. Next, in OFDM, each low-rate symbol stream is modulated onto its own carrier and sent out over the channel. The symbol stream-to-carrier mapping in OFDM can be described as follows: the spreading code $c_k(t) = \sum_{i=0}^{N-1} \beta_k^i e^{j2\pi i \Delta f t}$ is applied to symbol stream k where $\beta_k^k = 1$ and $\beta_k^j = 0$ $(j \neq k)$.

In CI/OFDM, on the other hand, *each* low-rate symbol stream is spread onto *all* of the N carriers. Specifically, the spreading code $c_k(t) = \sum_{i=0}^{N-1} \beta_k^i e^{j2\pi i \Delta f t}$ is applied to symbol stream k, where $\beta_k^i = e^{j\theta_k^i}$, and $\theta_k^i = \frac{2\pi}{N} \cdot k \cdot i$ has been carefully selected to allow symbol stream k to be separable at the receiver from the other symbols located on identical carriers. In other words, the spreading sequence $\{\beta_k^0, \beta_k^1, \ldots, \beta_k^{N-1}\} = \{e^{j\theta_k^0}, e^{j\theta_k^1}, \ldots, e^{j\theta_k^{N-1}}\}$ applied to symbol stream k is selected to ensure orthogonality between $K = N$ transmitted symbol streams, even though symbol streams occupy the same carriers at the same time.

That is, CI/OFDM's spreading sequences (referring to Chapter 3) simultaneously support $K = N$ orthogonal symbol streams by selecting N spreading sequences corresponding to:

$$\{\beta_k^0, \beta_k^1, \ldots, \beta_k^{N-1}\} = \{e^{j\theta_k^0}, e^{j\theta_k^1}, \ldots, e^{j\theta_k^{N-1}}\} = \left\{e^{j\frac{2\pi}{N}\cdot 0\cdot k}, e^{j\frac{2\pi}{N}1\cdot k}, \ldots, e^{j\frac{2\pi}{N}(N-1)k}\right\} \quad (7.1)$$

The transmitted signal for the k^{th} symbol stream (k^{th} branch out of the serial-to-parallel converter) in CI/OFDM (and therefore CI-WLAN) is:

$$s_k(t) = A \cdot \mathrm{Re}\{a_k^n c_k(t) e^{j2\pi f_c t}\} \quad (7.2)$$

$$s_k(t) = A \cdot \mathrm{Re}\left\{ a_k^n \sum_{i=0}^{N-1} e^{j\vartheta_k^i} e^{j2\pi i\Delta ft} e^{j2\pi f_c t} \right\} \tag{7.3}$$

$$s_k(t) = A \cdot \sum_{i=0}^{N-1} a_k^n \cos\left(2\pi f_c t + 2\pi f_i t + \frac{2\pi}{N} i \cdot k \right) \tag{7.4}$$

where: (1) a_k^n is the n^{th} symbol in the k^{th} symbol stream and is assumed to be +1 or –1 with equal probability (in this chapter, for ease in presentation); (2) $f_i = i\Delta f$, and $\Delta f = 1/T_S$ (T_S is the symbol rate after serial-to-parallel conversion) to assure orthogonality among carriers; and (3) A is a parameter used to establish the symbol energy.

When this strategy is applied to the 802.11a transmission train model of Figure 7.1, the transmitter operates as follows: (1) each m input bits (e.g., m = 1) are first channel coded to n output bits (e.g., n = 2) (puncturing is applied to create lower rate FECs as necessary); (2) interleaving follows where the n coded bits are interleaved such that they are sent at different OFDM symbol times (with a time separation selected to create a time diversity benefit); (3) next is bit-to-PSK or bit-to-QAM symbol mapping; (4) followed by the CI/OFDM modulator block characterized by Figures 7.2(b) and (c) and equations (7.1) – (7.4). Hence, CI-WLAN benefits from (1) coding gain, (2) time diversity benefit, and (3) frequency diversity gain via the spreading. Figure 6.2 illustrates the CI-WLAN PHY transmitter architecture.

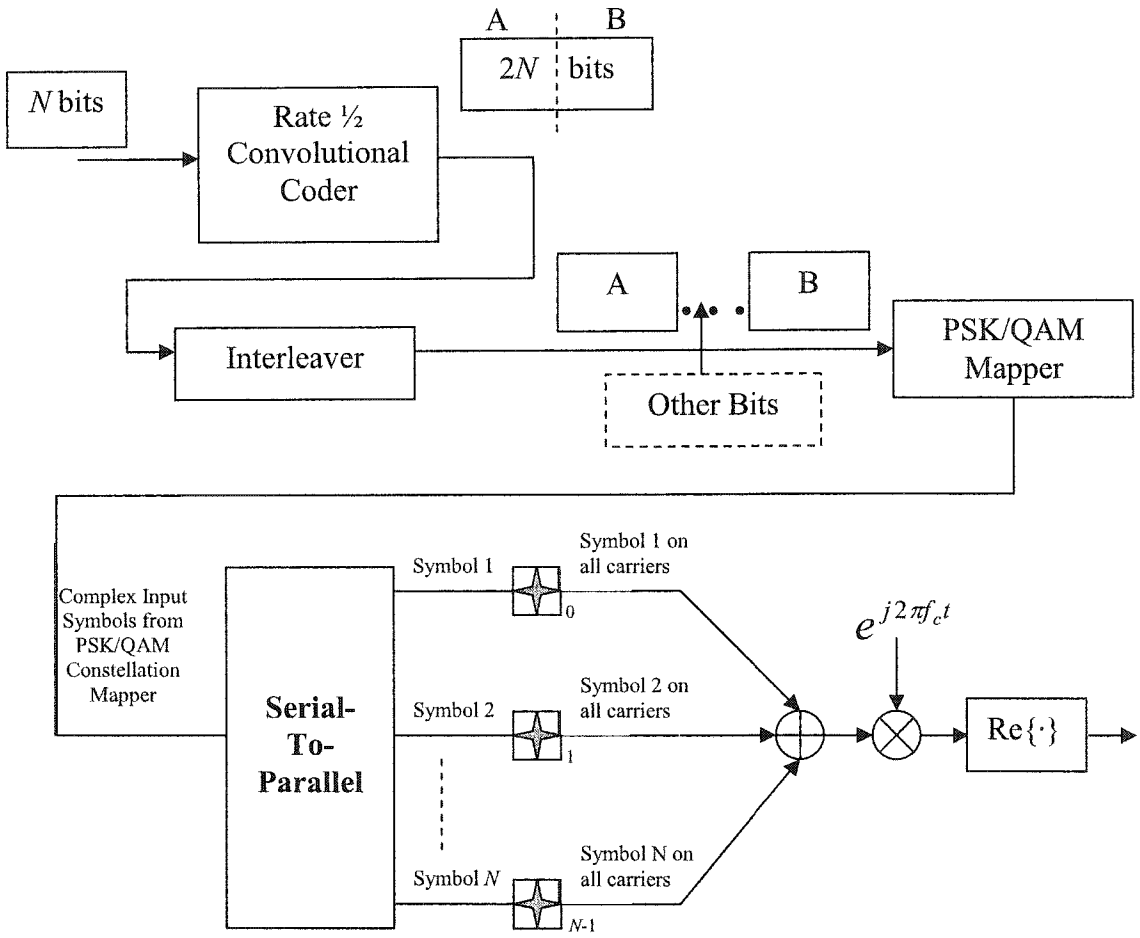

Figure 7.2: CI-WLAN

7.4 Receiver Architecture

After transmission over a slow frequency-selective fading channel (typical of WLAN transmissions), each received carrier experiences a unique flat fade. Assuming the sent signal *s(t)* from (7.4), the received signal is mathematically characterized by the following equation:

$$r(t) = A \cdot \sum_{k=0}^{N-1} \sum_{i=0}^{N-1} \alpha_i a_k^n \cos\left(2\pi f_c t + 2\pi f_i t + \frac{2\pi}{N} i \cdot k + \phi_i \right) + n(t) \tag{7.5}$$

where (1) α_i and ϕ_i are the fade parameter and phase offset, respectively, introduced into the i^{th} carrier by the frequency selective fading channel, and (2) *n(t)* is additive white Gaussian noise (AWGN). Perfect phase synchronization is assumed for simplicity in presentation.

Figure 7.3 depicts the CI-WLAN receiver for detection of the k^{th} symbol stream (conceptually).

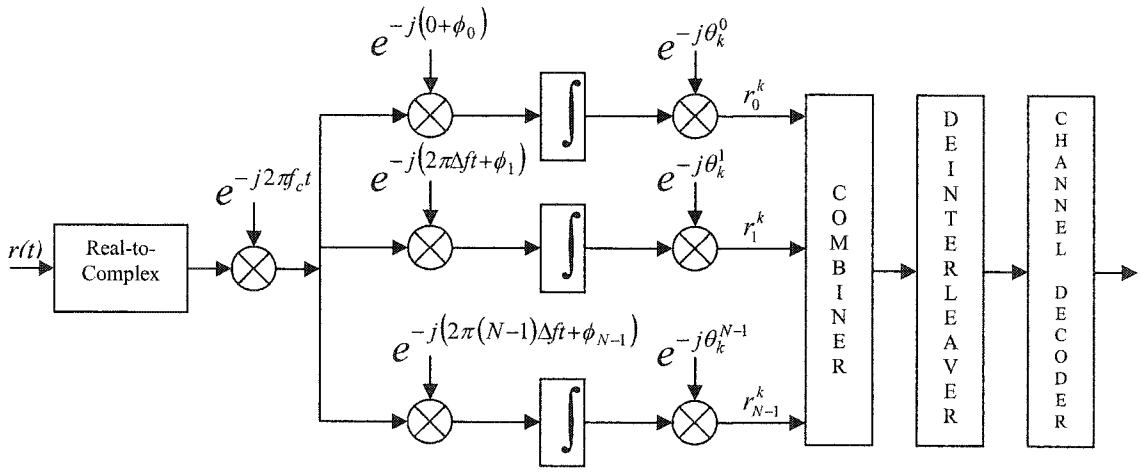

Figure 7.3: CI-WLAN receiver

The receiver separates *r(t)* into its *N* orthogonal carriers (typically implemented as an FFT), then removes the k^{th} symbol stream's phase offset from each carrier (i.e., despreads). This results in the decision vector,

$$\underline{r}_k^n = \left(r_k^n(0), r_k^n(1), \ldots, r_k^n(N-1)\right) \tag{7.6}$$

$$r_k^n(i) = A \cdot \alpha_i a_k^n + A \cdot \sum_{j=0, j\neq k}^{N-1} \alpha_i a_j^n \cos\left(i\left(\frac{2\pi}{N}k - \frac{2\pi}{N}j\right)\right) + n_i \tag{7.7}$$

The first term in (7.7) represents the presence of the desired symbol in the i^{th} carrier, the second term represents the presence of the *N-1* other symbols spread onto the same carrier, and the final term is a Gaussian random variable of mean 0 and variance $N_o/2$ representing the impact of AWGN. A combining strategy is then employed to help restore orthogonality between symbol streams, maximize frequency diversity benefits, and/or minimize noise. In an AWGN or flat fading channel, i.e., whenever $\alpha_1 = \alpha_2 = \cdots = \alpha_N$, the optimal combining is equal gain combining (EGC). That is, by performing $C_k^n = \sum_{i=0}^{N-1} r_k^n(i)$, we restore orthogonality between codes, minimizes correlation between pseudo-orthogonal codes, and minimize noise. The equal gain combining across decision vector components $r_k^n(i)$, however, is not an optimal strategy in a frequency selective channel (due to the carrier dependent fade, α_i). In such channels, a minimum mean square error combining (MMSEC) offers a performance close to that of optimal

ML (Maximum Likelihood) methods [75]. Specifically, MMSEC jointly minimizes interference from other spreading codes and noise, while exploiting frequency diversity. Employing MMSE combining in the receiver leads to the decision variable:

$$C_k^n = \sum_{i=0}^{N-1} r_k^n(i) \bullet \left[\frac{\alpha_i}{N p_i \alpha_i^2 + N_o / 2} \right] \tag{7.8}$$

where p_i is a known constant for carrier i: When N symbol streams are spread over the N OFDM carriers with orthogonal CI codes,

$$p_i = \begin{cases} 1, & i = 0, \frac{N}{2} \\ \frac{1}{2}, & else \end{cases} \tag{7.9}$$

Returning to the CI-WLAN receiver cascade of Figure 7.3, the combiner output C_k^n is then input into a deinterleaver, followed by a soft decision decoding Viterbi Algorithm (VA) performing channel decoding.

7.5 Simulated Performance Results

For simulation purposes, WLAN system parameters were carefully selected. At the WLAN transmitter, (1) the convolutional coding applied is rate ½ with constraint length 3; and, (2) bit-to-BPSK mapping is employed. To emulate realistic wireless environments, we assume a Rayleigh fading channel with frequency selectivity over the entire bandwidth, *BW*, but flat fading over each of the *N* carriers. Since it is possible for root mean squared (rms) values of delay spread (T_m) to vary from 20-50 ns for small office/home office (SOHO) and from 50-100 ns for large office buildings [76], rms delay spreads of 35 ns and 100 ns, as specified by the UMTS channel model [77], were utilized. These delay spreads create a 2.8-fold and an 8.125-fold frequency diversity, respectively, over the entire bandwidth. With this characterization, the correlation of the channel fades (α_i's) corresponds to [55]:

$$R_{i,j} = \frac{1}{1+\left(\frac{\Delta f_{i,j}}{(\Delta f_c)}\right)^2} \tag{7.10}$$

where $R_{i,j}$ is the correlation between carrier *i's* fade and carrier *j's* fade, $\Delta f_{i,j}$ is the frequency separation (312.5(i-j) kHz) between these two carriers, and $(\Delta f)_c$ is the channel coherence bandwidth (well approximated by $1/5T_m$).

Simulation results are presented in Figure 7.4, where curves are labeled using the following definitions. (1) AWGN, demonstrated by a dashed line, refers to the ideal

performance of BPSK in an additive white Gaussian noise (AWGN) channel. (2) WLAN refers to the performance of IEEE 802.11a as proposed in the standard (with BPSK) and with traditional Coded OFDM transmitting 24 information bits on its 48 carriers (the remaining 24 bits are redundant bits generated from the channel coder). (3) CI-WLAN refers to WLAN employing CI/OFDM to replace traditional OFDM, when $N = 48$ symbol streams are sent on $N = 48$ carriers by application of the CI orthogonal spreading codes (equation (7.1)). Here, of the 48 BPSK symbol streams, 24 are information bearing and 24 contain the redundancy generated by channel coding.

Referring to Figure 7.4, we observe, at a BER of 10^{-3}, the CI-WLAN system in the large office building environment (i.e., $T_m = 100$ ns) outperforms current WLAN by 3 dB. Even in the SOHO environment (i.e., $T_m = 35$ ns), where frequency diversity is small, the CI-WLAN system outperforms WLAN by 1 dB. We can also see that variation in delay spread, from 35 ns to 100 ns, has no effect on the traditional WLAN system. This is because only a limited frequency diversity is exploited in current WLAN systems. The CI-WLAN architecture, on the other hand, exploits the full frequency diversity available on the channel. Preliminary results for channels with higher delay spreads (i.e., large warehouses and outdoor pedestrian) show the performance gain of CI-WLAN, relative to WLAN, continuing to increase.

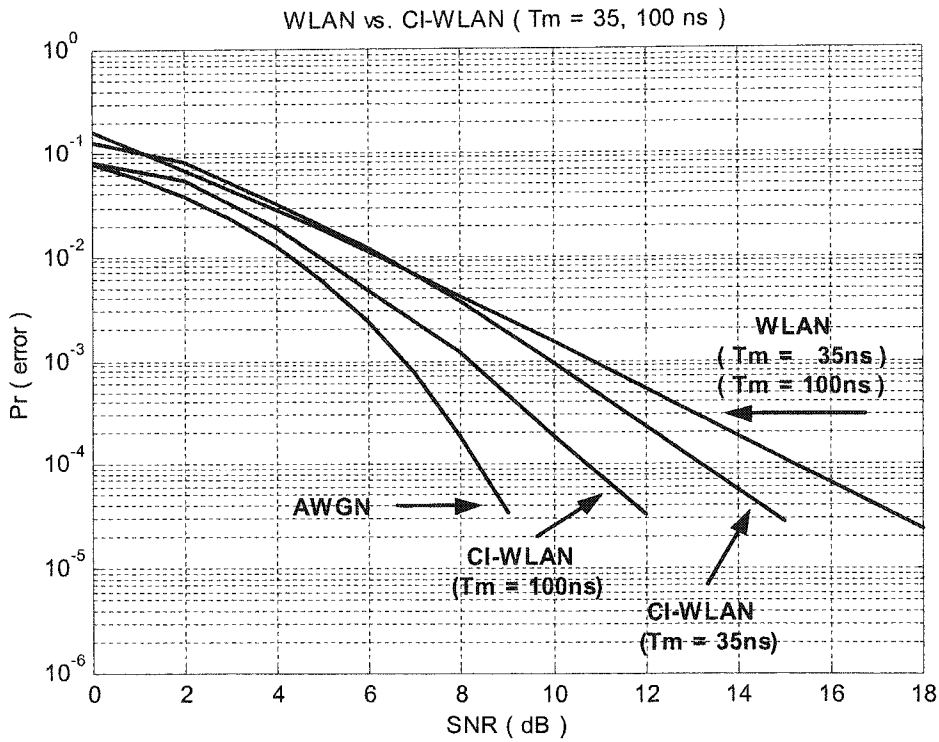

Figure 7.4: Performance results for WLAN vs. CI-WLAN

7.6 RF Testing of the CI-WLAN System

RF testing was performed in May 2002 to compare WLANs and CI-WLANs. The equipment setup is illustrated in Figure 7.6. Referring to Figure 7.6, a laptop computer, running the Agilent Signal Studio software package, generates OFDM and COFDM transmit signals in a manner consistent with the IEEE 802.11a standard. That is, the output of the laptop corresponds to the output of the transmit chain of Figure 7.5. Specifically, (1) pseudo-random bits are input into a convolutional encoder, (2) encoded bits are fed into the interleaver, (3) encoded and interleaved bits enter a bit-to-symbol

mapper (e.g., bit-to-BPSK mapper), (4) header information is appended to the data, and finally, (5) the header and data enter an IFFT (Inverse Fast Fourier Transform), which acts as the OFDM modulator block (here, the 4 pilot tones are inserted).

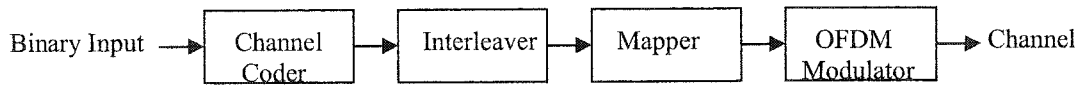

Figure 7.5: Simplified PHY Transmission Train for WLAN

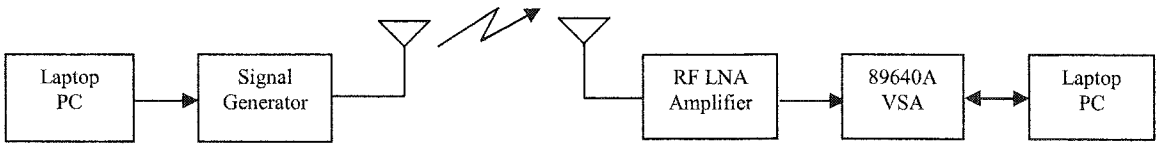

Figure 7.6: Generalized block diagram of testing setup

To generate a WLAN and CI-WLAN, the "OFDM modulator block," in Figure 7.5, is replaced by a "CI/OFDM modulator block," matching Figure7.2. This change was enabled in the software of the Agilent Signal Studio software package (with the direct support of Agilent software engineers). This allowed each incoming data symbol to be spread across all N (48) carriers by application of CI spreading codes. It is important to note that the CI spreading codes were *only* applied to the data portion of the signal -- *the header information (as well as the pilot tones) were left untouched.* Specifically, the

short and long training sequences, along with the cyclic prefixes, *were not* CI encoded, enabling traditional detection of header (and training) information at the receiver (the Agilent 89640A Vector Signal Analyzer). Figure 7.7 shows the Agilent Signal Studio software's interactive screen.

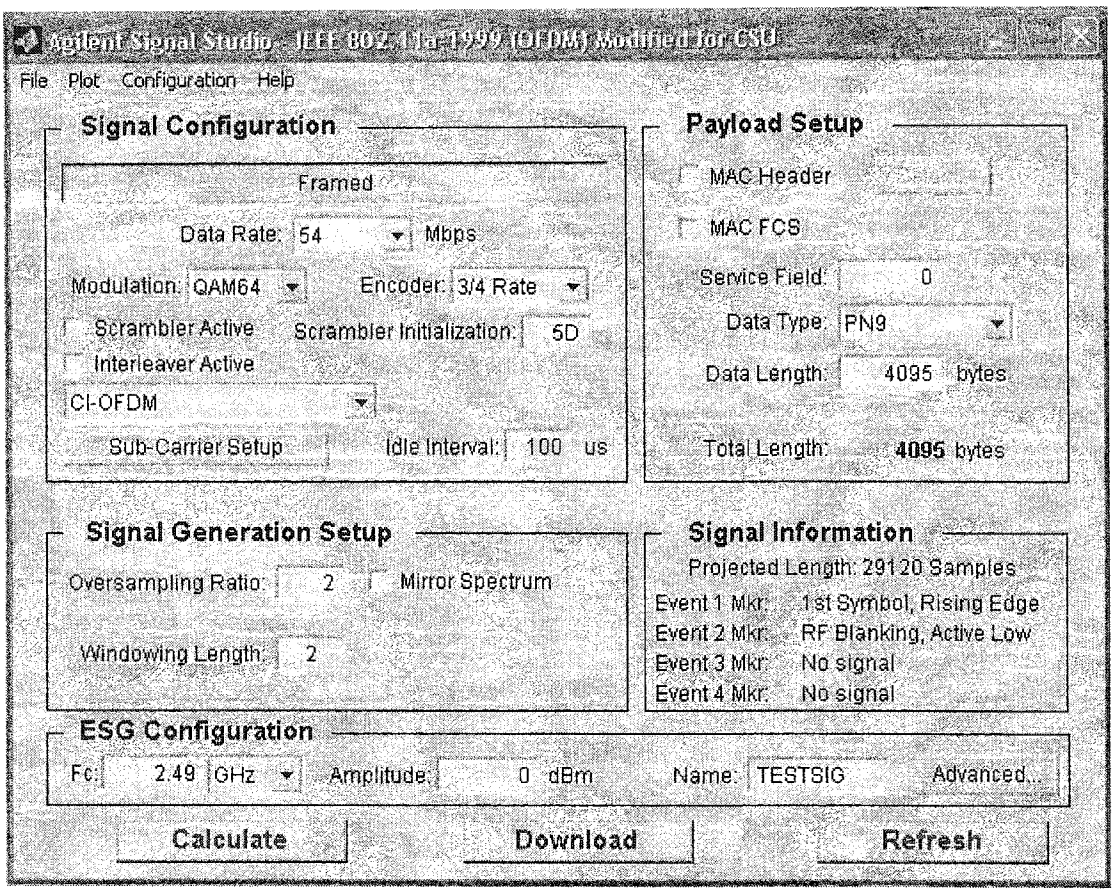

Figure 7.7: Modified Agilent Signal Studio Interactive Program

Referring to Figure 7.7, it can be seen that any of the IEEE 802.11a characteristics can be defined (e.g., modulation (shown as QAM64) and coding rate (shown as ¾ Rate). The "OFDM Modulator" block (OFDM transmitter of Figure 2.1) can also be updated to

reflect the CI/OFDM modulator block (shown in Figure 7.7 as CI-OFDM). Finally, the software also grants the ability to change the input data stream (shown in Figure 7.7 as Data Type: PN9). Input data sequences for both OFDM and CI/OFDM (or COFDM and CI/COFDM) were generated via binary pseudo-random input generators. Each trial consisted of 198 symbols x 48 carriers x 1 BPSK bit/symbol, or 9,504 data bits/packet. When rate ½ channel coding was enabled, the number of information bits per packet corresponded to 4,752 information bearing data bits/packet.

Returning to Figure 7.6, the OFDM symbols or CI/OFDM symbols were downloaded from the laptop to an Agilent E4438C Signal Generator via a standard bi-directional LAN cable. The E4438C signal generator output corresponds to the OFDM or CI/OFDM packet modulated to 2.49 GHz. The RF signal was fed into an omnidirectional antenna with 4 dBi gain, and the transmission power was varied up to +3 dBm. The transmit RF signal traveled over the indoor office test environment, discussed next.

Figure 7.8 illustrates the office test environment in Superior, Colorado, consisting of component cubical offices. As seen in Figure 7.8, two transmit locations were selected, with transmitter/receiver separation distances of 87 feet and 117 feet respectively. In both cases, the reflectors include four walls, a stairwell, and several office cubicles. The transmit antenna was located at a height of 4 feet, while the receive antenna was located at a height of 6 feet (to emulate an access point on an average shelf).

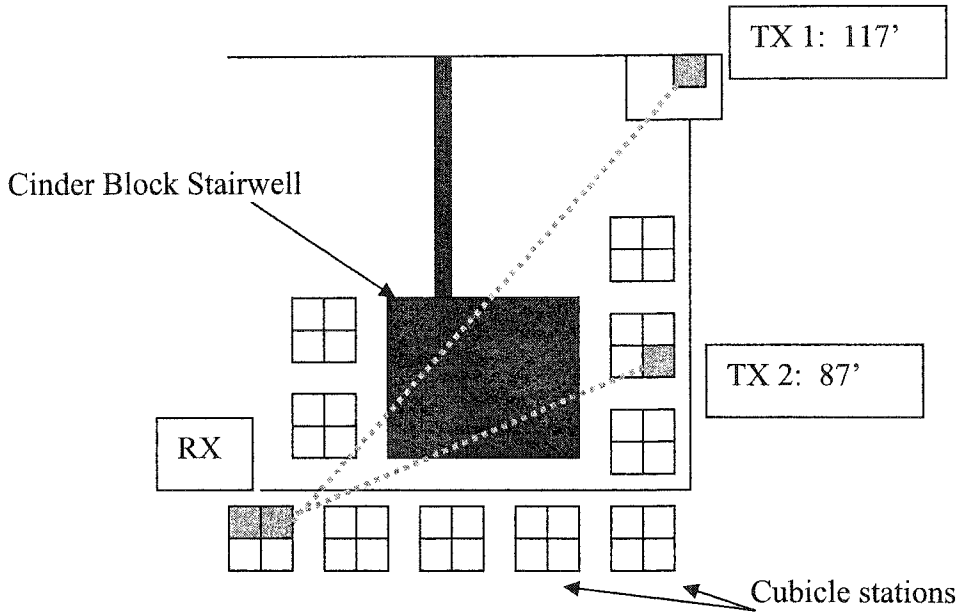

Figure 7.8: Indoor Office Test Environment

At the receive side (Figure 7.6), the signal is received via an omnidirectional antenna with 4 dBi gain, and is passed through a 26 dB gain Low Noise Amplifier (LNA). Finally, the received signal enters the Agilent 89640A Vector Signal Analyzer (VSA). The VSA is configured to receive an IEEE 802.11a formatted signal at 2.49 GHz. This Agilent VSA (1) utilizes the short and long training sequences to perform frequency and phase synchronization, (2) removes the cyclic prefix, and (3) performs a decomposition of the OFDM symbol into multiple carriers, by application of an FFT (Fast Fourier Transform). Using an IEEE 1394 firewire, this data is restored in a laptop where the remainder of the receiver operations are implemented via Matlab. (For

example, in COFDM, signals are deinterleaved and fed into a soft decision decoding Viterbi Algorithm (VA).)

In CI/OFDM, the laptop (via Matlab code) implements the MMSE combiner of Section 7.4 (which utilizes the channel fade information as well as an estimate of the noise power). The output of this MMSEC operation is then input through the deinterleaver, followed by the soft decision decoding VA.

A BER analysis was performed upon completion of the respective receive processes. The results of the analysis are detailed next.

7.7 RF Testing of the CI-WLAN System: Results

Figure 7.9 illustrates the bit error rate (BER) versus transmit power for OFDM, COFDM, CI/OFDM, and CI/COFDM when implementing the RF testing detailed in Section 7.6. Referring to Figure 7.9, we see that at BERs between 10^{-3} and 10^{-4}, the CI/OFDM WLAN system consistently outperforms traditional OFDM WLAN by 5-7 dB. This is a direct consequence of the frequency diversity gain exploited by the spreading codes of the CI/OFDM architecture. The loss due to inter-symbol interference in CI/OFDM reception (equation (7.7)), is more then compensated for by the gain achieved via diversity (sending the same symbol over the $N = 48$ carriers).

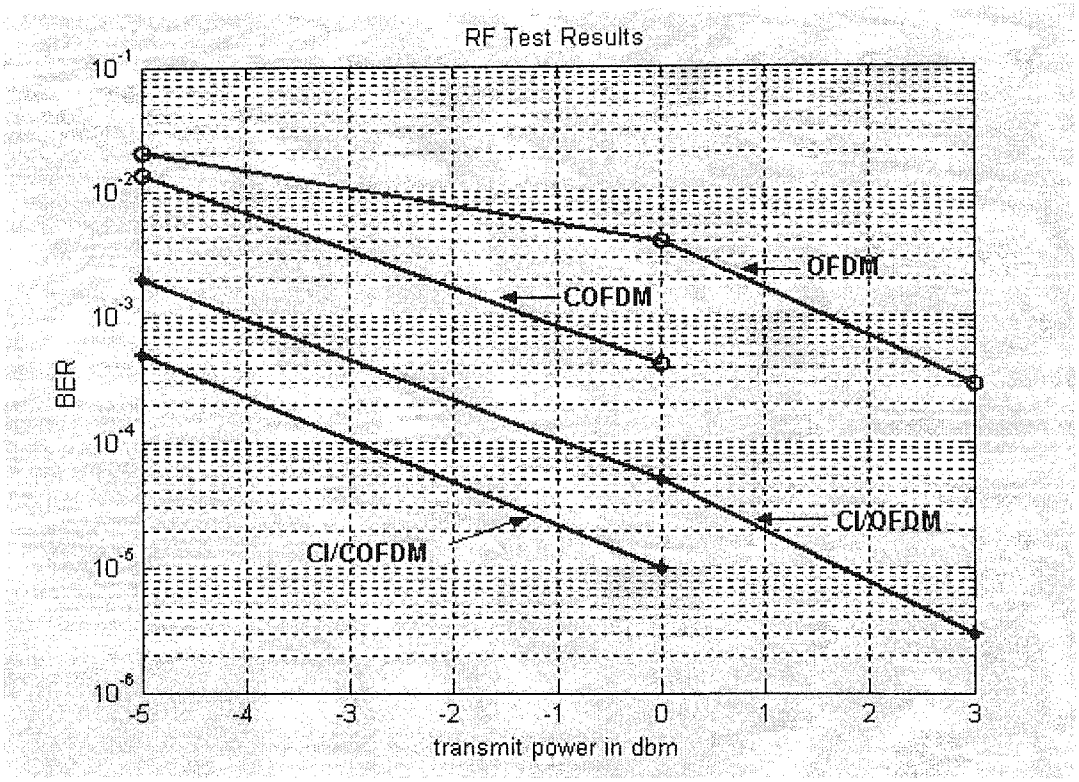

Figure 7.9: Probability of a bit error (BER) vs. Transmit Power in dBm

Figure 7.10 shows the computer emulations from Section 7.5, where an IEEE 802.11a WLAN system was compared to the same system with the OFDM modulator replaced by a CI/OFDM modulator. The dB gain observed for CI/COFDM in the simulation ranges from 1 to 4 dB for BERs between 10^{-3} and 10^{-4}, depending on the channel delay spread, T_m (larger delay spreads create larger gains), and BER of interest (lower BER implies larger gain). That is, the actual RF testing (by application of CI technology) suggests gains even larger than those observed in the computer-based emulation.

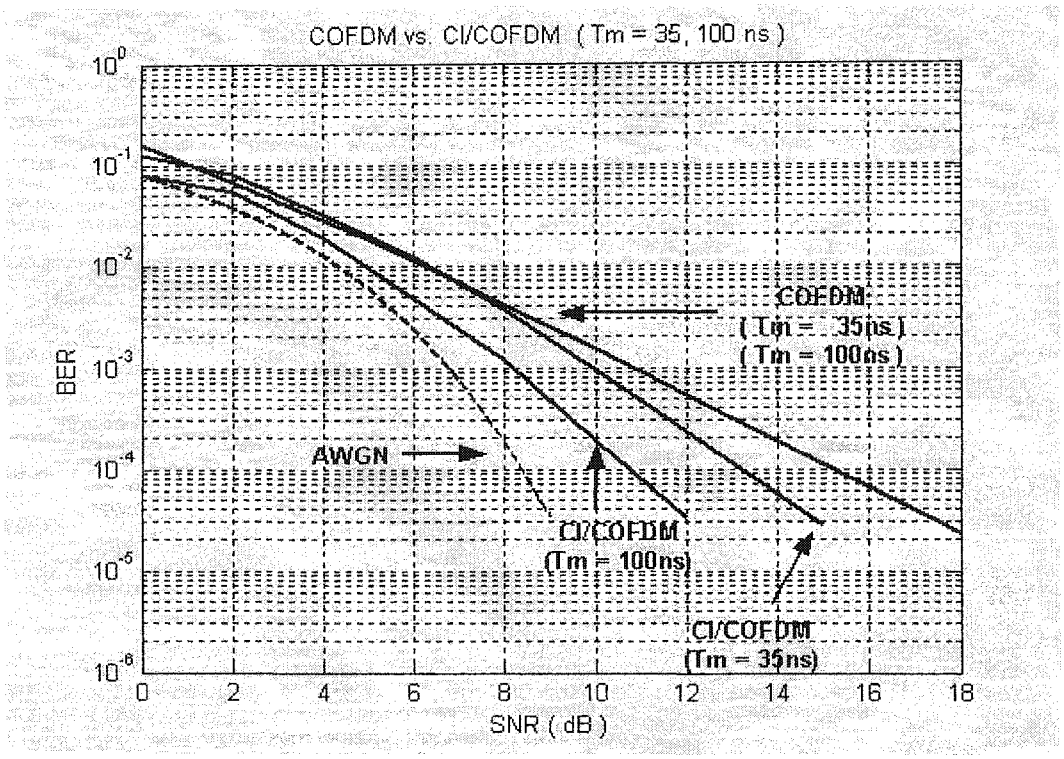

Figure 7.10: Simulated performance results for WLAN vs. CI-WLAN

7.8 Conclusions

In this chapter, RF test performance results of CI/OFDM and CI/COFDM versus OFDM and COFDM were presented. In the frequency selective indoor office, CI-WLAN gains 5-7 dB over traditional WLAN at a BERs between 10^{-3} and 10^{-4}. This gain is a result of CI/OFDM's inherent ability to exploit frequency diversity by spreading each information symbol over all N carriers. Therefore CI-WLAN's performance benefits far outweigh the cost of a small addition to transmitter and receiver complexity.

Chapter 8 Application of CI/OFDM to Fixed Broadband: RF Testing

Wireless technologies are currently being developed that rival traditional, long distance cabled networks such as fiber optic links, coaxial cable modems, and digital subscriber lines. These systems hope to mesh dependable high-rate data transfer with the ease of wireless networks, moving from the indoor WLAN (Wireless Local Area Networks), to vast outdoor environments. The emerging technologies represent tether-less broadband networks capable of supporting a variety of multimedia applications over building-to-building or metropolitan areas.

Orthogonal Frequency Division Multiplexing (OFDM) is one of the physical layer schemes under development for future Fixed Broadband networks and fourth generation cellular applications (4G) [15][78-80]. As discussed in previous chapters, OFDM avoids multipath effects while supporting high data rates: By serial-to-parallel converting one high-rate symbol stream into N low rate symbol streams, and transmitting each parallel stream over its own orthogonal carrier, the data rate in OFDM (per carrier) is effectively reduced by a factor of N from the original data rate. Hence, the bandwidth per carrier is only $(1/N)^{th}$ of the overall system bandwidth and, as a result, each carrier now experiences a flat fade upon transmission [19]. Utilizing this OFDM strategy in Fixed Broadband, or other outdoor, distance architectures, the impact of the high-multipath, frequency selective channels can be mitigated.

In an outdoor Fixed Broadband or 4G scenario, each carrier experiences a flat fade, and, hence, each carrier arrives at the receiver with a different amplitude. Even in the presence of very sensitive equalizers, data is lost in deep fades. Similar to WLAN systems, Fixed Broadband systems like IEEE 802.16, combat this problem via the addition of redundancy, incorporating Forward Error Correction (FEC) convolutional coding (of rate $1/n$) into the PHY prior to OFDM modulation and transmission, effectively allowing each symbol to be sent over n distinct frequencies [20]. This introduction of redundancy and frequency diversity overcomes much of the signal degradation due to fading. The downside of such a coding is reduced throughput (by a factor of n).

As presented in Chapters 3-6, the problems incurred by OFDM may be overcome by the introduction of Carrier Interferometry (CI) spreading codes. These CI spreading codes dramatically improve the performance of OFDM and COFDM. Frequency diversity benefits are introduced into the OFDM architecture by *simultaneously* modulating *each* of the N low rate parallel symbol streams onto *all* N carriers via application of a unique orthogonal complex spreading sequence (applied in the frequency domain). These frequency diversity benefits for each symbol stream lead to high performances *without* a decrease in throughput.

In this chapter, we illustrate the effectiveness of Carrier-Interferometry OFDM in outdoor, terrestrial networks, creating CI-Fixed Broadband. Using RF tests, we

demonstrate how, in the outdoor test environment, our CI-Fixed Broadband system offers significant performance benefits.

8.1 Physical Layer

Figure 8.1 demonstrates the typical, generalized physical layer (PHY) for terrestrial systems utilizing OFDM, such as IEEE 802.16 Fixed Broadband [81]. Similar to the WLAN systems of Chapter 7, the incoming data stream is first channel coded ("channel coder" block). Coding is typically a rate ½, constraint length 7 convolutional code, but current research is being conducted including, e.g., block coding strategies [82]. The channel coded bits then enter an "interleaver" (Figure 8.1), which serves a two-fold purpose: First, it ensures adjacent, coded bits are sent on non-adjacent carriers, and second, it alternates assignment of the adjacent, coded bits to constellation bits of greater and lesser importance. Following the interleaver is the "mapper," where, the carrier modulation scheme (BPSK, QPSK, 16QAM, or 64QAM) is employed. The mapped symbols then enter an "OFDM modulator" block. In the OFDM scheme explored for use in IEEE 802.16, a 256 point IFFT is utilized to modulate the data symbols onto 216 carriers.

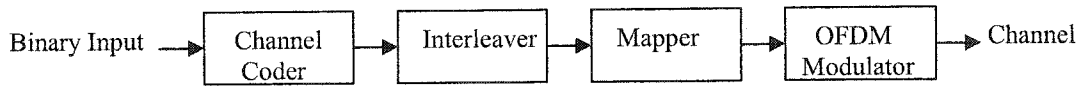

Figure 8.1: Simplified PHY Transmission Train for Fixed Broadband

8.2 RF Testing of the CI-Fixed Broadband System

RF testing was performed in January 2003 to compare CI/OFDM and CI/COFDM with similar OFDM and COFDM over terrestrial links. In order to utilize previously constructed CI test equipment, the IEEE 802.11a setup of Chapter 7 was employed. The equipment setup is illustrated in Figure 8.2. Referring to Figure 8.2, a laptop computer, running the Agilent Signal Studio software package, generates OFDM and COFDM transmit signals in a manner consistent with the IEEE 802.11a standard. That is, the output of the laptop corresponds to the output of the transmit chain of Figure 8.1. Specifically, (1) pseudo-random bits are input into a convolutional encoder, (2) encoded bits are fed into the interleaver, (3) encoded and interleaved bits enter a bit-to-symbol mapper (e.g., bit-to-BPSK mapper), (4) header information is appended to the data, and finally, (5) the header and data enter an IFFT (Inverse Fast Fourier Transform), which acts as the OFDM modulator block (here, the 4 pilot tones are inserted).

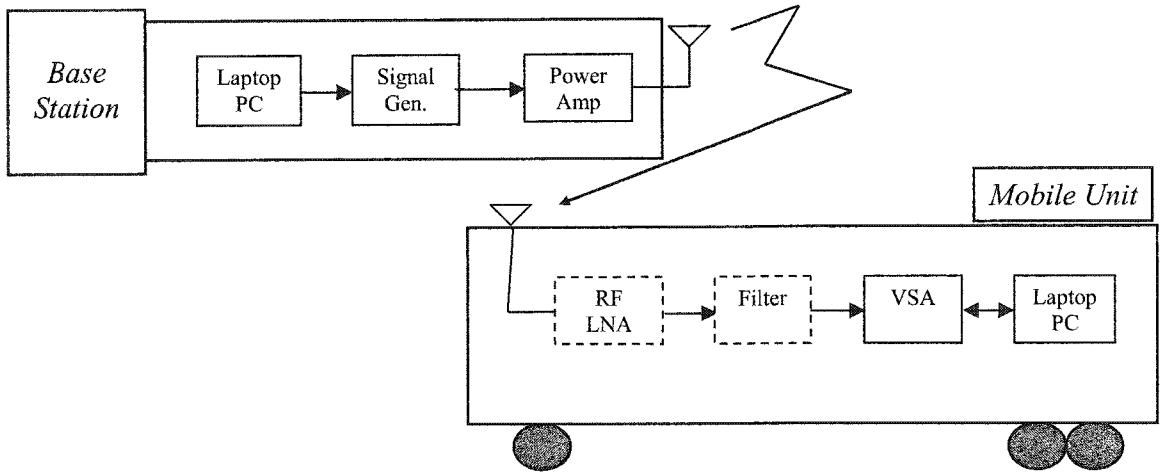

Figure 8.2: Generalized block diagram of testing setup

To generate CI/OFDM and CI/COFDM in Fixed Broadband, the "OFDM modulator block," of (Figure 2.1), is replaced by a "CI/OFDM modulator block," matching Figures 3.1(b) and 3.1(c).

In RF testing, this change at the transmitter is enabled in the software of the Agilent Signal Studio software package (with the direct support of Agilent software engineers). Here, each incoming data symbol is spread across all N (48) carriers by application of CI spreading codes. It is important to note that the CI spreading codes were *only* applied to the data portion of the signal -- *the header information (as well as the pilot tones) were left untouched.* Specifically, the short and long training sequences, along with the cyclic prefixes, *were not* CI encoded, enabling traditional detection of header (and training) information at the receiver (the Agilent 89640A Vector Signal Analyzer).

For the purposes of RF testing, input data sequences for both OFDM and CI/OFDM (or COFDM and CI/COFDM) were generated via binary pseudo-random input generators. Each trial consisted of 198 symbols x 48 carriers x 1 BPSK bit/symbol, or 9,504 data bits/packet. When, rate ½ channel coding was enabled, the number of information bits per packet corresponded to 4,752 information bearing data bits/packet.

The OFDM symbols or CI/OFDM symbols were downloaded from the laptop to an Agilent E4438C Signal Generator via a standard bi-directional LAN cable. The E4438C signal generator output corresponds to the OFDM or CI/OFDM packet modulated to the appropriate frequency. The RF signal was fed into a power amplifier, and finally into a wideband (approximately 100 MHz) directional antenna.

At the receive side, the signal is received via a wideband (approximately 100 MHz) Yagi antenna. Next, frequency band specific LNA's (low noise amplifiers) and filtering were applied when available: unfortunately, the LNAs were only available for the lower UHF frequency of test. Therefore, the upper UHF frequency tests did not benefit from amplification or filtering to overcome equipment noise figures. Finally, the received signal enters the Agilent 89640A Vector Signal Analyzer (VSA). A screen capture of the received signal in the high-multipath outdoor environment is shown in Figure 8.3. Referring to Figure 8.3, the lower, left hand portion displays the spectrum of the received CI/OFDM signal. As is evident from this spectrum, frequency selectivity is substantial across the transmit bandwidth. The VSA (1) utilizes short and long training

sequences to perform frequency and phase synchronization, (2) removes the cyclic prefix, and (3) performs a decomposition of the OFDM symbol into multiple carriers, by application of an FFT (Fast Fourier Transform). Using an IEEE 1394 firewire, this data is restored in a laptop where the remainder of the receiver operations are implemented via Matlab. (For example, in COFDM, signals are deinterleaved and fed into a soft decision decoding Viterbi Algorithm (VA).)

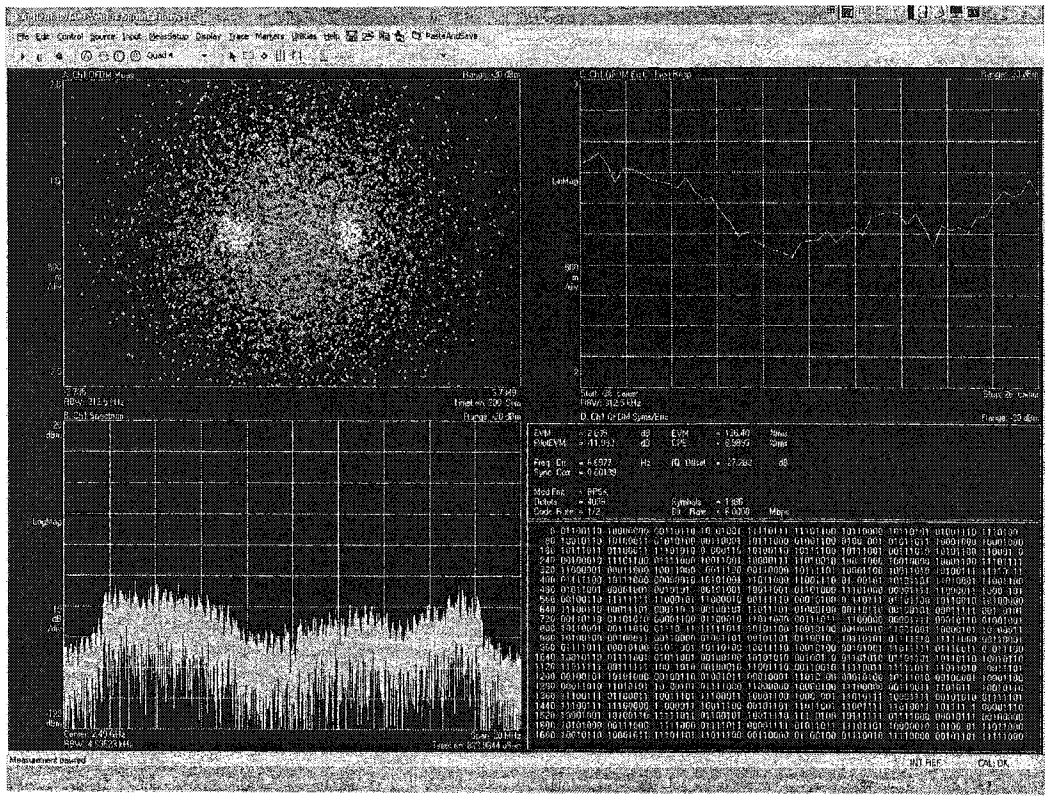

Figure 8.3: Screen Capture of the Received CI Signal in the Terrestrial Environment

In CI/OFDM, the laptop (via Matlab code) implements the MMSE combiner of Section 4.4 (which utilizes the channel fade information as well as an estimate of the

noise power). The output of this MMSEC operation is then input through the deinterleaver, followed by the soft decision decoding VA.

A BER analysis was performed upon completion of the receive processes. The results and an analysis are detailed next. (In the results that follow, a 0 (zero) BER was observed in a number of instances. Due to equipment limitations regarding the number of bits we could receive and process at one time, the 0 BER relates to a BER that is less than $6x10^{-7}$ for BPSK, less than $3x10^{-7}$ for QPSK, less than $2x10^{-7}$ for 16-QAM, and less than $1x10^{-7}$ for 64-QAM, based upon a 95% confidence interval.)

8.3 RF Testing of the CI-Fixed Broadband System: Results

Using the mobile receive arrangement of Figure 8.2, a location was chosen at approximately 1.6 miles for the purposes of this RF test. The system was first configured to transmit and receive the CI/OFDM signal in the lower UHF band. This test only examines the feasibility of reception, and as such, consists of three data points taken at the transmit power levels illustrated in Table 8.1 (0.4, 0.295, and 0.2 W), with 64QAM and no channel coding, no filtering, and no LNA. In essence, this test portrays the absolute worst case scenario at the distance of 1.6 miles, as an unnecessarily wideband Yagi antenna was used for reception and no filtering or amplification is applied to overcome the Agilent equipment's internal noise figures.

Protocol	(Un)Coded	Modulation	Power (W)	Frequency	BER
CI/OFDM	uncoded	64QAM	0.4	Lower UHF	0
CI/OFDM	uncoded	64QAM	0.295	Lower UHF	0
CI/OFDM	uncoded	64QAM	0.2	Lower UHF	0.2627

Table 8.1: Test Matrix at 1.6 Miles for the Preliminary CI/OFDM Reception

Referring to Table 8.1, the CI/OFDM signal, with no channel coding and 64QAM, represents a 72 Mbps transmission over 1.6 miles. At a transmitted power of equal to, or more than 300 mW, a zero bit-error-rate (BER) is achieved. Again, it is important to note that no LNA or filtering were utilized, even with a ~100 MHz-wide Yagi antenna.

Next, a full BER analysis (analysis where 10 independent BERs were calculated and then averaged) was conducted for BPSK OFDM and CI/OFDM at a lower UHF frequency. Again, no LNA or filtering is used in the receive chain. Tables 8.2 and 8.3 display three sets of 10 received BERs for OFDM and CI/OFDM (respectively) at 1.6 miles.

Referring to Tables 8.2 and 8.3, it can be seen that the lack of a receive LNA and/or filtering attributed to large transmit powers, necessary to fully synchronize the receive equipment to the signal. While these transmit powers correspond to illogical values in actual systems, they work to prove the viability of the CI/OFDM architecture for the terrestrial links. As will be shown later in this section, application of an LNA and

filtering within the receive chain act to overcome the noise figures of the receive equipment and allow for dramatically lower transmit powers.

Protocol	(Un)Coded	Modulation	Power (W)	Frequency	BER
OFDM	**uncoded**	BPSK	*18*	Upper UHF	0.0119
OFDM	**uncoded**	BPSK	*18*	Upper UHF	0.018
OFDM	**uncoded**	BPSK	*18*	Upper UHF	0.0122
OFDM	**uncoded**	BPSK	*18*	Upper UHF	0.0104
OFDM	**uncoded**	BPSK	*18*	Upper UHF	0.0133
OFDM	**uncoded**	BPSK	*18*	Upper UHF	0.0093
OFDM	**uncoded**	BPSK	*18*	Upper UHF	0.0079
OFDM	**uncoded**	BPSK	*18*	Upper UHF	0.0036
OFDM	**uncoded**	BPSK	*18*	Upper UHF	0.0176
OFDM	**uncoded**	BPSK	*18*	Upper UHF	0.0097
				AVE BER at 18W	**0.01139**
OFDM	**uncoded**	BPSK	*15.4*	Upper UHF	0.0212
OFDM	**uncoded**	BPSK	*15.4*	Upper UHF	0.0169
OFDM	**uncoded**	BPSK	*15.4*	Upper UHF	0.0269
OFDM	**uncoded**	BPSK	*15.4*	Upper UHF	0.051
OFDM	**uncoded**	BPSK	*15.4*	Upper UHF	0.023
OFDM	**uncoded**	BPSK	*15.4*	Upper UHF	0.0334
OFDM	**uncoded**	BPSK	*15.4*	Upper UHF	0.0273
OFDM	**uncoded**	BPSK	*15.4*	Upper UHF	0.0442
OFDM	**uncoded**	BPSK	*15.4*	Upper UHF	0.0108
OFDM	**uncoded**	BPSK	*15.4*	Upper UHF	0.0183
				AVE BER at 15.4W	**0.0273**
OFDM	**uncoded**	BPSK	*12.6*	Upper UHF	0.0284
OFDM	**uncoded**	BPSK	*12.6*	Upper UHF	0.0262
OFDM	**uncoded**	BPSK	*12.6*	Upper UHF	0.0427
OFDM	**uncoded**	BPSK	*12.6*	Upper UHF	0.0611
OFDM	**uncoded**	BPSK	*12.6*	Upper UHF	0.0223
OFDM	**uncoded**	BPSK	*12.6*	Upper UHF	0.074
OFDM	**uncoded**	BPSK	*12.6*	Upper UHF	0.0133
OFDM	**uncoded**	BPSK	*12.6*	Upper UHF	0.0273
OFDM	**uncoded**	BPSK	*12.6*	Upper UHF	0.0862
OFDM	**uncoded**	BPSK	*12.6*	Upper UHF	0.0363
				AVE BER at 12.6W	**0.04178**

Table 8.2: Test Matrix at 1.6 Miles for the BPSK OFDM Reception

Protocol	(Un)Coded	Modulation	Power (W)	Frequency	BER
CI/OFDM	uncoded	BPSK	*15.523*	Upper UHF	0.019
CI/OFDM	uncoded	BPSK	*15.523*	Upper UHF	0.018
CI/OFDM	uncoded	BPSK	*15.523*	Upper UHF	0.0097
CI/OFDM	uncoded	BPSK	*15.523*	Upper UHF	0.014
CI/OFDM	uncoded	BPSK	*15.523*	Upper UHF	0.0065
CI/OFDM	uncoded	BPSK	*15.523*	Upper UHF	0.0111
CI/OFDM	uncoded	BPSK	*15.523*	Upper UHF	0.0108
CI/OFDM	uncoded	BPSK	*15.523*	Upper UHF	0.018
CI/OFDM	uncoded	BPSK	*15.523*	Upper UHF	0.0338
CI/OFDM	uncoded	BPSK	*15.523*	Upper UHF	0.009
				AVE BER at 15.5W	**0.01499**
CI/OFDM	uncoded	BPSK	*18*	Upper UHF	**0.0018**
CI/OFDM	uncoded	BPSK	*18*	Upper UHF	**0.0122**
CI/OFDM	uncoded	BPSK	*18*	Upper UHF	**0.0032**
CI/OFDM	uncoded	BPSK	*18*	Upper UHF	**0.0101**
CI/OFDM	uncoded	BPSK	*18*	Upper UHF	**0.018**
CI/OFDM	uncoded	BPSK	*18*	Upper UHF	**0.0119**
CI/OFDM	uncoded	BPSK	*18*	Upper UHF	**0.0216**
CI/OFDM	uncoded	BPSK	*18*	Upper UHF	**0.019**
CI/OFDM	uncoded	BPSK	*18*	Upper UHF	**0.0075**
CI/OFDM	uncoded	BPSK	*18*	Upper UHF	**0.0111**
				AVE BER at 18W	**0.01164**
CI/OFDM	uncoded	BPSK	*12.618*	Upper UHF	0.0251
CI/OFDM	uncoded	BPSK	*12.618*	Upper UHF	0.0216
CI/OFDM	uncoded	BPSK	*12.618*	Upper UHF	0.0223
CI/OFDM	uncoded	BPSK	*12.618*	Upper UHF	0.0162
CI/OFDM	uncoded	BPSK	*12.618*	Upper UHF	0.0172
CI/OFDM	uncoded	BPSK	*12.618*	Upper UHF	0.0108
CI/OFDM	uncoded	BPSK	*12.618*	Upper UHF	0.0406
CI/OFDM	uncoded	BPSK	*12.618*	Upper UHF	0.0341
CI/OFDM	uncoded	BPSK	*12.618*	Upper UHF	0.018
CI/OFDM	uncoded	BPSK	*12.618*	Upper UHF	0.019
				AVE BER at 12.6W	**0.02249**

Table 8.3: Test Matrix at 1.6 Miles for the BPSK CI/OFDM Reception

Figure 8.4 plots the resulting average BERs from Tables 8.2 and 8.3. Referring to Figure 8.4, the CI/OFDM architecture outperforms OFDM in the terrestrial environment. While performance gain is observed, it is hard to equate the overall benefit to SNR gains as the transmit powers are un-realistic due to lack of an LNA in the receive chain. However, we are able to observe CI/OFDM's ability to exploit the frequency diversity of the channel, allowing it to outperform its OFDM counterpart.

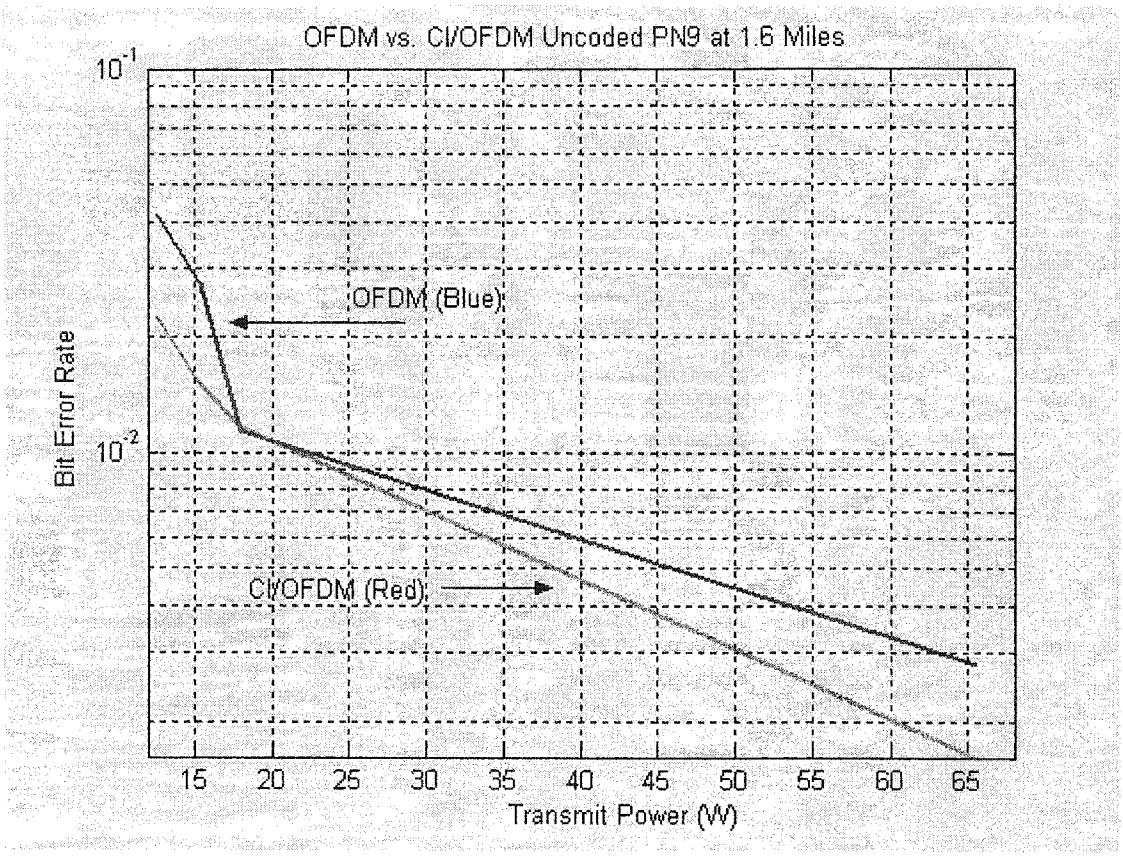

Figure 8.4: OFDM vs. CI/OFDM uncoded at 1.6 miles (upper UHF)

Following testing at a low UHF frequency band, the equipment was reconfigured to the upper UHF frequency band, and an average BER was conducted for a transmit power level of 287 mW. In this case, an LNA was included in the receive chain and both uncoded and coded cases were tested. Tables 8.4 and 8.5 display the test matrices for (C)OFDM and CI/(C)OFDM respectively. Due to time constraints, only one transmit power level was tested.

Protocol	(Un)Coded	Modulation	Power (W)	Frequency	BER
OFDM	**uncoded**	BPSK	*0.287*	Upper UHF	0.0124
OFDM	**uncoded**	BPSK	*0.287*	Upper UHF	0.021
OFDM	**uncoded**	BPSK	*0.287*	Upper UHF	0.0185
OFDM	**uncoded**	BPSK	*0.287*	Upper UHF	0.0305
OFDM	**uncoded**	BPSK	*0.287*	Upper UHF	0.021
OFDM	**uncoded**	BPSK	*0.287*	Upper UHF	0.0146
OFDM	**uncoded**	BPSK	*0.287*	Upper UHF	0.0472
OFDM	**uncoded**	BPSK	*0.287*	Upper UHF	0.0504
OFDM	**uncoded**	BPSK	*0.287*	Upper UHF	0.0437
OFDM	**uncoded**	BPSK	*0.287*	Upper UHF	0.0405
				AVE BER at 287mW	**0.02998**
OFDM	**Coded**	BPSK	*0.287*	Upper UHF	0.0029
OFDM	**Coded**	BPSK	*0.287*	Upper UHF	0.0168
OFDM	**Coded**	BPSK	*0.287*	Upper UHF	0.0154
OFDM	**Coded**	BPSK	*0.287*	Upper UHF	0.0548
OFDM	**Coded**	BPSK	*0.287*	Upper UHF	0.0475
OFDM	**Coded**	BPSK	*0.287*	Upper UHF	0.0066
OFDM	**Coded**	BPSK	*0.287*	Upper UHF	0.1491
OFDM	**Coded**	BPSK	*0.287*	Upper UHF	0.1382
OFDM	**Coded**	BPSK	*0.287*	Upper UHF	0.0768
OFDM	**Coded**	BPSK	*0.287*	Upper UHF	0.1016
				AVE BER at 287mW	**0.06097**

Table 8.4: Test Matrix at 1.6 Miles for the BPSK (C)OFDM Reception

Protocol	(Un)Coded	Modulation	Power (W)	Frequency	BER
CI/OFDM	uncoded	BPSK	*0.283*	Upper UHF	0.0039
CI/OFDM	uncoded	BPSK	*0.283*	Upper UHF	0.0021
CI/OFDM	uncoded	BPSK	*0.283*	Upper UHF	0.0018
CI/OFDM	uncoded	BPSK	*0.283*	Upper UHF	0.0337
CI/OFDM	uncoded	BPSK	*0.283*	Upper UHF	0.0014
CI/OFDM	uncoded	BPSK	*0.283*	Upper UHF	0.0437
CI/OFDM	uncoded	BPSK	*0.283*	Upper UHF	0.0053
CI/OFDM	uncoded	BPSK	*0.283*	Upper UHF	0.0156
CI/OFDM	uncoded	BPSK	*0.283*	Upper UHF	0.0011
CI/OFDM	uncoded	BPSK	*0.283*	Upper UHF	0.0195
				AVE BER at 283mW	**0.01281**
CI/OFDM	Coded	BPSK	*0.283*	Upper UHF	0.0015
CI/OFDM	Coded	BPSK	*0.283*	Upper UHF	0.00074
CI/OFDM	Coded	BPSK	*0.283*	Upper UHF	0
CI/OFDM	Coded	BPSK	*0.283*	Upper UHF	0.0081
CI/OFDM	Coded	BPSK	*0.283*	Upper UHF	0
CI/OFDM	Coded	BPSK	*0.283*	Upper UHF	0.0148
CI/OFDM	Coded	BPSK	*0.283*	Upper UHF	0
CI/OFDM	Coded	BPSK	*0.283*	Upper UHF	0.0022
CI/OFDM	Coded	BPSK	*0.283*	Upper UHF	0
CI/OFDM	Coded	BPSK	*0.283*	Upper UHF	0
				AVE BER at 283 mW	**0.002734**

Table 8.5: Test Matrix at 1.6 Miles for the BPSK CI/(C)OFDM Reception

Referring to Tables 8.4 and 8.5, we observe that the incorporation of an LNA into the receive chain dramatically lowers the necessary transmit power (the transmit power necessary for synchronization at the receiver), bringing power levels to realistic levels. Also referring the Tables 8.4 and 8.5, the uncoded CI/OFDM system offers a small performance benefit relative to uncoded OFDM. When channel coding is employed, the COFDM system performance degrades from that of its uncoded counterpart (OFDM). This is due to low SNRs creating well-known failures in the channel decoding. The

CI/COFDM system, on the other hand, dramatically improves its performance over its uncoded counterpart (CI/OFDM). The CI/COFDM system is observed outperforming its COFDM counterpart by more than an order of magnitude (0.0027 vs. 0.06)..

Further testing conducted at the upper UHF frequency band included adding Doppler effects into the transmit signal. This was accomplished via incorporation of a function generator (used at the signal generator. The Doppler scenarios are as follows: (1) a 4 kHz shift to the right, (2) A +/- 4 kHz sweep through the entire spectrum (creating a jitter effect), and (3) simulated communication with an airplane traveling 500 knots overhead. The (C)OFDM scenario was only tested under cases (1) and (3), whereas the CI/(C)OFDM system was tested under all three. Tables 8.6 and 8.7 display the test matrices for (C)OFDM and CI/(C)OFDM respectively, with an LNA in the receive chain.

Protocol	(Un)Coded	Modulation	Power (W)	Frequency (MHz)	BER	Doppler Testing Notes
OFDM	**uncoded**	BPSK	1.4	Upper UHF	0.0022	Doppler shift 4 kHz right
OFDM	**uncoded**	BPSK	1.4	Upper UHF	0.0102	500 Knot Aircraft overhead
OFDM	**Coded**	BPSK	1.4	Upper UHF	0.0039	Doppler shift 4 kHz right
OFDM	**Coded**	BPSK	1.4	Upper UHF	0.0078	500 Knot Aircraft overhead

Table 8.6: Test Matrix at 1.6 Miles for the BPSK (C)OFDM Doppler Testing

Protocol	(Un)Coded	Modulation	Power (W)	Frequency (MHz)	BER	Doppler Testing Notes
CI/OFDM	uncoded	BPSK	1.4	Upper UHF	0	Doppler shift 4 kHz right
CI/OFDM	uncoded	BPSK	1.4	Upper UHF	0	4 kHz sweep
CI/OFDM	uncoded	BPSK	1.4	Upper UHF	0	500 Knot Aircraft overhead
CI/OFDM	Coded	BPSK	1.4	Upper UHF	0.0036	Doppler shift 4 kHz right
CI/OFDM	Coded	BPSK	1.4	Upper UHF	0	4 kHz sweep
CI/OFDM	Coded	BPSK	1.4	Upper UHF	0	500 Knot Aircraft overhead

Table 8.7: Test Matrix at 1.6 Miles for the BPSK CI/(C)OFDM Doppler Testing

Referring to Table 8.6, it can be seen, in the presence of Doppler, noteable BERs result in both OFDM and COFDM. Referring to Table 8.7, Doppler effects created no errors in the CI/OFDM system, and only case (1) created errors in the CI/COFDM system. Due to time constraints, the results shown only represent a one-time capture and not a full BER analysis, but do indicate a resilience of the CI/OFDM architecture to Doppler.

The mobile receive chain of Figure 8.2 was moved to a location of approximately 4 miles. Tables 8.8 and 8.9 display the test matrix for BPSK OFDM and CI/OFDM respectively at the various transmit power levels. In this case, no LNA was utilized in the receive chain.

Protocol	(Un)Coded	Modulation	Power (W)	Frequency	BER
OFDM	**uncoded**	BPSK	*19.275*	Lower UHF	0.0302
OFDM	**uncoded**	BPSK	*19.275*	Lower UHF	0.0765
OFDM	**uncoded**	BPSK	*19.275*	Lower UHF	0.0129
OFDM	**uncoded**	BPSK	*19.275*	Lower UHF	0.033
OFDM	**uncoded**	BPSK	*19.275*	Lower UHF	0.032
OFDM	**uncoded**	BPSK	*19.275*	Lower UHF	0.0223
OFDM	**uncoded**	BPSK	*19.275*	Lower UHF	0.0223
OFDM	**uncoded**	BPSK	*19.275*	Lower UHF	0.0223
OFDM	**uncoded**	BPSK	*19.275*	Lower UHF	0.0374
OFDM	**uncoded**	BPSK	*19.275*	Lower UHF	0.0284
				AVE BER at 19.2W	**0.03173**
OFDM	**uncoded**	BPSK	*25*	Lower UHF	0.023
OFDM	**uncoded**	BPSK	*25*	Lower UHF	0.0205
OFDM	**uncoded**	BPSK	*25*	Lower UHF	0.0169
OFDM	**uncoded**	BPSK	*25*	Lower UHF	0.0115
OFDM	**uncoded**	BPSK	*25*	Lower UHF	0.0119
OFDM	**uncoded**	BPSK	*25*	Lower UHF	0.0154
OFDM	**uncoded**	BPSK	*25*	Lower UHF	0.037
OFDM	**uncoded**	BPSK	*25*	Lower UHF	0.0126
OFDM	**uncoded**	BPSK	*25*	Lower UHF	0.0205
OFDM	**uncoded**	BPSK	*25*	Lower UHF	0.0165
				AVE BER at 25 W	**0.01858**
OFDM	**uncoded**	BPSK	*41*	Lower UHF	0.0072
OFDM	**uncoded**	BPSK	*41*	Lower UHF	0.0072
OFDM	**uncoded**	BPSK	*41*	Lower UHF	0.004
OFDM	**uncoded**	BPSK	*41*	Lower UHF	0.004
OFDM	**uncoded**	BPSK	*41*	Lower UHF	0.004
OFDM	**uncoded**	BPSK	*41*	Lower UHF	0.0025
OFDM	**uncoded**	BPSK	*41*	Lower UHF	0.005
OFDM	**uncoded**	BPSK	*41*	Lower UHF	0.0047
OFDM	**uncoded**	BPSK	*41*	Lower UHF	0.0075
OFDM	**uncoded**	BPSK	*41*	Lower UHF	0.0126
				AVE BER at 41W	**0.00587**

Table 8.8: Test Matrix at 4 Miles for the BPSK OFDM Reception

Protocol	(Un)Coded	Modulation	Power (W)	Frequency	BER
CI/OFDM	uncoded	BPSK	*19.186*	Lower UHF	**0.0111**
CI/OFDM	uncoded	BPSK	*19.186*	Lower UHF	**0.014**
CI/OFDM	uncoded	BPSK	*19.186*	Lower UHF	**0.0097**
CI/OFDM	uncoded	BPSK	*19.186*	Lower UHF	**0.0108**
CI/OFDM	uncoded	BPSK	*19.186*	Lower UHF	**0.018**
CI/OFDM	uncoded	BPSK	*19.186*	Lower UHF	**0.0237**
CI/OFDM	uncoded	BPSK	*19.186*	Lower UHF	**0.0108**
CI/OFDM	uncoded	BPSK	*19.186*	Lower UHF	**0.004**
CI/OFDM	uncoded	BPSK	*19.186*	Lower UHF	**0.0108**
CI/OFDM	uncoded	BPSK	*19.186*	Lower UHF	**0.0298**
				AVE BER at 19.2W	**0.01427**
CI/OFDM	uncoded	BPSK	*25*	Lower UHF	0.0047
CI/OFDM	uncoded	BPSK	*25*	Lower UHF	0.0036
CI/OFDM	uncoded	BPSK	*25*	Lower UHF	0.0057
CI/OFDM	uncoded	BPSK	*25*	Lower UHF	0.005
CI/OFDM	uncoded	BPSK	*25*	Lower UHF	0.0029
CI/OFDM	uncoded	BPSK	*25*	Lower UHF	0.004
CI/OFDM	uncoded	BPSK	*25*	Lower UHF	0.0022
CI/OFDM	uncoded	BPSK	*25*	Lower UHF	0.0029
CI/OFDM	uncoded	BPSK	*25*	Lower UHF	0.0079
CI/OFDM	uncoded	BPSK	*25*	Lower UHF	0.0018
				AVE BER at 25W	**0.00407**
CI/OFDM	uncoded	BPSK	*41*	Lower UHF	**0.0025**
CI/OFDM	uncoded	BPSK	*41*	Lower UHF	**0.000718**
CI/OFDM	uncoded	BPSK	*41*	Lower UHF	**0.000718**
CI/OFDM	uncoded	BPSK	*41*	Lower UHF	**0.000718**
CI/OFDM	uncoded	BPSK	*41*	Lower UHF	**0.0018**
CI/OFDM	uncoded	BPSK	*41*	Lower UHF	**0.0025**
CI/OFDM	uncoded	BPSK	*41*	Lower UHF	**0.0011**
CI/OFDM	uncoded	BPSK	*41*	Lower UHF	**0.0079**
CI/OFDM	uncoded	BPSK	*41*	Lower UHF	**0.0011**
CI/OFDM	uncoded	BPSK	*41*	Lower UHF	**0.0018**
				AVE BER at 41W	**0.002086**

Table 8.9: Test Matrix at 4 Miles for the BPSK CI/OFDM Reception

Figure 8.5 plots the resulting average BERs from Tables 8.8 and 8.9. Referring to Figure 8.5, we observe the CI/OFDM architecture with a pronounced performance gain over OFDM. Again, it is hard to equate the overall benefit to SNR gains as the transmit powers are un-realistic due to lack of an LNA in the receive chain.

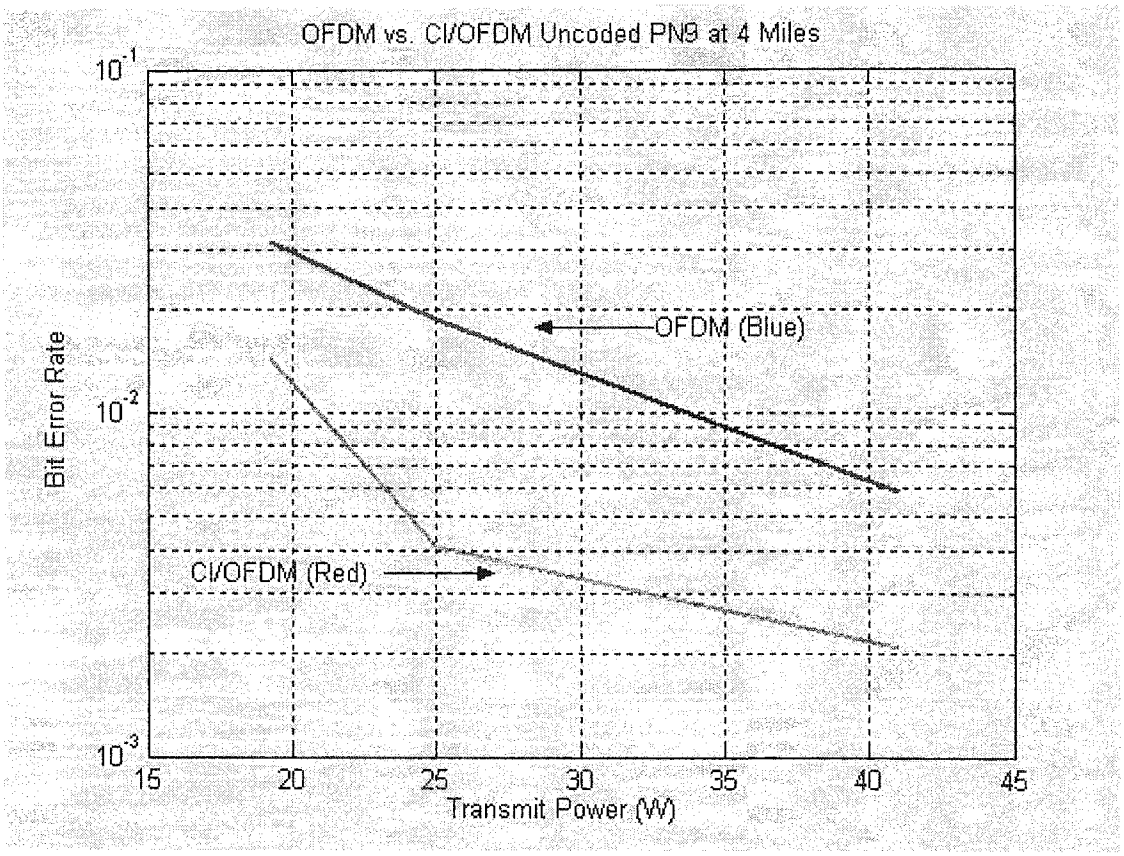

Figure 8.5: OFDM vs. CI/OFDM uncoded at 4 miles (lower UHF)

8.4 Conclusions

In this chapter, RF test performance results of CI/OFDM and CI/COFDM versus OFDM and COFDM were presented for the outdoor terrestrial environment. Performance results were limited to small sample results due to the constraint imposed by the equipment operations. In all case samples, the CI/(C)OFDM architecture outperforms the (C)OFDM architecture. When appropriate LNAs were available, this performance gain of the CI system was greater than an order of magnitude. This gain is a result of CI/OFDM's inherent ability to exploit frequency diversity by spreading each information symbol over all N carriers. Therefore CI-Fixed Broadband's performance benefits far outweigh the cost of a small addition to transmitter and receiver complexity.

Furthermore, Doppler test results show that CI systems may mitigate the plagues associated with Doppler shifts. This is an important result because it indicates that even with complex spreading codes, the Doppler effects present no barrier to excellent system performance.

While not all of the results were achieved with realistic system transmit powers, the tests suggest the benefits that CI architectures can grant (in terms of increased performance). In a carefully-designed system with appropriate antenna design, power amplification, LNAs, and filtering, the CI/OFDM system is likely to represent a high-performance alternative to OFDM in outdoor terrestrial networks.

Chapter 9 Application of CI/OFDM to the Satellite Environment

Future generation satellite communications shall be capable of high-performances, high-data rates, and the ability to integrate into existing terrestrial communications protocols.

Orthogonal Frequency Division Multiplexing (OFDM) is becoming more and more widespread as the technology of choice for many land-based wireless schemes, and as such is a possible choice for satellite architectures. Research is currently being conducted on the integration of OFDM into satellite communications protocols (e.g., [83-86]). The benefits of OFDM to the satellite channel include high-bandwidth efficiency, low receiver complexity, and reduced intersymbol interference.

In this chapter, we explore the performance capabilities of Carrier-Interferometry OFDM within satellite systems. Through RF testing of the CI/OFDM architecture at C-band, we show the CI technique slightly outperforms its OFDM counter-part. Furthermore, we show that CI/OFDM with channel coding can enable a 64-QAM satellite system, ensuring high-throughput.

9.1 Transmit Structure

Figure 9.1 illustrates the generalized transmission blocks for the satellite system. Similar to the WLAN system of Chapter 7, the incoming data stream is first channel coded ("channel coder" block). Coding is typically a rate ½, constraint length 7 convolutional code. The channel coded bits then enter an "interleaver" (Figure 8.1), which serves a two-fold purpose: First, it ensures adjacent, coded bits are sent on non-adjacent carriers, and second, it alternates assignment of the adjacent, coded bits to constellation bits of greater and lesser importance. Following the interleaver is the "mapper," where, the carrier modulation scheme (BPSK, QPSK, 16QAM, or 64QAM) is employed. The mapped symbols then enter an "OFDM modulator" block.

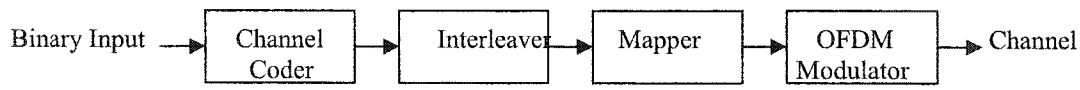

Figure 9.1: Simplified Satellite PHY Transmission Train

When CI/OFDM is applied to the satellite transmission train model of Figure 9.1, the transmitter operates as follows: (1) each m input bits (e.g., m = 1) are first channel coded to n output bits (e.g., n = *2*) (puncturing is applied to create lower rate FECs as necessary); (2) interleaving follows where the n coded bits are interleaved such that they are sent at different OFDM symbol times (with a time separation selected to create a time diversity benefit); (3) next is bit-to-PSK or bit-to-QAM symbol mapping; (4) followed by the CI/OFDM modulator block of Figures 3.1(b) and (c). Hence, CI/OFDM satellite links benefit from (1) coding gain, (2) time diversity benefit, and (3) frequency diversity gain via the spreading. Figure 9.2 illustrates the CI-Satellite transmitter architecture.

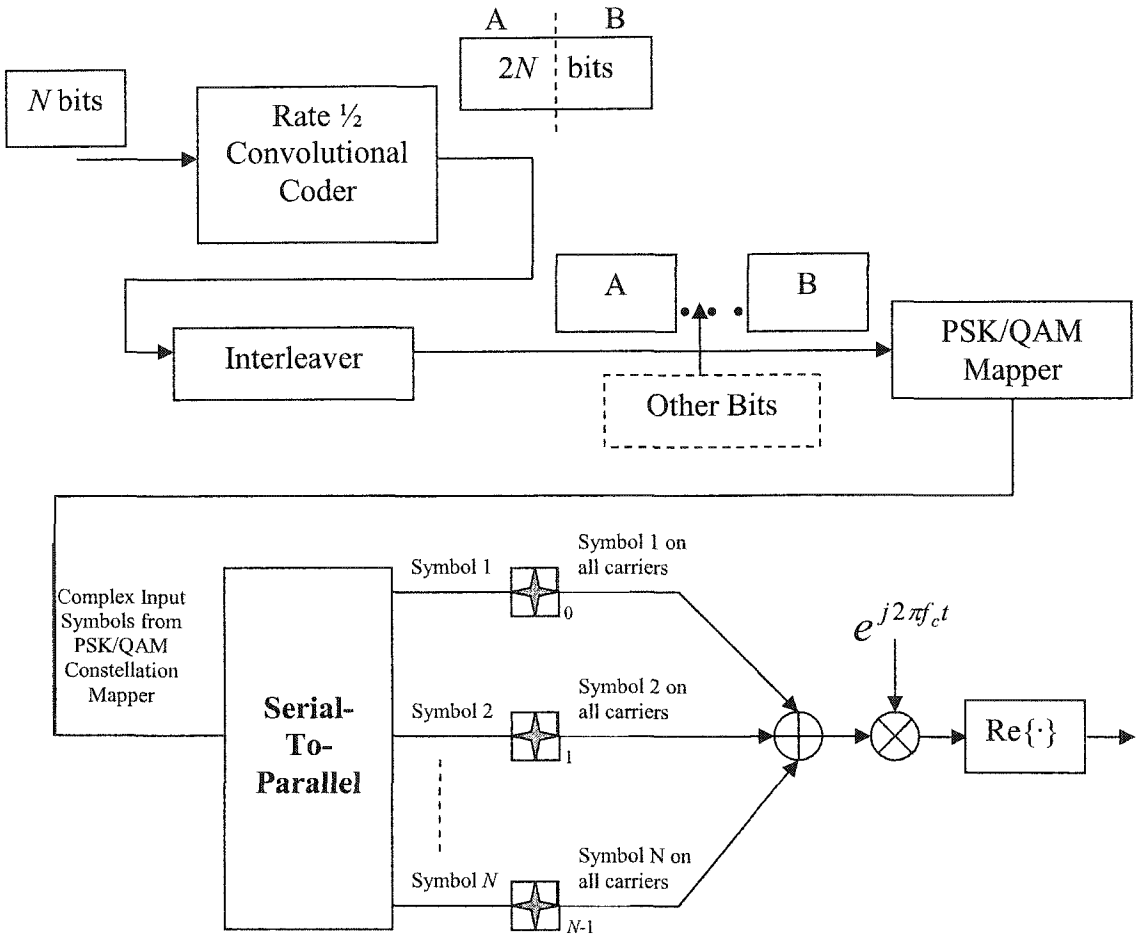

Figure 9.2: CI-Satellite PHY

9.2 RF Testing of the CI-Satellite System

RF testing was performed in January 2003 to compare CI/OFDM and CI/COFDM satellite architectures to OFDM and COFDM satellite architectures. The equipment setup is illustrated in Figure 9.3. Referring to Figure 9.3, a laptop computer, running the Agilent Signal Studio software package, generates OFDM and COFDM transmit signals in a manner consistent with the IEEE 802.11a standard. That is, the output of the laptop corresponds to the output of the transmit chain of Figure 9.1. Specifically, (1) pseudo-random bits are input to a convolutional encoder, (2) encoded bits are fed into the interleaver, (3) encoded and interleaved bits enter a bit-to-symbol mapper (e.g., bit-to-BPSK mapper), (4) header information is appended to the data, and finally, (5) the header and data enter an IFFT (Inverse Fast Fourier Transform), which acts as the OFDM modulator block (here, the 4 pilot tones are inserted).

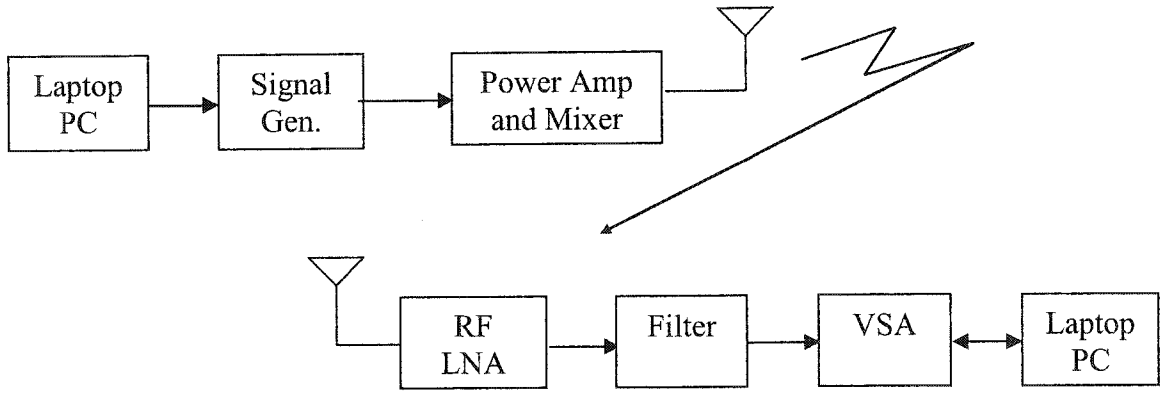

Figure 9.3: Generalized block diagram of testing setup

To generate a CI/OFDM and CI/COFDM, the "OFDM modulator block," of (Figure 2.1), is replaced by a "CI/OFDM modulator block," matching Figures 3.1(b) and 3.1(c). This change was enabled in the software of the Agilent Signal Studio software package (with the direct support of Agilent software engineers). This allowed each incoming data symbol to be spread across all N (48) carriers by application of CI spreading codes. It is important to note that the CI spreading codes were *only* applied to the data portion of the signal -- *the header information (as well as the pilot tones) were left untouched.* Specifically, the short and long training sequences, along with the cyclic prefixes, *were not* CI encoded, enabling traditional detection of header (and training) information at the receiver (the Agilent 89640A Vector Signal Analyzer).

Referring to Figure 9.3, the OFDM symbols or CI/OFDM symbols are downloaded from the laptop to an Agilent E4438C Signal Generator via a standard bi-directional LAN cable. The E4438C signal generator output corresponds to the OFDM or CI/OFDM packet modulated to 70 MHz IF. The IF signal was fed into a power

amplifier and mixer, and then to a directional antenna. The C-band satellite acts as a transponder, and does nothing more than signal amplification and frequency downcoversion for retransmission back to Earth.

At the receive side (Figure 9.3), the signal is received via a directional antenna, and is passed through a Low Noise Amplifier (LNA). The signal is then downconverted to 70 MHz and enters the Agilent 89640A Vector Signal Analyzer (VSA). The VSA is configured to receive an IEEE 802.11a formatted signal at the 70 MHz IF. A screen capture of the received signal in the flat fading satellite environment is shown in Figure 9.4. Referring to Figure 9.4, the lower, left hand portion displays the spectrum of the received CI/OFDM signal. As is evident from this spectrum, the multipath profile is very flat across the 20 MHz bandwidth (the raised-middle portion), proving a low-level of frequency selectivity. This Agilent VSA (1) utilizes the short and long training sequences to perform frequency and phase synchronization, (2) removes the cyclic prefix, and (3) performs a decomposition of the OFDM symbol into multiple carriers, by application of an FFT (Fast Fourier Transform). Using an IEEE 1394 firewire, this data is restored in a laptop where the remainder of the receiver operations are implemented via Matlab.

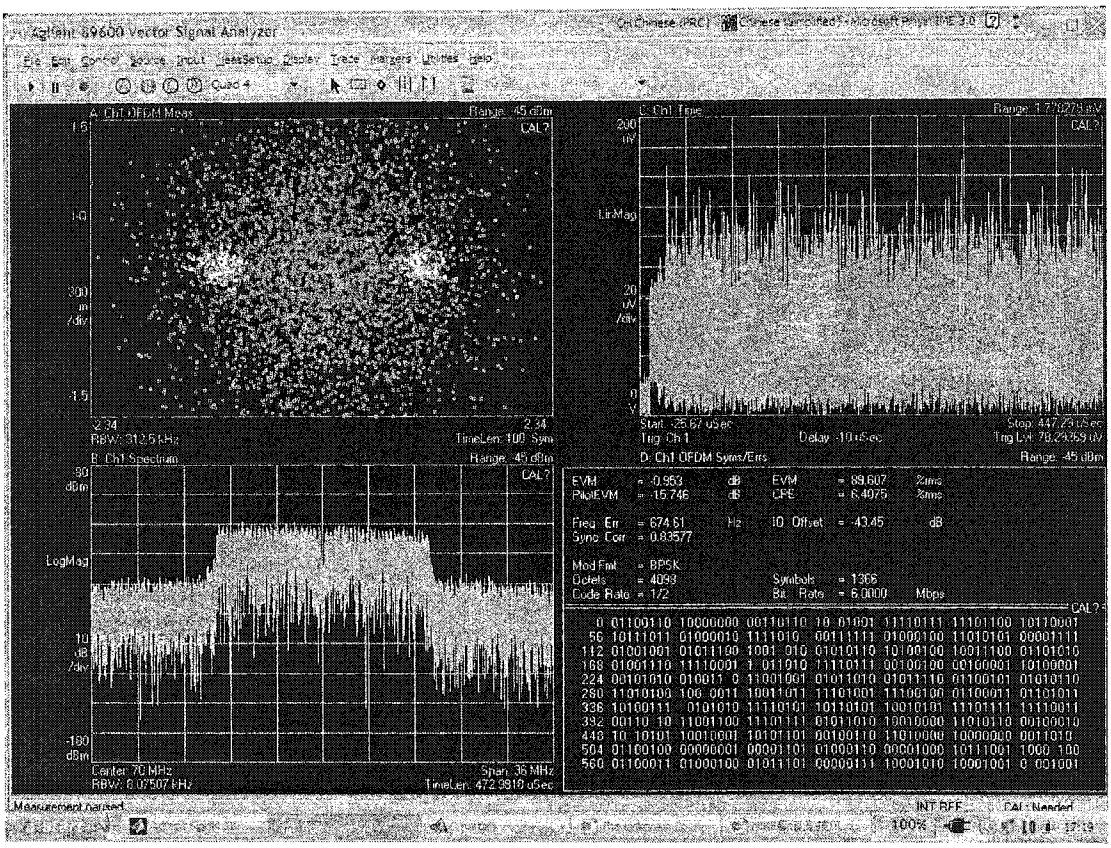

Figure 9.4: Screen Capture of the CI/OFDM Receive Signal in the Satellite Channel

A BER analysis was performed upon completion of the respective receive processes. The results of the analysis are detailed next.

9.3 RF Testing of the CI-Satellite System: Results

Performance measurements were conducted during the satellite test by adjusting the power of the transmitted signal at C-band. Due to operating constraints set by the satellite provider, the maximum permitted transmit power was –25 dBm at the signal generator. This translates to a maximum power of 7 dB back-off from the saturation region of the transmit power amplifier, and more importantly, 7 dB back-off from the maximum transmit power of the band as dictated by FCC regulations [87].

Bit Error Rate (BER) calculations were performed for signal powers lowered from the –25 dBm maximum transmit power in 2 dBm increments. For BPSK, the BER calculations began at –28 dBm, because at –25 dBm BPSK showed no errors. Each point (on the BER curves) was calculated from an average of at least ten measurements or until there was little variation in the data to obtain a reasonably accurate value. The results for BPSK, QPSK, 16QAM and 64QAM modulation schemes are shown in Figures 9.5 – 9.9.

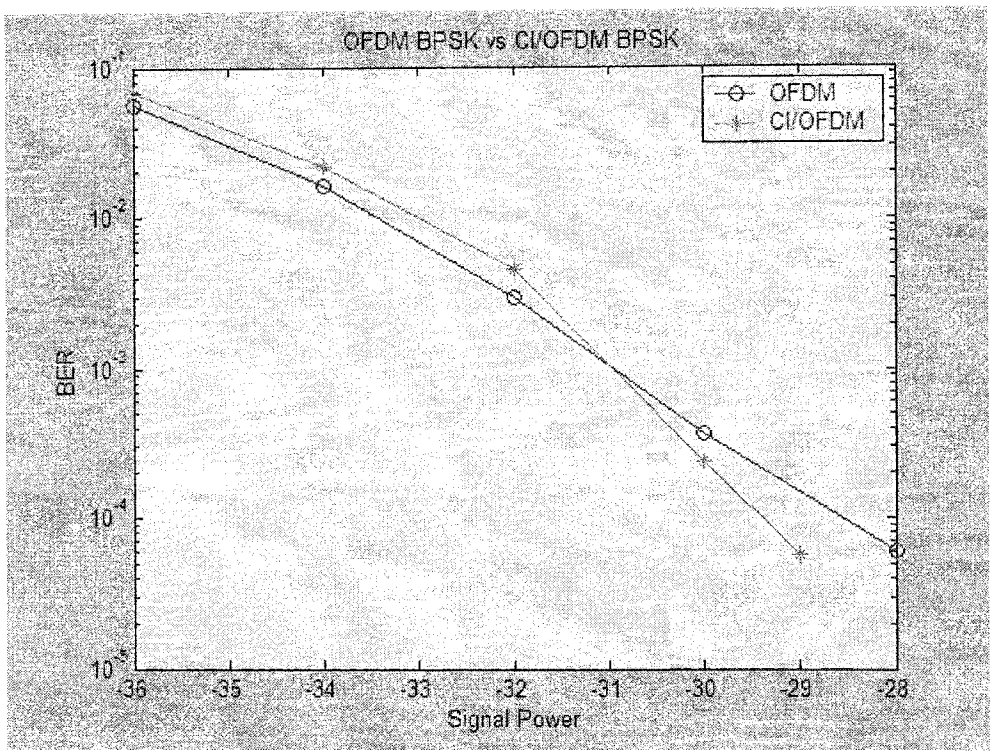

Figure 9.5: Performance Results for BPSK OFDM vs. CI/OFDM

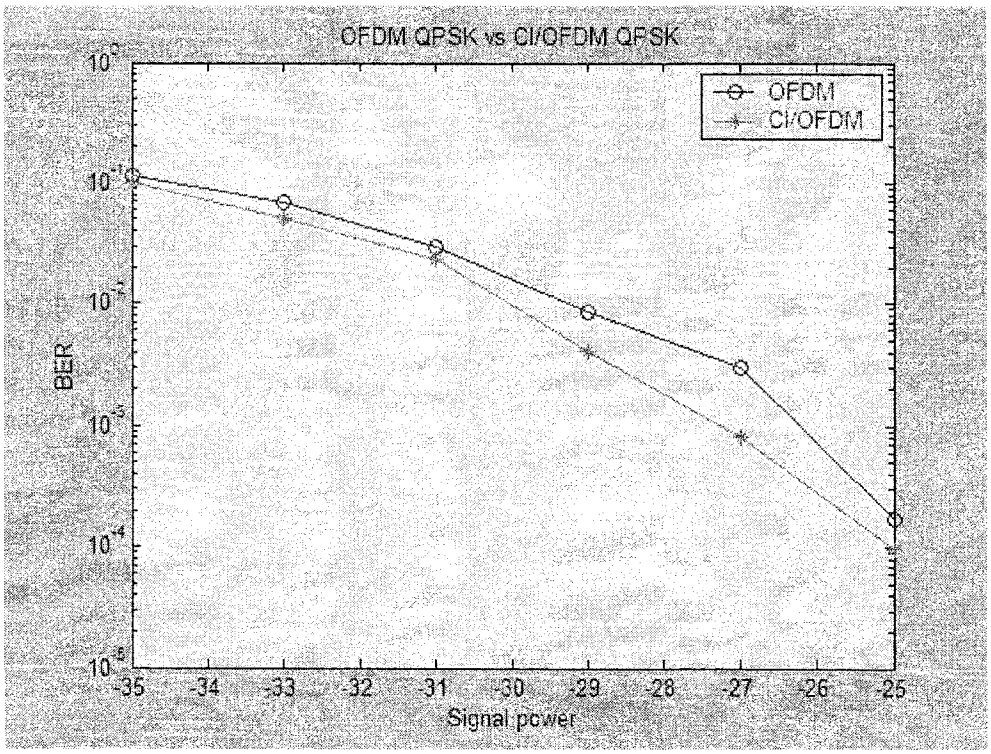

Figure 9.6: Performance Results for QPSK OFDM vs. CI/OFDM

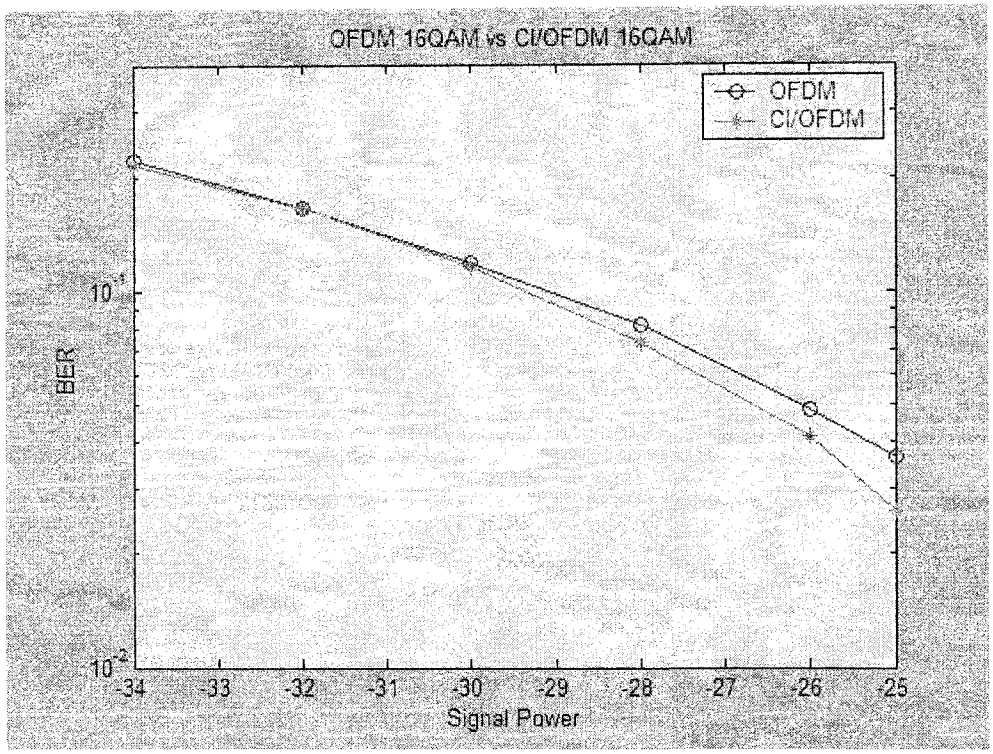

Figure 9.7: Performance Results for 16QAM OFDM vs. CI/OFDM

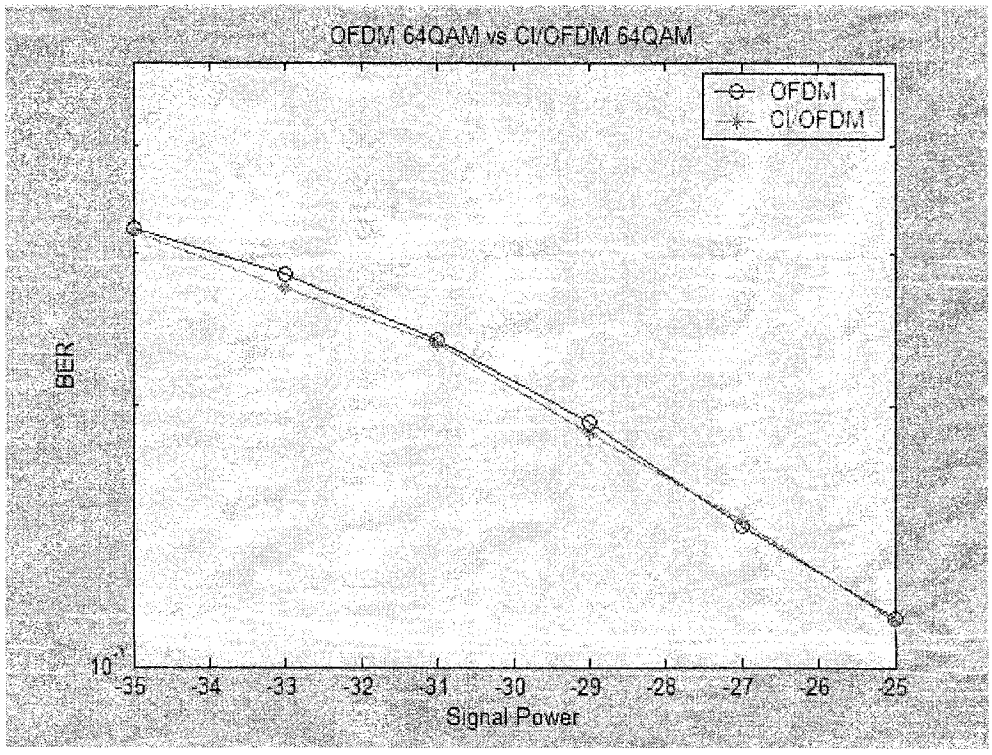

Figure 9.8: Performance Results for 64QAM OFDM vs. CI/OFDM

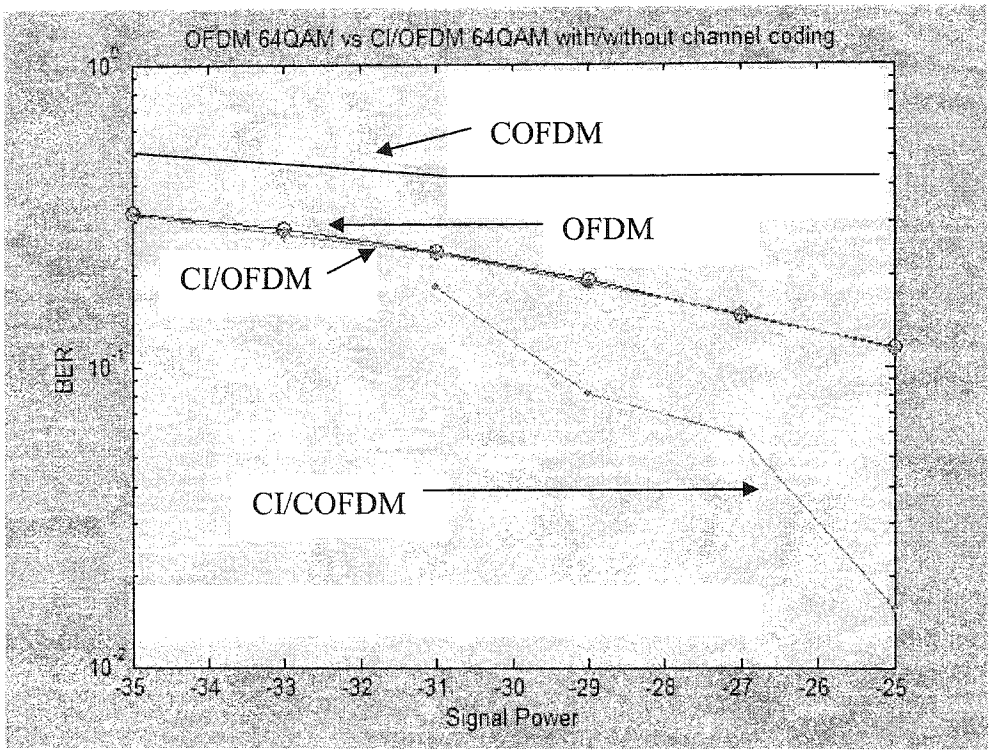

Figure 9.9: Performance Results for 64QAM OFDM vs. CI/(C)OFDM

Referring to Figures 9.5 – 9.7, the BPSK, QPSK, and 16QAM CI/OFDM systems offer small performance gains relative to the OFDM systems. These small gains are a consequence of the small frequency diversity that exists within the transmit bandwidth. However, referring to Figure 9.8, the 64QAM OFDM and CI/OFDM systems are very similar. It is also observed that the performance of CI/OFDM over OFDM improves at higher SNR. Unfortunately, because transmissions are required to be below a –25dBm threshold, we are not able to directly measure how much of an improvement CI/OFDM is able to achieve over OFDM as we approach the saturation region of the power amplifier.

Finally, referring to Figure 9.9, which includes performance results when channel coding is implemented, the performance of the 64QAM COFDM system is entirely unacceptable, whereas the CI/COFDM 64QAM system significantly benefits from channel coding. Even if these worse case scenarios only happened 1% of the time, it may prevent 64QAM OFDM from ever being practical. In other words, these worse case data scenarios could dominate the operation of the system and cause the transmission to consistently timeout and fail. With a stronger coding strategy, the CI/COFDM architecture could present a viable 64QAM transmission protocol, offering high-data rates for satellite systems.

9.4 Conclusions

In this chapter, RF test performance results of CI/OFDM and CI/COFDM versus OFDM and COFDM were presented for the satellite channel. It was anticipated that the BER performance curves for OFDM and CI/OFDM may be the same, due to the approximate flat fading nature of the satellite channel. However, up to a 1 dB gain in BER was measured for CI/OFDM relative to conventional OFDM. This is believed to be due to a small degree of diversity over the channel. Even though the satellite channel response is relatively flat, there was still a slight frequency selectivity, resulting in

CI/OFDM performance gains (relative to conventional OFDM). In 64QAM satellite links, CI/COFDM grants significant performance gains over 64QAM COFDM. With this enhanced performance, 64QAM CI/COFDM provides a high-throughput system for satellite links.

Chapter 10 Conclusions

In this dissertation, an innovation is introduced to improve upon the performance, throughput, and peak-to-average power ratio characteristics of current Orthogonal Frequency Division Multiplexing (OFDM) systems.

This dissertation began by introducing novel Carrier Interferometry spreading codes into current OFDM systems, creating the innovative CI/OFDM system (Chapters 3 and 4). It is shown (in Chapters 4, 5, and 6) that this CI/OFDM system significantly improves performance relative to traditional OFDM. Specifically, by applying CI spreading codes to the data symbols of the OFDM system, receivers can better exploit the frequency diversity of the multipath fading channel. That is, at receiver side, the CI/OFDM received signal is decomposed into its carriers, and optimally recombined to best exploit diversity and minimize interference and noise. In this way, the poor performance exhibited by traditional uncoded OFDM systems can be overcome. Simulation results showed the dramatically improved BER performance when this new architecture is applied.

Moreover, the carefully selected CI spreading codes have been shown to exhibit a second benefit, significant reduction in peak-to-average power ratio (PAPR) (Chapter 3).

The same CI codes which grant significant performance increases over OFDM, also average the transmit power for the N data symbols over the entire transmit time frame. Specifically, when one data symbol's transmission reaches a maximum, the remaining $N-1$ data symbols' pulses are at minima, alleviating the possibility of an in-phase coherent addition. The resulting instantaneous signal power tightly hugs its mean and has small variance, ultimately allowing transmit power amplifiers to operate more efficiently, i.e., closer to the saturation region.

This dissertation also introduces two orthogonal CI spreading code sets that are pseudo-orthogonal to each other, creating PO-CI/OFDM (Chapters 3 and 4). The two code sets demonstrate minimum cross correlation (between the orthogonal sets). In this way, $2N$ real symbols are supported on a traditional N carrier OFDM system, without bandwidth expansion or increased transmit power. Simulations indicate that the novel PO-CI/OFDM system outperforms traditional OFDM while doubling its throughput.

Similar to the CI/OFDM system, PO-CI/OFDM also eliminates the PAPR issues that plague OFDM (Chapter 3). In the OFDM time frame, each PO-CI/OFDM symbol peaks in power at a unique moment in time, and as such, the overall transmit power is well averaged over the total OFDM symbol time. PAPR issues are essentially eliminated.

This research also examined CI/OFDM systems employing very high-order constellation mapping (Chapter 6). Simulation results show that CI/OFDM with high-order modulations, continues to significantly outperform traditional OFDM in the frequency selective fading channel, and continues to demonstrate excellent PAPR properties.

Through RF testing, CI/OFDM was applied to today's real world systems, further demonstrating the benefits of the CI strategy. RF testing of CI/OFDM was conducted in (1) the IEEE 802.11a Wireless LAN indoor environment (Chapter 7), (2) the terrestrial Fixed Broadband architectures (Chapter 8), and (3) the C-band satellite system (Chapter 9). When CI/OFDM replaces the traditional OFDM of the IEEE 802.11a Wireless LAN physical layer, performance gains of 5-7 dB at a probability of error of 10^{-3} are seen in the RF test results. When CI/OFDM was tested in the terrestrial environment, significant BER gains of (up to) an order of magnitude were observed. The terrestrial testing also suggested CI/OFDM's ability to overcome Doppler effects. Finally, when CI/OFDM was applied to the satellite system, small performance gains were observed for BPSK, QPSK, and 16QAM mapping techniques. With coding applied to the CI/OFDM 64QAM system, dramatic gains were observed relative to traditional Coded OFDM.

This thesis provides novel, powerful techniques that enable OFDM to overcome its limitations, and, as a result, satisfy the needs of future generation wireless networks.

Chapter 11 Future Work via Extensions to CI/OFDM

Some directions for future research are highlighted in this final chapter.

11.1 MIMO CI/OFDM

Multiple-input multiple-output (MIMO) antenna array systems, such as, e.g., space-time codes, have gained a great deal of attention as of late [88-89]. One such scheme, proposed by Alamouti, offers significant increases in performance, while maintaining fairly low complexity [90]. Further work has been conducted to merge similar transmit diversity schemes with the OFDM architecture, leading to MIMO-OFDM [91]-[93]. The proposed CI/COFDM systems can be merged with MIMO systems, leading to very high-performance MIMO-CI/OFDM systems.

11.2 Carrier Selective CI/OFDM

FD-MC-CDMA (Frequency Division Multi-Carrier Code Division Multiple Access) systems are novel architectures which exploit frequency diversity while minimizing MAI [94-97]. These systems benefit from true ML (Maximum-Likelyhood) MUD (Multi-user Detection) detection at the receiver, which is constructed to combat both ISI and noise in an exact ML sense [75]. Based upon this body of research, the FD-MC-CDMA concept can be extended to CI/OFDM systems.

Here, we divide the N carriers of CI/OFDM into N/M groups, where each group contains M (where $M<<N$) non-contiguous carriers that are maximally separated over the transmit bandwidth (i.e., M is selected based upon the available frequency diversity gain within the channel). We spread each data symbol over one of the N/M sets of M non-contiguous carriers (instead of spreading over all N carriers). The total number of interfering data symbols drops from N-1 (in CI/OFDM) to M-1. By decreasing the number of interfering data symbols in this manner, all the while maintaining the diversity of the channel, the complexity of an optimal ML MUD detection scheme becomes viable. This may lead to higher-performances than the MMSEC receiver utilized within this thesis.

11.3 Security Aspects of CI/OFDM

Security of wireless transmissions is a hot topic in today's research [98-100]. The CI spreading codes scramble traditional constellations. Figures 11.1-11.4 illustrate the I/Q locations of transmit symbols in OFDM and CI/OFDM for BPSK, QPSK, 16QAM and 64QAM, with and without noise. Figure 11.5 shows *only* a noise on the I/Q constellation plane *without modulation of any form.*

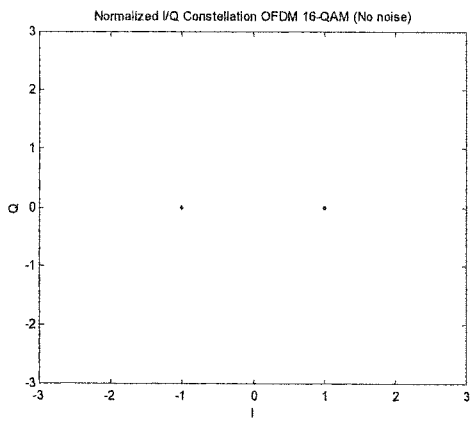

(a)

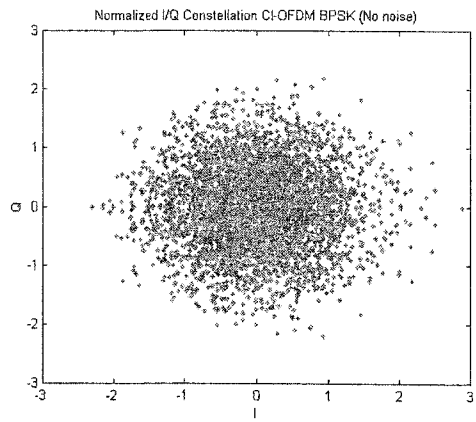

(b)

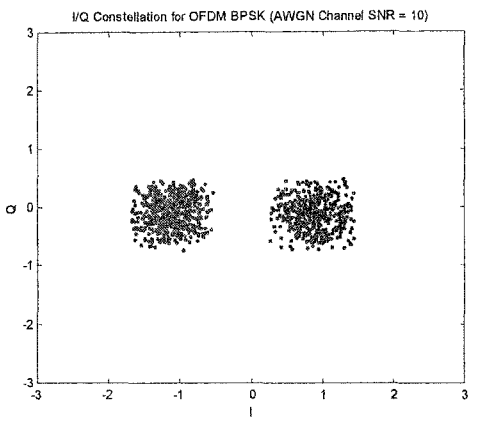

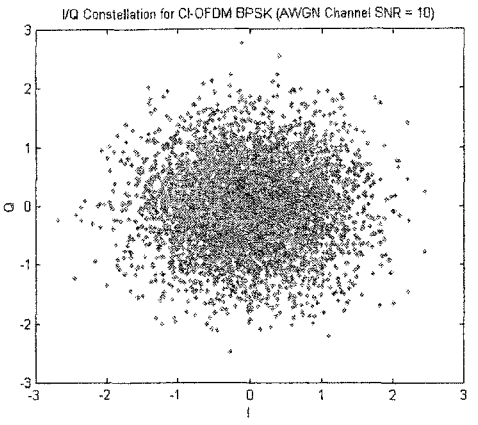

(c) (d)

Figure 11.1: BPSK (a) OFDM without noise, (b) CI/OFDM without noise, (c) OFDM with noise (SNR = 10 dB), and (d) CI/OFDM with noise (SNR = 10 dB)

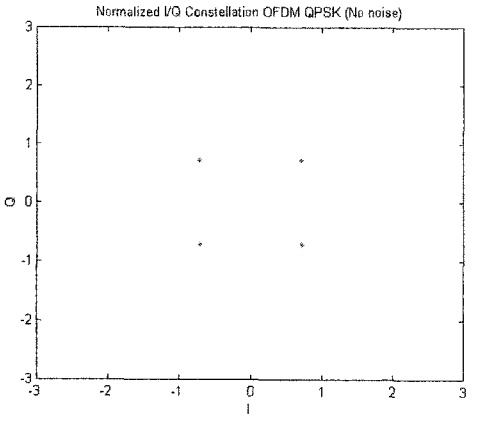

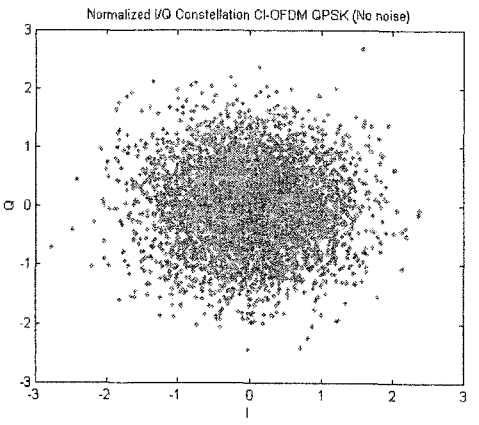

(a) (b)

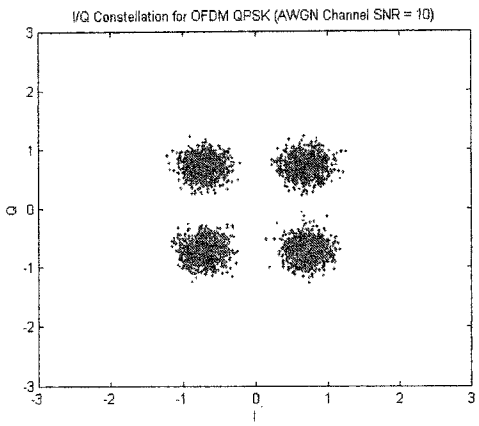

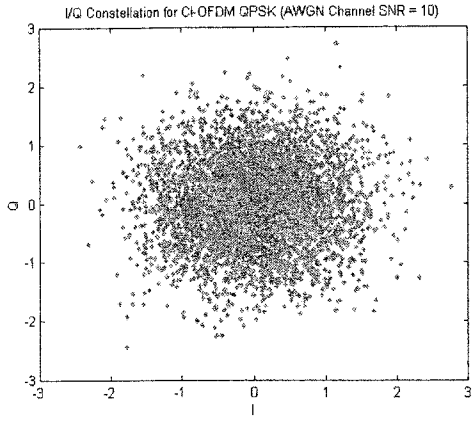

(c) (d)

Figure 11.2: QPSK (a) OFDM without noise, (b) CI/OFDM without noise, (c) OFDM with noise (SNR = 10 dB), and (d) CI/OFDM with noise (SNR = 10 dB)

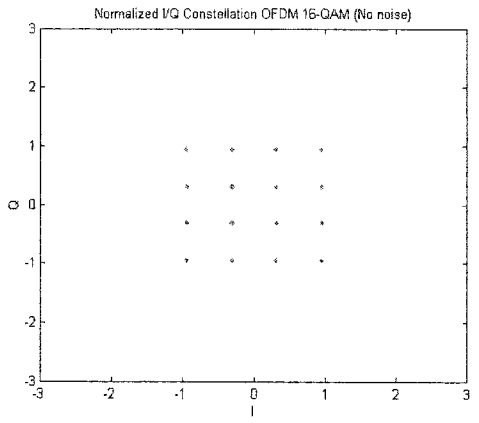

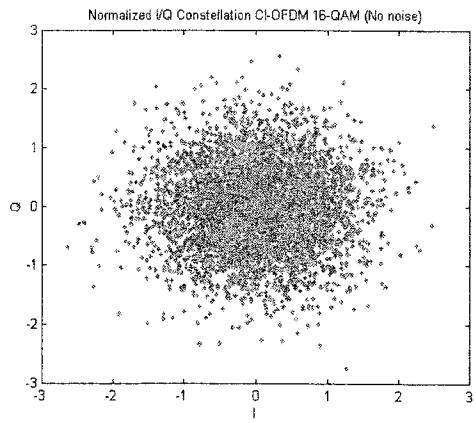

(a) (b)

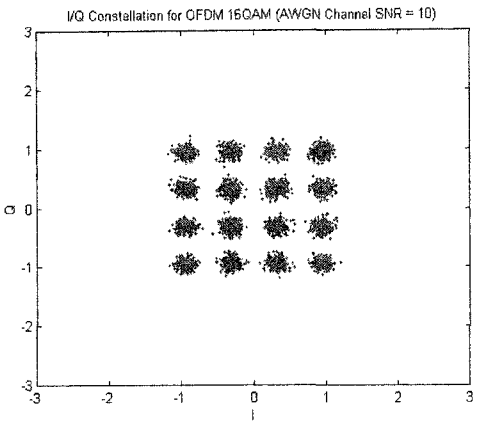

(c)

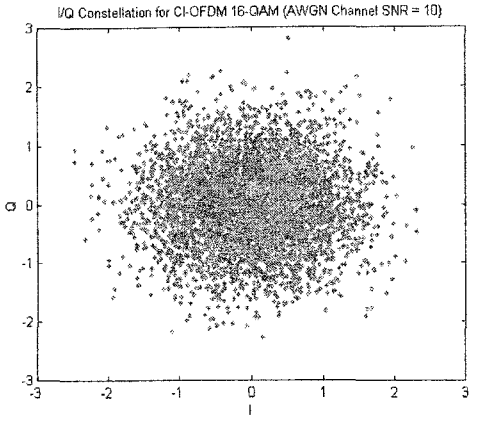

(d)

Figure 11.3: 16QAM (a) OFDM without noise, (b) CI/OFDM without noise, (c) OFDM with noise (SNR = 10 dB), and (d) CI/OFDM with noise (SNR = 10 dB)

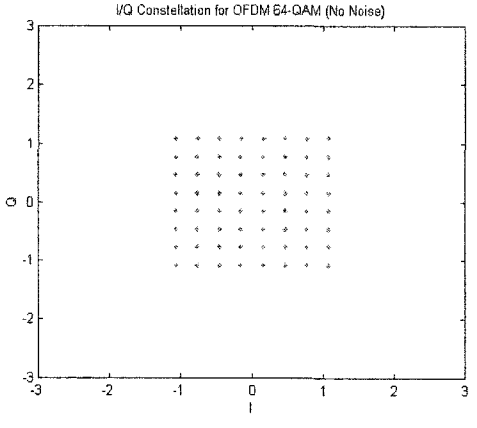

(a)

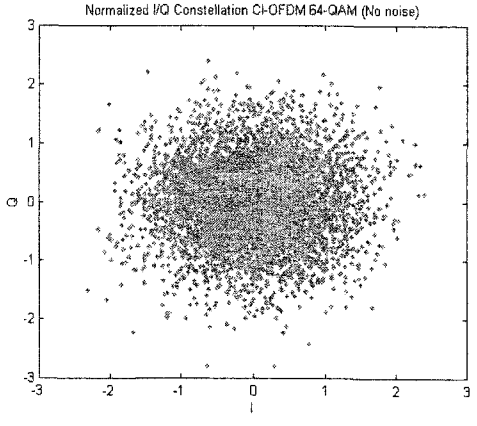

(b)

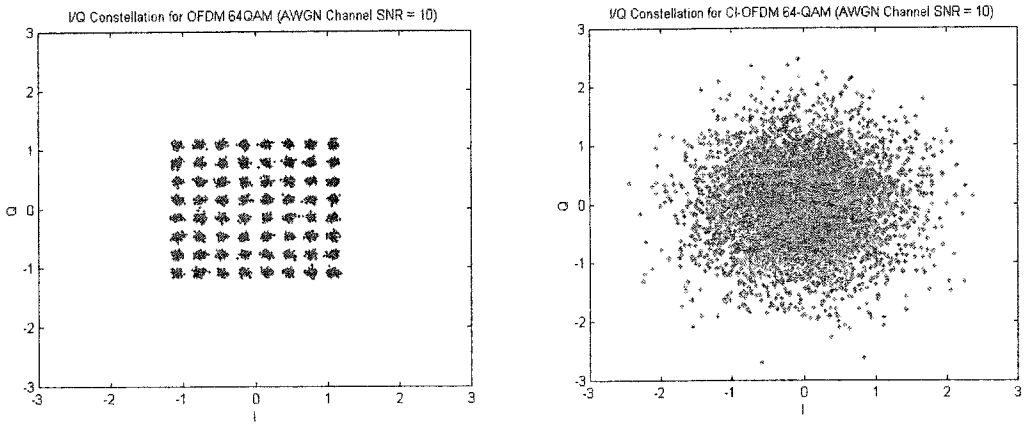

(c) (d)

Figure 11.4: 64QAM (a) OFDM without noise, (b) CI/OFDM without noise, (c) OFDM with noise (SNR = 10 dB), and (d) CI/OFDM with noise (SNR = 10 dB)

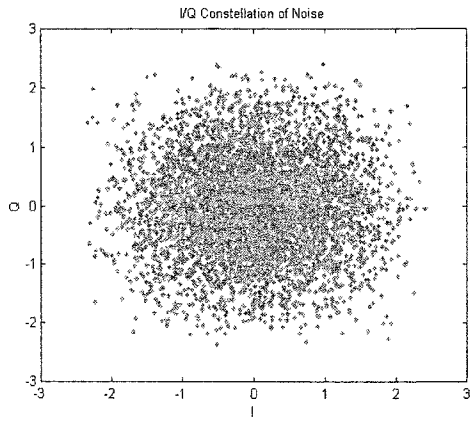

Figure 11.5: Reception of the noise (SNR = 10 dB) without Modulation

Referring to Figures 11.1-11.4, it can be seen that the CI/OFDM constellations appear completely random in nature. It can also be seen that the CI/OFDM I/Q constellations look similar regardless of symbol mapping technique (BPSK, QPSK, 16QAM, or 64QAM). Finally, in comparing the CI/OFDM constellations with the

constellation of noise (shown in Figure 11.5), we see that the CI constellations looks very similar to a pure noise.

Based upon these preliminary results, it is easy to see that advantages can be exploited for secure transmission of CI signaling. While it is well-known that a receiving strategy could be employed to extract CI/OFDM's data symbols (Chapter 4), a code scrambling (of the CI codes), or phase masking, in addition to scrambling across both CI codes and PO-CI codes, could easily hide the transmit signal.

These three subsections illustrate some of the many directions to be studied in the near future. There is no doubt that OFDM and COFDM systems will continue to be important areas of research and development for years to come.

APPENDIX A: Derivation of PO-CI Spreading Codes

Consider 2 sets of N orthogonal spreading sequences: the first set is defined by equation (1), and the second set is defined by equation (2). We now determine the value for $\Delta\theta$ that ensures a minimal cross-correlation between these sets. Let $R_{1,2}(j,k)$ refer to the cross correlation between the j^{th} spreading sequence in orthogonal code set *1* (equation (1)), and the k^{th} spreading sequence in orthogonal code set *2* (equation (2)). Also, let

$$R_{1,2} = [\frac{1}{N^2}\sum_{j=0}^{N-1}\sum_{k=0}^{N-1}(R_{1,2}(j,k))^2]^{\frac{1}{2}} \tag{A1}$$

represent the root mean square (rms) cross correlation that exists between spreading sequences in group 1 and group 2. Now, it is easily shown that for real signaling

$$\begin{aligned} R_{1,2}(j,k) &= \frac{1}{2\Delta f}\sum_{i=0}^{N-1}\cos[\ i(\theta_j - (\theta_k + \Delta\theta))] \\ &= \frac{1}{2\Delta f}\sum_{i=0}^{N-1}\cos[\ i(\frac{2\pi}{N}j - \frac{2\pi}{N}k - \Delta\theta)]) \end{aligned} \tag{A2}$$

It is also easy to show that

$$\sum_{j=0}^{N-1}(R_{1,2}(j,k))^2 = \sum_{j=0}^{N-1}(R_{1,2'}(j,k'))^2 \qquad k \neq k' \tag{A3}$$

That is, the total cross-correlation between the k^{th} spreading sequence in orthogonal group 2 and all spreading sequences in group 1 is identical to the cross-correlation

between the k'^{th} spreading sequence in orthogonal group 2 and all spreading sequences in group 1. Using equation (A3), we can rewrite equation (A1) as

$$R_{1,2} = [\frac{1}{N}\sum_{j=0}^{N-1}(R_{1,2}(j,0))^2]^{\frac{1}{2}} \tag{A4}$$

and, using equation (A2), this becomes

$$R_{1,2} = [\frac{1}{N}\sum_{j=0}^{N-1}[\frac{1}{2\Delta f}\sum_{i=0}^{N-1}\cos[\ i(\frac{2\pi}{N}j - \Delta\theta)]]^2]^{\frac{1}{2}} \tag{A5}$$

Let us now determine the selection of $\Delta\theta$ for group 2 that minimizes the root mean square correlation between the two orthogonal groups. To do this, we select

$$\frac{\partial R_{1,2}}{\partial\Delta\theta} = 0 \tag{A6}$$

Now,

$$\frac{\partial R_{1,2}}{\partial\Delta\theta} = \frac{1}{2}[\frac{1}{N}\sum_{j=0}^{N-1}(R_{1,2}(j,0))^2]^{-\frac{1}{2}}\frac{1}{N}\frac{\partial[\sum_{j=0}^{N-1}(R_{1,2}(j,0))^2]}{\partial\Delta\theta} = \frac{1}{2}[\frac{1}{N}\sum_{j=0}^{N-1}(R_{1,2}(j,0))^2]^{-\frac{1}{2}}\frac{1}{N}\cdot I \tag{A7}$$

where

$$I = \frac{\partial[\sum_{j=0}^{N-1}(R_{1,2}(j,0))^2]}{\partial\Delta\theta} = \frac{\partial[\sum_{j=0}^{N-1}(\sum_{i=0}^{N-1}\cos[\ i(\frac{2\pi}{N}j - \Delta\theta)])^2]}{\partial\Delta\theta} \tag{A8}$$

Now,

$$
\begin{aligned}
I &= \sum_{j=0}^{N-1} 2\left[\sum_{i=0}^{N-1}\cos[i(\frac{2\pi}{N}j-\Delta\theta)]\right]\cdot\left[\sum_{k=0}^{N-1}k\sin[k(\frac{2\pi}{N}j-\Delta\theta)]\right] \\
&= \sum_{j=0}^{N-1}\sum_{i=0}^{N-1}\sum_{k=0}^{N-1}2k\cos[i(\frac{2\pi}{N}j-\Delta\theta)]\sin[k(\frac{2\pi}{N}j-\Delta\theta)] \\
&= \sum_{j=0}^{N-1}\sum_{i=0}^{N-1}\sum_{k=0}^{N-1}k\left\{\sin[(k+i)(\frac{2\pi}{N}j-\Delta\theta)]+\sin[(k-i)(\frac{2\pi}{N}j-\Delta\theta)]\right\} \\
&= \mathrm{Im}(\sum_{j=0}^{N-1}\sum_{i=0}^{N-1}\sum_{k=0}^{N-1}k\{e^{j(k+i)(\frac{2\pi}{N}j-\Delta\theta)}+e^{j(k-i)(\frac{2\pi}{N}j-\Delta\theta)}\}) \\
&= \mathrm{Im}(\sum_{i=0}^{N-1}\sum_{k=0}^{N-1}ke^{-j(k+i)\Delta\theta}\sum_{j=0}^{N-1}e^{j\frac{2\pi}{N}j(k+i)}+\sum_{i=0}^{N-1}\sum_{k=0}^{N-1}ke^{-j(k-i)\Delta\theta}\sum_{j=0}^{N-1}e^{j\frac{2\pi}{N}j(k-i)}) \\
&= \mathrm{Im}(\sum_{i=0}^{N-1}\sum_{k=0}^{N-1}ke^{-j(k+i)\Delta\theta}\delta(k+i-N)N+\sum_{i=0}^{N-1}\sum_{k=0}^{N-1}ke^{-j(k-i)\Delta\theta}\delta(k-i)N) \\
&= \mathrm{Im}(\sum_{i=0}^{N-1}(N-i)e^{-jN\Delta\theta}+\sum_{i=0}^{N-1}i)N
\end{aligned}
\tag{A9}
$$

Hence, when $\Delta\theta=\frac{k\pi}{N}, k=0,1,2,...$, we have $I=0$ and, therefore, from equation (A7), $\frac{\partial R_{1,2}}{\partial\Delta\theta}=0$.

Seeking to determine which $\Delta\theta$ are maxima and which are minima, we calculate the second order partial derivative at $\Delta\theta=\frac{k\pi}{N}$ and determine:

$$
\begin{aligned}
&\frac{\partial R^2}{\partial^2\Delta\theta} > 0 \qquad when \qquad \Delta\theta = \frac{(2k+1)\pi}{N} \\
&\frac{\partial R^2}{\partial^2\Delta\theta} < 0 \qquad when \qquad \Delta\theta = \frac{2k\pi}{N}
\end{aligned}
\tag{A10}
$$

Hence, $\Delta\theta=\frac{2k\pi}{N}$ corresponds to maxima and $\Delta\theta=\frac{(2k+1)\pi}{N}$ provides minima. Selecting $k=0$, we choose $\Delta\theta=\frac{\pi}{N}$ as our minima. Figure A2 plots the root mean square cross

correlation $R_{1,2}$ between the two groups of codes as a function of $\Delta\theta$, verifying our selection of $\Delta\theta$.

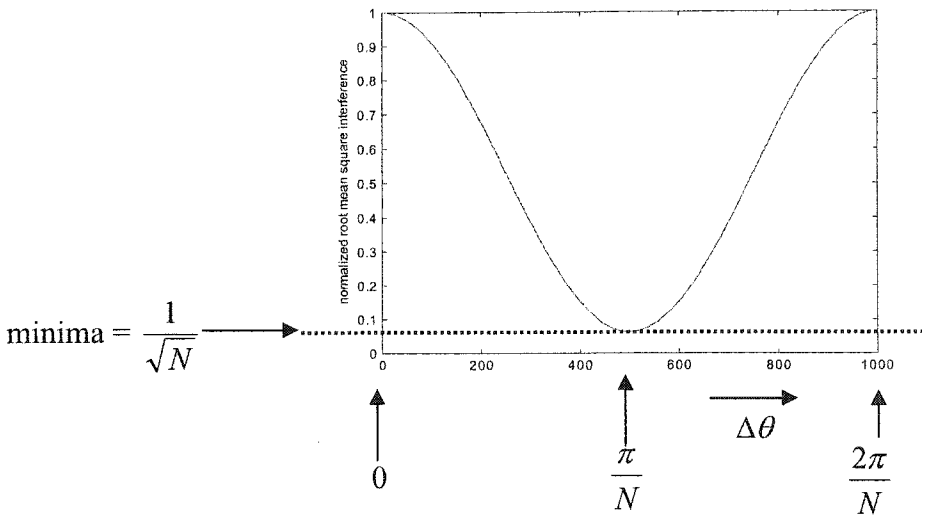

Figure A1: Root Mean Square Cross Correlation versus $\Delta\theta$

Hence, if we have one set of N orthogonal spreading sequences, specified via equation (1), and we want to increase system capacity via the addition of spreading sequences of equation (2), we can introduce the second set of N orthogonal spreading sequences with phase offset $\Delta\theta = \frac{\pi}{N}$. This selection minimizes the cross-correlation between code sets.

It is interesting to note that these codes demonstrate an rms cross-correlation provided by the minima of Figure A1. As shown in this figure, the rms cross-correlation is proportional to $\frac{1}{\sqrt{N}}$. When N is small, e.g., $N = 2$ or $N = 4$, the rms cross-correlation is large (rendering the codes impractical); fortunately, when N is large (e.g., $N \geq 16$), the rms cross-correlation is low and the codes represent an excellent selection. In most

practical systems, N is very large, e.g., N = 52 in IEEE 802.11a and N = 1,024 in proposed 4G systems, making PO-CI codes an excellent choice.

References

[1] Mosier, R. R., and R.G. Clabaugh, "Kineplex, a Bandwidth Efficient Binary Transmission System," *AIEE Trans.*, Vol. 76, pp. 723 - 728, Jan.1958.

[2] Saltzberg, B. R., "Performance of an efficient parallel data transmission system," *IEEE Trans. Comm.*, Vol. COM-15, pp. 805 – 813, Dec. 1967.

[3] G. C. Porter, "Error distribution and diversity performance of a frequency differential PSK HD modem," *IEEE Transactions on Communications*, Vol., COM-16, pp. 567-575, August 1968.

[4] M. S. Zimmerman and A. L. Kirsch, "The AN/GSC-10 (KATHRYN) variable rate data modem for HF radio," *IEEE Transactions on Communications*, Vol., COM-15, pp. 197-205, April 1967.

[5] R. W. Chang, "Synthesis of band-limited orthogonal signals for multichannel data transmission," *Bell System Technical Journal*, Vol., 45, pp. 1775-1796, December 1966.

[6] S. B. Weinstein and P. M. Ebert, "Data transmission by frequency division multiplexing using the discrete fourier transform," *IEEE Transactions on Communications*, Vol. COM-19, pp. 628-634, October 1971.

[7] W. Y. Zou and Y. Wu, "COFDM: an overview," *IEEE Transactions on Broadcasting*, Vol. 41, No. 1, pp. 1-8, March 1995.

[8] W. E. Keasler, and D. L. Bitzer, "High speed modem suitable for operating with a switched network," U.S. Patent No. 4,206,320, June 1980.

[9] P. S. Chow, J. C. Tu and J. M. Cioffi, "Performance evaluation of a multichannel transceiver system for ADSL and VHDSL services," *IEEE J. Selected Area*, Vol., SAC-9, No. 6, pp. 909 – 919, Aug. 1991.

[10] P. S. Chow, J. C. Tu and J. M. Cioffi, "A discrete miltitone transceiver system for HDSL applications," *IEEE J. Selected Areas in Comm.*, Vol. SAC-9, No. 6, pp. 909 – 919, Aug. 1991.

[11] H. Sari, G. Karma, and I. Jeanclaude, "Transmission techniques for digitial terrestrial TV broadcasting," *IEEE Communications Magazine*, Vol. 33, pp. 100-109, February 1995.

[12] A. V. Oppenheim and R. W. Schaffer, *Discrete-time signal processing*, Prentice-Hall International, ISBN 0-13-216771-9, 1989.

[13]S. Hara, M. Mouri, M. Okada, and N. Morinaga, "Transmission performance analysis of multi-carrier modulation in frequency selective fast rayleigh fading channel," *Wireless Personal Communications*, Kluwer Academic Press, Vol. 2, pp. 335-356, 1996.

[14] R. V. Paiement, "Evaluation of single carrier and multicarrier modulation techniques for digital ATV terrestrial broadcasting," *CRC Report*, No. CRC-RP-004, Ottawa, Canada, Dec. 1994.

[15] R. B. Marks, "The IEEE 802.16 working group on broadband wireless," *IEEE Network*, Vol. 13, Issue 2, pp. 4-5, March-April 1999.

[16] Anna Hac, *Multimedia applications support for wireless ATM networks*. Prentice Hall PTR, Upper Saddle River, NJ, 2000.

[17] IEEE 802.11, "Draft supplement to standard for telecommunications and information exchange between systems – LAN/MSN specific requirements – Part 11:

wireless MAC and PHY specifications: High speed physical layer in the 5 GHz band," P802.11a/D6.0, May 1999.

[18] http://standards.ieee.org/announcements/80211gapp2.html

[19] P. Ramjee and R. van Nee, *OFDM for Wireless Multimedia Communications*. Artech House Publishers, Boston, MA, 2000.

[20] L. H. Charles Lee, *Convolutional coding: Fundamentals and Applications*, Artech House, London, England, 1997.

[21] B. Le Flock, M. Alard, and C. Berrou, "Coded orthogonal frequency division multiplex," *Proceedings of the IEEE*, Vol. 83, No. 6, June 1995, pp. 982-996.

[22] Q. Wang and L. Y. Onotera, "Coded QAM using a binary convolutional code," *IEEE Transactions on Communications*, Vol. 43, No. 6, pp. 2001-2004, June 1995.

[23] G. Ungerboeck, "Channel coding with multilevel/phase signals," *IEEE Transactions on Information Theory*, Vol. IT-28, No.1, pp.55-67, Jan. 1982.

[24] R. D. Wesel and J. M. Cioffi, "Fundamentals of coding for broadcast OFDM," *Proceedings of IEEE ASILOMAR-29*, 1996.

[25] L. H. Charles Lee, *Convolutional coding: fundamentals and applications*, Artech House, London, 1997.

[26] V. Tarokh and H. Jafarkhani, "On the computation and reduction of the peak-to-average power ratio in multicarrier communications," *IEEE Transactions on Communications*, Vol., 48, pp. 37-44, January 2000.

[27] T. A. Wilkinson and A. E. Jones, "Minimization of the peak to mean envelope power ratio in multicarrier transmission schemes by block coding," *IEEE Vehicular Technology Conference, VTC'95*, July 1995, pp. 825-831.

[28] A. De Wild, "The peak-to-average power ratio of OFDM," *M.S. Thesis*, Delft University of Technology, Delft, The Netherlands, September 1997.

[29] Y. Fu, S. G. Kang, and C. C. Ko, "A new scheme for PAPR reduction in OFDM systems with ICI self cancellation," *Proceedings of the IEEE Vechicular Technology Conference, VTC '02*, Vol., 3, pp. 1418-1421, 2002.

[30] S. H. Muller and J. B. Huber, "OFDM with reduced peak-to-average power ratio by optimum combination of partial transmit sequences," *Electronic Letters*, Vol. 33, No. 5, Feb 1997, pp. 368-369.

[31] J. A. Davis and J. Jedwab, "Peak-to-mean power control in OFDM, golay complement sequences, and reed-muller codes," *IEEE Transactions on Information Theory*, Vol. 45, No. 7, pp. 2397-2417, Nov. 1999.

[32] X. Li and L. J. Cimini, Jr., "Effects of clipping and filtering on the performance of OFDM," *IEEE Vehicular Technology Conference, VTC'97*, May 1997, pp. 1634-1638.

[33] C. R. Nassar, B. Natarajan, Z. Wu, D. Wiegandt, S. A. Zekavat, and S. Shattil, *Multi-carrier technologies for wireless communications*, Kluwer Academic Press, November 2001.

[34]C. R. Nassar, B. Natarajan, D. Wiegandt and Z. Wu, "Multi-carrier platform for wireless communications. Part 2: OFDM and MC-CDMA systems with high-performance, high-throughput via innovations in spreading," *Wireless Communications and Mobile Computing Journal,* Vol. 2, Issue 4, pp. 381-403, June 2002.

[35]D. A. Wiegandt, Z. Wu, and C. R. Nassar, "High-performance OFDM with excellent papr properties via carrier interferometry spreading," submitted for review to *IEEE Transactions on Vehicular Technology*, Feb. 2003.

[36]D. A. Wiegandt, Z. Wu, and C. R. Nassar, "A multiple constellation papr analysis of carrier interferometry ofdm," submitted for review to *IEEE Wireless Communication Letters*, Feb. 2003.

[37]D. A. Wiegandt and C. R. Nassar, "High performance OFDM via carrier interferometry," *IEEE International Conference on Third Generation Wireless and Beyond, 3Gwireless '01,* San Francisco, CA, pp. 404-409.

[38] Z. Wu, D.A. Wiegandt, and C.R. Nassar, "High-Performance 64-QAM OFDM via Carrier Interferometry Spreading Codes," Submitted for *review IEEE Vehicular Technologyl Conference VTC 2003.*

[39]C. R. Nassar, Zhiqiang Wu, B. Natarajan and D. Wiegandt, The Road to 4G: two paradigm shifts, one enabling technology, submitted to *IEEE Communications Magazine.*

[40] D. A. Wiegandt and C. R. Nassar, "High-throughput, high-performance orthogonal frequency division multiplexing via pseudo-orthogonal carrier interferometry spreading codes," accepted for publication in *IEEE Transactions on Communications*, January 2003.

[41]D. A. Wiegandt and C. R. Nassar, "High-throughput, high-performance OFDM via pseudo-orthogonal carrier interferometry coding," *IEEE 12th International Symposium on Personal, Indoor and Mobile Radio Communications, PIMRC 2001*, San Diego, CA, pp. G98-G102.

[42]D. A. Wiegandt and C. R. Nassar, "High-throughput, high-performance OFDM via pseudo-orthogonal carrier interferometry type 2," To be presented at the *5TH international Symposium on Wireless Personal Multimedia Communications (WPMC '02).*

[43]D. A. Wiegandt, C. R. Nassar, and Z. Wu, "Overcoming peak-to-average power ratio issues in OFDM via carrier interferometry codes," *IEEE Vehicular Technology Conference, VTC'01,* Atlantic City, NJ, pp. 660-663.

[44]D. A. Wiegandt, C. R. Nassar, and Z. Wu, "Peak-to-average power reduction in high-peformance, high-throughput OFDM via pseudo-orthogonal carrier interferometry coding," *2001 IEEE Pacific Rim Conference on Communications, Computers and Signal Processing, PACRIM 2001*, Victoria, British Columbia, Canada, pp. 453-456.

[45]D. A. Wiegandt, Z. Wu, and C.R. Nassar, The elimination of peak-to-average power ratio concerns in OFDM via carrier interferometry spreading codes: a multiple constellation analysis, Submitted for review *IEEE Global Telecommunications Conference, GLOBECOM'03.*

[46]D. A. Wiegandt and C. R. Nassar, "High-performance 802.11a WLAN via carrier interferometry orthogonal frequency division multiplexing at 5 GHz," *IEEE Global Telecommunications Conference, GLOBECOM'01*, San Antonio, TX, Nov. 25-26, 2001, Vol. 6, pp. 3579-3582.

[47]D. A. Wiegandt and C. R. Nassar, "High-performance wireless ATM via carrier-interferometry orthogonal frequency division multiplexing," *IASTED International Conference on Wireless and Optical Communications, WOC 2001*, Banff, Alberta, Canada, pp. 82-86.

[48]D. A. Wiegandt and C. R. Nassar, "Higher-speed, higher-performance 802.11a wireless LAN via carrier interferometry orthogonal frequency division multiplexing," *IEEE International Conference on Communications, ICC 2002*, New York, New York, pp. 527-532.

[49]D.A. Wiegandt, Z. Wu, and C.R. Nassar, High-performance carrier interferometry OFDM WLANs: RF testing, Accepted for Publication in *Proceedings of IEEE International Conference on Communications, ICC 2003.*

[50] I. Koffman and V. Roman, "Broadband wireless access solutions based on OFDM access in IEEE 802.16," *IEEE Communications Magazine*, Vol., 40, pp. 96-103, April 2002.

[51] E. Ayanoglu, V. K. Jones, G. G. Raleigh, J. Gardner, D. Gerlach, and K. Toussi, "VOFDM broadband wireless transmission and its advantages over single carrier modulation," *IEEE International conference on Communications, ICC '01*, Vol., 6, pp. 1660-1664, 2001.

[52] R. B. Marks, "The IEEE 802.16 working group on broadband wireless," *IEEE Network*, Vol., 13, pp. 4-5, April 1999.

[53] W. A. C. Fernando and R. M. A. P. Rajatheva, "Performance of COFDM for LEO satellite channels in global mobile communications," *IEEE Vehicular Technology Conference, VTC '98*, Vol., 2, pp. 18-21, May 1998.

[54] Z. Ye, G. J. Saulnier, and M. J. Medley, "Rate adaptive OFDM (RA-OFDM) spread spectrum system for LEO satellite communications," *IEEE Military Communications Conference Proceedings, MILCOM '99*, Vol., 1, pp. 621-625, 1999.

[55] W. C. Jakes, Ed., *Microwave Mobile Communications*, IEEE Press, New York, NY, 1974.

[56] Natarajan, B., C.R. Nassar, and V. Chandrasekhar, "Generation of Rayleigh fading envelopes for spread spectrum applications," IEEE Communications Letters, Vol. 4, No.1, Jan.2000, pp.9-1

[57] B. Natarajan, C. R. Nassar, and V. Chandrasekar, "Correlated rayleigh fading envelopes with spread spectrum applications," *IEEE Radio and Wireless Conference, RAWCON '99*, pp. 45-48, 1999.

[58] M. Pauli, H.-P. Kuchenbecker, "On the reduction of the out-of-band radiation of OFDM-signals," *IEEE International Conference on Communications*, Vol. 3, June 1998, pp. 1304-1308.

[59] T. May and H. Rohling, "Reducing the peak-to-average power ratio in OFDM radio transmission systems," in *Proc. VTC '98*, (Ottawa, Canada), 18-21.5. 1998.

[60] S. Hara and R. Prasad, "Overview of multicarrier CDMA," *IEEE Communications Magazine*. Vol. 35, No.

[61] B. Natarajan, "Carrier interferometry for next generation CDMA and TDMA wireless systems: a multi-carrier framework," *Ph.D. Dissertation*, Colorado State University, Fort Collins, CO, May 2002.

[62] C.R. Nassar, M. Michelini, B. Natarajan, and S. Shattil, "Introduction of carrier interference to spread spectrum multiple access," *Symposium on Emerging Technologies in Wireless Communications and Systems*, Richardson, TX, April 12-13, 1999, pp. 4.1-4.5.

[63] B. Natarajan, C.R. Nassar, S. Shattil, M. Michelini, and Z. Wu, "High-performance MC-CDMA via carrier interferometry codes," *IEEE Transactions on Vehicular Technology*, Vol. 50, No. 6, pp. 1344-1353, Nov. 2001.

[64] S. Kaiser, "On the performance of different detection techniques for OFDM-CDMA in fading channels," *IEEE Global Telecommunications Conference 1995, Globecom '95*, pp. 2059-2063.

[65] D. Merouane, P. Loubaton, and M. de Courville, "Spread OFDM performance with MMSE equalization," *2001 IEEE Conference on Acoustics, Speech, and Signal Processing*, pp. 2385-2388.

[66] F. Vanhaverbeke, M. Moeneclaey and H. Sari, "DS/CDMA with Two Sets of Orthogonal Spreading Sequences and Iterative Detection," *IEEE Communications Letters*, Vol. 4, No. 9, Sep. 2000, pp. 289-291.

[67] J. G. Proakis, *Digital communications*, McGraw Hill, Inc., New York, NY, 1995.

[68] D. D. Falconer and S. L. Ariyavisitakul, "Broadband wireless using single carrier and frequency domain equalization," *5th International Symposium on Wireless Personal Multimedia Communications, WPMC '02*, Vol., 1, pp. 27-36, 2002.

[69] E. Lawrey and C. J. Kikkert, "Maximising signal strength inside buildings for wireless LAN systems using OFDM," *Microwave Conference*, pp. 257-260, 2000.

[70] P. Nobles and F. Halsall, "OFDM for high bit rate data transmission over measured indoor radio channels," IEE *Colloqium on Radio LANs and MANs*, pp. 5/1-5/5, 1995.

[71] J. Li, G. Liu, and G. B. Giannakis, "Carrier frequency offset estimation for OFDM-based WLANs," *IEEE Signal Processing Letters*, Vol., 8, pp. 80-82, March 2001.

[72] P. Vandenameele, S. Thoen, M. Engels, and H. De Mau, "A combined OFDM/SDMA approach for WLAN," *IEEE 49th Vehicular Technology Conference, VTC '99*, Vol., 2, pp. 1712-1716, 1999.

[73] S. Wu and Y. Bar-ness, "A phase noise suppression algorithm for OFDM-based WLANs," *IEEE Communications Letters,* Vol., 6, pp. 535-537, December 2002.

[74] ISO/IEC 8802.11:1999 (ANSI/IEEE Std 802.11, 1999 Edition), Information Technology—Telecommunications and Information Exchange Between Systems—Local

and Metropolitan Area Networks—Specific Requirements, Part 11: Wireless LAN Medium Access Control (MAC) and Physical Layer (PHY) Specifications—Amendment 1: High-speed Physical Layer in the 5 GHz band, May 1999.

[75] S. Verdu, *Multiuser Detection*, Cambridge University Press, New York, NY, 1998.

[76] H. Hashemi, "The indoor propagation channel," *Proc. IEEE*, vol.81, no. 7, July 1993, pp. 943-68.

[77] TR 101 112, "Universal mobile telecommunications system (UMTS); Selection procedures for the
choice of radio transmission technologies of the UMTS (UMTS 30.03 version 3.1.0)," November 1997.

[78] H. Sari, G. Karam, and I. Jeanclaud, "Frequency-domain equalization of mobile radio and terrestrial broadcast channels," *IEEE Global Telecommunications Conference, GLOBECOM '94*, Vol., 1, pp. 1-5, 1994.

[79] E. Viterbo and K. Fazal, "How to combat long echoes in OFDM transmission schemes: sub-channel equalization for more powerful channel coding," *IEEE Global Telecommunications Conference, GLOBECOM '95*, Vol., 3, pp. 2069-2074, 1995.

[80] A. Vahlin and N. Holte, "OFDM for broadcasting in presence of analogue co-channel interference," *IEEE Transactions on Broadcasting*," Vol., 41, pp. 89-93, September 1995.

[81] IEEE Standard for Local and Metropolitan Area Networks – Part 16: Air Interface for Fixed Broadband Wireless Access Systems – Amendment 1: Detailed System Profiles for 10-66 GHz, 2002.

[82] P. G. M. de Bot and P. M. J. Baggen, "Error correcting coding for OFDM broadcasting over frequency selective channels," *IEE Coloqium on Digital Terrestrial Television*, pp. 3/1-3/4, November 1993.

[83] B. Usevitch, "Code selection to eliminate interchannel interference in a multi-user OFDM satellite system," *Conference Record of the 34th Asilomar Conference on Signals, Systems, and Computers*, Vol., 1, pp. 137-141, 2000.

[84] L. Wan and V. K. Dubey, "Performance of frequency and time domain coded OFDM over fast fading LEO channels," *Information Systems for Enhanced Public Safety and Security, EUROCOMM 2000*, pp. 179-183, 2000.

[85] H. Lou, M. J. Fernandez-Getino Garcia, and V. Weerackody, "FEC scheme for a TDM-OFDM based satellite broadcasting system," *IEEE Transactions on Broadcasting*, Vol., 46, pp. 60-67, March 2000.

[86] C. J. Demeure and P. A. Laurent, "COFDM modem for terrestrial radio broadcasting," *8th International Conference on HF Radio Systems and Techniques*, pp.53-57, 2000.

[87] Federal Communications Commission, 25.204, FR 40255, September 6, 1983.

[88] H.E. Gamal and A. R. Hammons Jr., "On the design of algebraic space-time codes for MIMO block fading channels," *IEEE Transactions on Information Theory*, Vol., 49, pp. 151-163, January 2003.

[89] T. H. Liew and L. Hanzo, "Space-time codes and concatenated channel codes for wireless communications," *Proceedings of the IEEE*, Vol., 90, pp. 187-219, February 2002.

[90] S. M. Alamouti, "A simple transmit diversity technique for wireless communications," *IEEE Journal on Select Areas in Communications*, Vol. 16, pp. 1451-1458, October 1998.

[91] Z. Liu, G. B. Giannakis, A. Scaglione, and S. Barbarossa, "Decoding and equalization of unknown multipath channels based on block precoding and transmit-antenna diversity," *Conference Record of the Thirty-Third Asilomar Conference on Signals, Systems, and Computers*, Pacific Grove, CA, Vol. 2, pp. 1557-1561, October 1999.

[92] J. Ha, A. N. Mody, J. H. Sung, J. R. Barry, S. W. McLaughlin, and G. L. Stuber, "LDPC coded OFDM with Alamouti/SVD diversity technique," *International Symposium on Wireless Personal Multimedia*, Aalborg, Denmark, Vol. 3, pp. 1345-1350, September 2001.

[93] Z. Liu, G. B. Giannakis, S. Barbarossa, and A. Scaglione, "Transmit antennae space-time block coding for generalized OFDM in the presence of unknown multipath," *IEEE Journal on Selected Areas in Communications*, Vol. 19, pp. 1352-1364, July 2001.

[94] Z. Wu, C. R. Nassar, "FD-MC-CDMA: a frequency-based multiple acess architecture for high performance wireless communication, accepted for publication in *IEEE Transactions on Vehicular Technology.*

[95] Z. Wu and C. R. Nassar, "FD-MC-CDMA with multi user detection: exploiting frequency diversity for high performance wireless communications," *International Conference on Third Generation Wireless and Beyond*, San Francisco, CA, may 28-31, 2002, pp. 814-819.

[96] Z. Wu, C. R. Nassar and B. Natarajan, "FD-MC-CDMA: a frequency-based multiple access architecture for high performance wireless communication," *proceedings of IEEE Radio and Wireless Conference, RAWCON '01*, Waltham, MA, 2001, August 19-22.

[97] S.K. Miller, "Facing the challege of wireless security," *Computer*, Vol., 34, pp. 16-18, July 2001.

[98] J. J. Harrington and D. A. Pritchard, "Concepts and applications of wireless security systems for tactical, portable, and fixed sites," *IEEE 31st International Carnahan Conference on Security Technology*, pp. 133-139, October 1997.

[99] D. M. Johnson, "Wireless security: vulnerabilities and countermeasures," *Proceedings of the Computer Security Applications Conference*, pp. 91, 2002.

[100] P. Ashley, H. Hinton, and M. Vandenwauver, "Wired versus wireless security: the internet, WAP and imode for E-commerce," *Proceedings of the 17th Computer Security Applications Conference*, pp. 296-306, 2001.